Electrogenerated Hydrogen Peroxide and Fuel Cells
Ciaran James McDonnell-Worth
BScAdv (with Honours)

A thesis submitted for the degree of *Doctor of Philosophy* at
Monash University in 2016
School of Chemistry

Copyright notice

Abstract

This thesis focuses on the electrochemical production of H_2O_2 *via* water oxidation and its subsequent use as a fuel in direct H_2O_2 fuel cells.

H_2O_2 is a useful chemical both in industrial and scientific applications as it is not only a strong oxidant but also produces no harmful by-products when it is used as such. Shortly prior to the commencement of this thesis it was found that H_2O_2 may be produced electrochemically *via* water oxidation. This process only occurred in a specific electrolyte, namely one in which the salt contained an ammonium-based cation and free amine was present in solution. It was hypothesised that the presence of free amine helped to stabilise the H_2O_2. To further understand this phenomenon this research focused on changing the parameters involved in the water oxidation mechanism. This included using different ammonium-based salts in the electrolyte, measuring H_2O_2 production rates at different pHs and different oxidative potentials and observing the rate of H_2O_2 production over different oxidation times. It was found that H_2O_2 was only generated efficiently in a narrow range of oxidation potentials and pHs. It was proposed that the role of the free amine in solution was two-fold, one to help stabilise the H_2O_2 during water oxidation and prevent its further oxidation to O_2, and the other to act as a pH buffer at the surface of the water oxidation catalyst.

The research went on to attempt to utilise this electrogenerated H_2O_2 in direct H_2O_2 fuel cells (DHPFCs). DHPFCs are a fascinating alternative to H_2 gas or methanol fuel cells as H_2O_2 can be used as both the fuel and the oxidant. This is because H_2O_2 can be reduced *and* oxidised relatively easily compared to other fuels. As a consequence of this DHPFCs may be designed and utilised in a number of different ways which has certain advantages in cost, efficiency and safety. As part of this thesis novel catalysts for H_2O_2 reduction and oxidation were tested as anodes and cathodes in DHPFCs and were found to perform well. Specifically, using a mixed cobalt oxide-carbon black film as a cathode in combination with a heat treated nickel foam anode was found to give quite high open circuit potentials compared to other catalysts that have been used previously in similar conditions.

Ultimately, this thesis was able to demonstrate a fully reversible system in which H_2O_2 was generated electrochemically and then used to produce power in a single-electrolyte fuel cell without any processing of the fuel or electrolyte. This reversibility is important if such a system were to be used in real world applications and shows great promise for this technology.

Declaration

This thesis contains no material which has been accepted for the award of any other degree or diploma at any university or equivalent institution and that, to the best of my knowledge and belief, this thesis contains no material previously published or written by another person, except where due reference is made in the text of the thesis.

Publications during enrolment

McDonnell-Worth, C. and D. R. MacFarlane (2014). "Ion effects in water oxidation to hydrogen peroxide." <u>RSC Advances</u> **4**(58): 30551-30557.

Thesis including published works General Declaration

I hereby declare that this thesis contains no material which has been accepted for the award of any other degree or diploma at any university or equivalent institution and that, to the best of my knowledge and belief, this thesis contains no material previously published or written by another person, except where due reference is made in the text of the thesis.

This thesis includes 1 original paper published in peer reviewed journals and 2 unpublished publications. The core theme of the thesis is "electrochemical H_2O_2 production and its use in fuel cells". The ideas, development and writing up of all the papers in the thesis were the principal responsibility of myself, the candidate, working within the School of Chemistry under the supervision of Prof. Douglas R. MacFarlane

(The inclusion of co-authors reflects the fact that the work came from active collaboration between researchers and acknowledges input into team-based research.)

In the case of Chapter 2 my contribution to the work involved the following:

(If this is a laboratory-based discipline, a paragraph outlining the assistance given during the experiments, the nature of the experiments and an attribution to the contributors could follow.)

Thesis chapter	Publication title	Publication status*	Nature and extent (%) of students contribution
2	Ion Effects in Water Oxidation to Hydrogen Peroxide	Published	85%
1	Review of Progress in Direct Hydrogen Peroxide Fuel Cells (DHPFCs)	Ready to be submitted	90%
3	Cobalt and Nickel Oxide Catalysts for One-compartment, Direct Hydrogen Peroxide Fuel Cells (DHPFCs) in Ammonium-based Electrolytes	Ready to be submitted	85%

* e.g. 'published'/ 'in press'/ 'accepted'/ 'returned for revision'

I have renumbered sections of submitted or published papers in order to generate a consistent presentation within the thesis.

Student signature: ████████   **Date:**   25/02/2016

The undersigned hereby certify that the above declaration correctly reflects the nature and extent of the student and co-authors' contributions to this work.

Main Supervisor signature: **Date:** 25/02/2016

Acknowledgements

I would first like to thank my supervisor, Doug, for his constant input, advice and support over the course of my PhD. Also, thanks to my secondary supervisors Alex and Fengling as well as Peter for both their help in the labs and their friendship. My friends Mega, Alison and everyone else in and around the MacFarlane offices have made this journey a joy and I don't know what I would have done without them. I would also like to thank my parents, Mary and Chris, for their constant support and for being the best role models a son could ever ask for. Finally, I could not have done any of this without my partner, Madi. She has been alongside me for every part of my PhD and hopefully will be beside me for much, much more.

Table of Contents

Chapter 1

Introduction

1.1 Specific Declaration for Chapter 1.3

Monash University

Declaration for Thesis Chapter 1.3

Declaration by candidate

In the case of Chapter 1.3, the nature and extent of my contribution to the work was the following:

Nature of contribution	Extent of contribution (%)
Initiation, key ideas, data collection and interpretation, manuscript writing and preparation	90%

The following co-authors contributed to the work. If co-authors are students at Monash University, the extent of their contribution in percentage terms must be stated:

Name	Nature of contribution	Extent of contribution (%) for student co-authors only
Douglas R. MacFarlane	Initiation, key ideas, manuscript editing and preparation	10

The undersigned hereby certify that the above declaration correctly reflects the nature and extent of the candidate's and co-authors' contributions to this work*.

Candidate's Signature	██████████████	Date 25/02/2016

Main Supervisor's Signature	██████████████	Date 25/02/2016

*Note: Where the responsible author is not the candidate's main supervisor, the main supervisor should consult with the responsible author to agree on the respective contributions of the authors.

1.2 Introduction

With an ever increasing proportion of a population of 7 billion living lifestyles that consume an extraordinary amount of energy, our awareness of where that energy comes from and how it influences our environment is also increasing dramatically. In the past decade concern in governments and the general population energy needs and climate change has led to innumerable scientific inquests, policy changes and public protests that deal with matters from the development of new, clean energy sources to the economic ramifications of investigating and mitigating the effects of rising atmospheric CO_2 levels. Unsurprisingly, government expenditure on these issues has also risen. For example, the U.S. government's climate change expenditures reached as high as $22.6 billion in 2013, $6 billion of which was invested in clean energy technologies[†]. This is a clear indication that, while the source of clean energy in the future may be contested (solar, wind, geothermal, nuclear or, a more likely scenario, an amalgamation of several of these) a new energy economy is likely to take over from that of fossil fuels. The way that we store, transport and use energy will be very different and will have to take into account the intermittent nature of some sources of clean energy such as wind and solar. In these cases the energy storage medium is vitally important as it needs to be safe to store and transport, have a high energy density and be energy efficient. A wide array of energy storage systems such as batteries, capacitors and chemical fuels already exist in varying states of technological advancement. Out of these, chemical fuels offer relatively high energy densities and also benefit from taking advantage of the infrastructure used for the transportation and storage of fossil fuels today.

[†]http://www.whitehouse.gov/sites/default/files/omb/assets/legislative_reports/fcce-report-to-congress.pdf
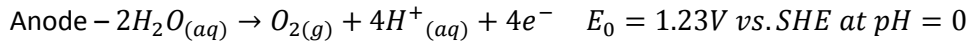
The Hydrogen Economy

As opposed to conventional motors or generators, fuel cells allow chemical fuels to be converted directly into electrical energy *via* a reduction/oxidation reaction. The H_2 fuel cell makes use of the oxidation of hydrogen gas, using $O_{2(g)}$ as the oxidant and produces only water as waste. There are a number of different ways to store hydrogen gas, offering different energy densities and safety concerns. $H_{2(g)}$ has the higher energy density by weight but a relatively low energy density by volume when compared to fossil fuels. This proves problematic when considering it as a fuel for automobiles. Pressurisation and cryogenics improve energy density but also increases the mass, volume and safety precautions necessary for the storage vessels. Other methods for hydrogen storage exist and are being researched including adsorption and physisorption of hydrogen molecules and incorporation of hydrogen into hydrocarbons or metal hydrides.
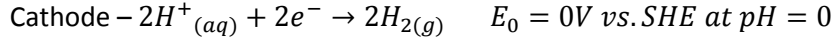
Water Oxidation

Given that hydrogen gas is not available "as is" in the environment the methods used to produce it determine its cost as a fuel. The largest source of hydrogen gas today is available *via* steam reforming which requires the consumption of natural gas and produces carbon monoxide and carbon dioxide. The alternative method utilising electrochemical water splitting ideally has no harmful by-products, uses only water and, as such, is ideal for sustainable hydrogen fuel production.

Hydrogen production in an electrochemical cell proceeds *via* the oxidation of water at the anode and H^+ reduction on the cathode:

Anode $- 2H_2O_{(aq)} \rightarrow O_{2(g)} + 4H^+{}_{(aq)} + 4e^-$ $E_0 = 1.23V \; vs. SHE \; at \; pH = 0$

(Equation 1)

Cathode $- 2H^+{}_{(aq)} + 2e^- \rightarrow 2H_{2(g)}$ $E_0 = 0V \; vs. SHE \; at \; pH = 0$

(Equation 2)

As indicated in Eq. 1 and 2 each reaction has an associated E_0 or standard redox (reduction/oxidation) potential that determines the minimum potential that must be applied for a reduction or oxidation reaction to occur at standard conditions (25°C, 1 atmosphere pressure and an effective activity of unity for each of the reactants). This standard redox potential is determined by the change in the Gibb's free energy of the reactants and products of the redox reaction. The Nernst equation (Eq. 3) can be used to determine the change to the redox potential when standard conditions are not used:

$$E_{red} = E^0{}_{red} + \frac{RT}{nF} ln \frac{a_{ox}}{a_{red}}$$

(Equation 3)

Where E_{red} is the reduction potential, $E^0{}_{red}$ is the reduction potential at standard conditions, R is the gas constant, n is the number of moles of electrons transferred in the reaction, F is Faraday's constant and a_{ox} and a_{red} are the activity of the oxidising species and reducing species respectively. For example, the potential at which water oxidation occurs (Eq. 1) will vary depending on the pH of the solution due to the change in proton activity.

Due to a variety of thermodynamic losses there is a difference in this theoretically determined potential and the actual potential required for a reaction to occur. Of the two reactions shown in Eq. 1 and 2 water oxidation (commonly referred to as the oxygen evolution reaction or OER) is considered to be more difficult to achieve. This is

due to the activation energy barriers present in the four electron transfer steps that occur in OER[1]. This is often described as an overpotential for electrochemical reactions and represents an activation energy that can be reduced through the use of electrocatalysts and different electrolytes.

Electrocatalytic Materials

The choice of a correct catalyst for water splitting is vital to determine not only the overpotential but also the rate of reaction and stability of the water oxidation cell. Platinum metal is a relatively good water oxidation catalyst but is costly and can be poisoned with exposure to carbon monoxide[2]. Other excellent water oxidation catalysts make use of ruthenium[3-5], palladium[6] or iridium complexes[7] and oxides[8, 9]. However, these catalysts are limited in practicality because of their rarity and cost. Therefore, cheaper and more abundant metals have been investigated[10, 11] including conducting polymers[12], cobalt[13-16], nickel[17, 18], iron and manganese[19-22] oxides. In fact, a large field of research is devoted towards mimicking the water oxidation system found in nature, Photosystem II[23]. Plants perform water oxidation as part of a photosynthetic process to convert CO_2 into hydrocarbons. The collection of proteins and metal oxides that perform the water oxidation reaction is known as Photosystem II. Water oxidation occurs specifically at a central oxygen-evolving complex (OEC) which has the molecular formula Mn_4CaO_5[24] arranged in a particular structure by coordination with the surrounding proteins[25]. Some catalysts or combinations of catalysts and other materials such as adsorbed dyes even make use of light, either partially or wholly, to reduce the overpotential required for water oxidation[26-29]

The number of water oxidation catalysts is large but the majority of them are designed to perform water oxidation *via* the four electron pathway to $O_{2(g)}$. However, an

alternative two electron pathway for water oxidation has been shown to be possible and provides a low oxidation pathway relative to the oxygen evolution reaction that also produces H_2O_2 with high faradaic efficiency.

Hydrogen Peroxide

As a strong oxidant H_2O_2 has a number of uses both industrially and chemically. As it produces only O_2 and water when it decomposes it is ideal for areas such as pulp bleaching[30], cleaning and degrading pollutants such as dyes[31-33]. The majority of H_2O_2 used industrially is produced by the anthraquinone auto-oxidation method[34]. This process is only viable in large scale facilities due to its reliance on a source of $H_{2(g)}$ (usually from steam reformation plants attached to the facility) and is quite energy intensive. As such there is some interest in H_2O_2 production techniques that can be scaled-down to be used as required "on-site" or even for *in situ* advanced oxidation processes (AOPs) such as epoxidation reactions[35-37]. Other methods that have been investigated are Izgorodin *et al.*[38] found that the combination of a water oxidation catalyst, a mixed-oxidation state manganese oxide, and an ammonium-based aqueous electrolyte containing free amine was able to oxidise water at low overpotentials (around 150mV) to produce H_2O_2. It was hypothesised that the H_2O_2 was stabilised in the electrolyte by hydrogen bonding to the free amine.

Aims of the project

This project aims to:

1. Investigate the water oxidation to H_2O_2 electrochemical reaction further by testing other ammonium salts. Originally, an aqueous solution of

butylammonium sulfate (ie. a salt composed of a 1:2 mixture of butylamine and sulfuric acid) to which butylamine was added was used as the electrolyte[38]. In **Chapter 2** salts with different cations (amines with different alkyl chain length and branches as well as secondary amines) and anions will be investigated as to how they behave electrochemically and what determines the rate and faradaic efficiency of H_2O_2 production. pH is another important factor that will be investigated as, given the role of hydrogen bonding hypothesised previously, both proton activity and free amine concentration will have a dramatic effect on the catalytic activity of these cells.

2. Given that H_2O_2 is a useful oxidant in many chemical processes this efficient, environmentally-friendly method to produce it provides a number of opportunities for exploitation. In particular, H_2O_2 has recently been used in direct H_2O_2 fuel cells due to its ease of storage and its relatively high theoretical open circuit potential. Later in this chapter, the recent research into these types of fuel cells will be discussed as well as how they may be integrated with electrochemical methods to produce H_2O_2. **Chapter 3** will explore some novel catalysts for both H_2O_2 reduction and oxidation and their incorporation into direct H_2O_2 fuel cells.

3. **Chapter 4** aims to integrate the water oxidation to H_2O_2 process into a direct H_2O_2 fuel cell to demonstrate a fully reversible fuel production and fuel cell system. The concept of a reversible fuel cell will be discussed and linked to the unique properties of H_2O_2 as both a fuel and an oxidant.

The following section (**Chapter 1.3**) has been written in the form of a review ready to be submitted which discusses reversible H_2O_2 fuel cells including recent advances in electrochemical H_2O_2 production and electrode materials for H_2O_2 oxidation and reduction.

1.7 References

1.   H. Dau, C. Limberg, T. Reier, M. Risch, S. Roggan and P. Strasser, *ChemCatChem*, 2010, **2**, 724-761.

2.   A. Ponrouch, S. Garbarino and D. Guay, *Electrochemistry Communications*, 2009, **11**, 834-837.

3.   L. Wang, L. L. Duan, L. P. Tong and L. C. Sun, *J. Catal.*, 2013, **306**, 129-132.

4.   Y. M. Badiei, D. E. Polyansky, J. T. Muckerman, D. J. Szalda, R. Haberdar, R. F. Zong, R. P. Thummel and E. Fujita, *Inorg. Chem.*, 2013, **52**, 8845-8850.

5.   R. Ramaraj, A. Kira and M. Keneko, *Journal of the Chemical Society, Chemical Communications*, 1987, 227-228.

6.   G. Kwon, G. A. Ferguson, C. J. Heard, E. C. Tyo, C. R. Yin, J. DeBartolo, S. Seifert, R. E. Winans, A. J. Kropf, J. Greeley, R. L. Johnston, L. A. Curtiss, M. J. Pellin and S. Vajda, *ACS Nano*, 2013, **7**, 5808-5817.

7.   J. M. Thomsen, S. W. Sheehan, S. M. Hashmi, J. Campos, U. Hintermair, R. H. Crabtree and G. W. Brudvig, *Journal of the American Chemical Society*, 2014, **136**, 13826-13834.

8.   J. D. Blakemore, N. D. Schley, M. N. Kushner-Lenhoff, A. M. Winter, F. D'Souza, R. H. Crabtree and G. W. Brudvig, *Inorg. Chem.*, 2012, **51**, 7749-7763.

9.   J. Rossmeisl, Z. W. Qu, H. Zhu, G. J. Kroes and J. K. Nørskov, *Journal of Electroanalytical Chemistry*, 2007, **607**, 83-89.

10.   A. Singh and L. Spiccia, *Coord. Chem. Rev.*, 2013, **257**, 2607-2622.

11.   R. D. L. Smith, M. S. Prevot, R. D. Fagan, S. Trudel and C. P. Berlinguette, *Journal of the American Chemical Society*, 2013, **135**, 11580-11586.

12.   O. Winther-Jensen, B. Winther-Jensen and D. R. MacFarlane, *Electrochemistry Communications*, 2011, **13**, 307-309.

13. G. Mattioli, P. Giannozzi, A. A. Bonapasta and L. Guidonili, *Journal of the American Chemical Society*, 2013, **135**, 15353-15363.

14. J. D. Blakemore, H. B. Gray, J. R. Winkler and A. M. Muller, *ACS Catal.*, 2013, **3**, 2497-2500.

15. Y.-H. Lai, C.-Y. Lin, Y. Lv, T. C. King, A. Steiner, N. M. Muresan, L. Gan, D. S. Wright and E. Reisner, *Chemical Communications*, 2013, **49**, 4331-4333.

16. M. W. Kanan, Y. Surendranath and D. G. Nocera, *Chemical Society Reviews*, 2009, **38**, 109-114.

17. W. J. Zhou, X. J. Wu, X. H. Cao, X. Huang, C. L. Tan, J. Tian, H. Liu, J. Y. Wang and H. Zhang, *Energy & Environmental Science*, 2013, **6**, 2921-2924.

18. Y. Zhang, B. Cui, C. Zhao, H. Lin and J. Li, *Physical Chemistry Chemical Physics*, 2013, **15**, 7363-7369.

19. M.-R. Gao, Y.-F. Xu, J. Jiang, Y.-R. Zheng and S.-H. Yu, *Journal of the American Chemical Society*, 2012, **134**, 2930-2933.

20. F. Zhou, A. Izgorodin, R. K. Hocking, L. Spiccia, D.R. MacFarlane, *Advanced Energy Materials*, 2012, **In print**.

21. F. Jiao and H. Frei, *Energy & Environmental Science*, 2010, **3**, 1018-1027.

22. M. Wiechen, H.-M. Berends and P. Kurz, *Dalton Transactions*, 2012, **41**, 21-31.

23. R.-Z. Liao, M. D. Kärkäs, B.-L. Lee, B. Åkermark and P. E. M. Siegbahn, *Inorg. Chem.*, 2015, **54**, 342-351.

24. M. Yagi, M. Toda, S. Yamada and H. Yamazaki, *Chemical Communications*, 2010, **46**, 8594-8596.

25. M. Suga, F. Akita, K. Hirata, G. Ueno, H. Murakami, Y. Nakajima, T. Shimizu, K. Yamashita, M. Yamamoto, H. Ago and J.-R. Shen, *Nature*, 2015, **517**, 99-103.

26. T. Bak, J. Nowotny, M. Rekas and C. C. Sorrell, *International Journal of Hydrogen Energy*, 2002, **27**, 991-1022.

27. A. Kudo and Y. Miseki, *Chemical Society Reviews*, 2009, **38**, 253-278.

28. A. Fujishima and K. Honda, *Nature*, 1972, **238**, 37-38.

29. J. H. Park, O. O. Park and S. Kim, *Applied Physics Letters*, 2006, **89**, 163106-163103.

30. U. Suess Hans, *Pulp Bleaching Today*, 2010.

31. I. Oller, S. Malato and J. A. Sánchez-Pérez, *Science of The Total Environment*, 2011, **409**, 4141-4166.

32. A. Aleboyeh, H. Aleboyeh and Y. Moussa, *Dyes and Pigments*, 2003, **57**, 67-75.

33. V. M. Daskalaki, E. S. Timotheatou, A. Katsaounis and D. Kalderis, *Desalination*, 2011, **274**, 200-205.

34. J. M. Campos-Martin, G. Blanco-Brieva and J. L. G. Fierro, *Angewandte Chemie International Edition*, 2006, **45**, 6962-6984.

35. G. Fioroni, F. Fringuelli, F. Pizzo and L. Vaccaro, *Green Chemistry*, 2003, **5**, 425-428.

36. G. B. Payne, *Journal of the American Chemical Society*, 1959, **81**, 4901-4904.

37. M. C.-Y. Tang, K.-Y. Wong and T. H. Chan, *Chemical Communications*, 2005, 1345-1347.

38. A. Izgorodin, E. Izgorodin, D. R. MacFarlane, *Energy & Enviroonmental Science*, 2012, **5**, 9496-9501.

Review of Progress in Direct Hydrogen Peroxide Fuel Cells (DHPFCs)

C.J. McDonnell-Worth[a] and D. R. MacFarlane[a].

This review introduces the concept of direct H_2O_2 fuel cells and discusses the merits of these systems in comparison to other "clean" energy fuels. Through electrochemical methods H_2O_2 fuel can be generated from environmentally benign energy sources such as wind and solar. It also produces only water and oxygen when it is utilised in a direct H_2O_2 fuel cell making it a fully reversible system. The electrochemical methods for H_2O_2 production are discussed here as well as the recent research aimed at increasing the efficiency and power of direct H_2O_2 fuel cells.
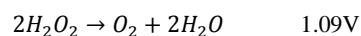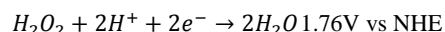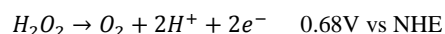
Introduction

Phasing out fossil fuels as an energy storage system is an inevitability as sources of oil become harder to access both physically and politically[1]. The influence of carbon dioxide and other greenhouse gases on weather patterns and the environment has also become a serious cause for concern[3]. The amount of renewable energy generated by wind, solar, hydro and geothermal sources is on the rise and will likely begin to eclipse fossil fuels in the future. Unfortunately many of these renewable energy sources are either intermittent or limited to certain geographic regions, and as such cannot fully replicate the ubiquity afforded by petrol, coal or natural gas. To sustain the same modes of energy transportation and utilisation that our society is comfortable with today the energy produced by renewable sources must be stored in efficient and inexpensive media. Electro-chemically generated chemical fuels are ideal for this purpose as they can be produced on demand with renewable energies and stored and transported when those energy sources are unavailable.

Rather than being burned in conventional combustion engines chemical fuels can also be used in fuel cells to convert their stored chemical potential energy directly into electrical energy. In general a fuel cell is composed of two compartments, one containing an anode on which the fuel is electrochemically oxidised and the other containing a cathode on which an oxidant (usually O_2) is reduced. Separating these two segments is a membrane that allows for charge to pass through the fuel cell but keeps the fuel and the oxidant from coming in direct contact with each other, or the opposite electrodes. The power that is generated by the fuel cell is a result of the difference in the electrochemical potential of the oxidation of the fuel and the reduction of the oxidant.

The fuel most famously associated with clean energy is undoubtedly H_2 gas which has garnered media attention for its use in real-world applications[4] as well as its long pedigree of intense scientific research[5-7]. H_2 gas can be generated electrochemically by the water splitting process in which an electrochemical cell is used to oxidise water while simultaneously reducing protons to H_2 gas. This gas can be collected and later utilised as a fuel.

While it ticks many of the boxes that are desirable in a 'green' fuel (its products when it is burned are only water and energy), H_2 gas has a number of drawbacks that are not trivial to overcome. One of these is the storage of H_2 gas, which is largely a problem of both cost and efficiency. H_2 storage has long been a problem for its utilisation as a fuel, as its energy density by volume at atmospheric pressure is far below that which would be practicable in a vehicle or even a stationary fuel storage facility. In order for it to be viable, H_2 gas must either be compressed to around 70MPa pressure, cryogenically stored as a liquid below 21K or be physically or chemically captured in other materials[8]. In terms of compression, storage at higher pressures allow for more fuel to be stored per unit volume, but also increases the amount of external equipment required to maintain that pressure safely[9, 10]. This raises the cost of any system incorporating pressurised H_2 gas and also increases its weight. There is also a certain amount of energy required to pressurise the H_2 gas in the first place, all of which lowers the efficiency of these types of storage systems. Other options are physiochemical storage (using materials such as a metal organic frameworks[11-14]) or chemical storage (such as in metal hydrides[15, 16]) to adsorb or chemically bind H_2. These materials are certainly safer than pressurised or liquid storage of H_2, but usually necessitate energy losses such as heating to release H_2 from the storage material during operation[17] and may suffer from impurities which lower their performance over time[18].

One particularly interesting alternative fuel to H_2 that has garnered some attention in the past decade is H_2O_2. H_2O_2 is well-known as an oxidant and is used in a number of chemical and industrial processes that make use of this property[19-24]. It has even been used as the oxidant in other types of fuel cells where it has been shown to perform even better than O_2 in some cases[25-28]. However, H_2O_2 is relatively unique when applied to fuel cells because it can be both oxidised *and* reduced with each process occurring at a different electrochemical potential:

$$H_2O_2 \rightarrow O_2 + 2H^+ + 2e^- \quad 0.68\text{V vs NHE}$$

$$H_2O_2 + 2H^+ + 2e^- \rightarrow 2H_2O \quad 1.76\text{V vs NHE}$$

$$2H_2O_2 \rightarrow O_2 + 2H_2O \quad 1.09\text{V}$$

This opens up the possibility of using H_2O_2 as the fuel and the oxidant in the same fuel cell with a maximum theoretical potential of 1.09V which is reasonably close to other fuel cells such as those using methanol/air (1.21V) and H_2/air (1.23V). The major advantage that a H_2O_2 fuel cell has over H_2 is that H_2O_2 can be made up into a solution that is liquid at room temperature, thus requiring no pressurisation or additional storage media. The energy density of a H_2O_2 fuel cell can be estimated and will ultimately depend on the concentration of H_2O_2 that can be safely used. As H_2O_2 is a reasonably strong oxidant the higher the concentration the more dangerous the solution becomes, until eventually it becomes reactive enough to be used as an oxidant in rocket fuel (around 85w%[29]). At a conservative concentration of 70w% the theoretical energy density can be calculated from the Gibbs free energy of the state of the system before and after fuel cell operation. The total energy generated by the simultaneous reduction and oxidation of two moles of H_2O_2 to one mole of O_2 and two moles of H_2O is -234kJ/mol[30]. For a concentration of 70w% of H_2O_2 in pure water ($0.89kg_{H2O2}L^{-1}$) we can calculate the number of moles per litre of H_2O_2 in this fuel to be $26.2molL^{-1}$. This is equivalent to 3.06MJ per litre of 70w% H_2O_2. On the other hand, in the simplest case (ie. following the ideal gas law), a tank which compresses $H_{2(g)}$ to 70MPa at room temperature will have a molar concentration of $28.7molL^{-1}$. The Gibbs free energy change for the reaction:

$$H_{2(g)} + 0.5O_{2(g)} \rightarrow H_2O_{(l)}$$
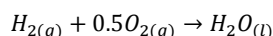
is $-237.1kJmol^{-1}$ which means that the compressed $H_{2(g)}$ will theoretically produce $6.8MJL^{-1}$ when operated in a fuel cell. However, an estimated 20% of that energy is used to compress the $H_{2(g)}$ in the first place[8] which lowers the maximum practical energy to approximately $5.4MJL^{-1}$. While this statistic may favour the use of compressed $H_{2(g)}$ it is not only the volume of the fuel that needs to be considered in the practical application of these systems. As mentioned above, pressurisation inevitably requires additional and specialised equipment for compressing the gas[14] and to prevent leakage and relieve pressure in case of faults[10]. In total the gravimetric capacity of compressed $H_{2(g)}$ is around 13wt%[18] meaning that most of the weight of the system is taken up by the storage vessel. Alternatively, liquid H_2 has a much higher energy density per volume than either aqueous H_2O_2 or compressed $H_{2(g)}$ but loses approximately 40% of that through the energy required to cool it to 21°K and has higher associated losses due to boil off and higher costs from liquefaction equipment and storage tanks.

Methods for hydrogen peroxide production

Hydrogen peroxide is known as a 'green' oxidant because it only produces water and oxygen when it decomposes. As such there is a much interest in using it for advanced oxidation processes such as the decolourisation of waste dye[21, 31-33] and as the oxidant in chemical reactions[20, 23, 34-39]. Large-scale H_2O_2 production is almost exclusively performed *via* the anthraquinone auto-oxidation process in which O_2 is reduced by 2-alkyl-anthrahydroquinone. First, $H_{2\ (g)}$ is produced (usually *via* steam reformation) and used to hydrogenate the quinone over a Pd catalyst. The hydrogenated quinone must then be filtered and then oxidised with air to form H_2O_2 which is subsequently extracted and distilled into an aqueous phase. This method is

unsuitable in the context of renewable fuels primarily because of its reliance on hydrogen gas which, when produced by steam reformation, is inherently non-renewable and ultimately energy inefficient. The Pd catalyst must also be roasted to clean it of organics and some toxic by-products must be treated or disposed of which is energy intensive and adds to the cost of the process[40]. The process is also only economically viable when it is performed on a large scale which requires more space than would be suitable for a roadside refuelling station, for example.

One of the benefits of electrochemical generation of H_2O_2 is that the devices used to produce the fuel can be constructed on a smaller or larger scale depending on their specific use. Much interest has been shown in designing electrocatalytic H_2O_2 batch reactors[41] for on-site industrial facilities that make use of advanced oxidation processes (AOPs)[35, 42, 43], pulp bleaching[19] or waste management[44] by H_2O_2. It may even be possible to downsize an electrochemical H_2O_2 production unit to the size that would fit into a household garage so that a steady supply of fuel could be generated and stored in homes.

There are two pathways available for electrochemical H_2O_2 production, O_2 reduction and water oxidation. Both pathways may yield H_2O_2 in conjunction with other products such as water in the case of O_2 reduction and O_2 in the case of water oxidation, depending on the specificity of the production method. H_2O_2 may also be produced by the direct reaction of $H_{2(g)}$ and $O_{2(g)}$[45] however, a source of $H_{2(g)}$ is necessary for this process.. In the following sections we explore these process in more detail.

Electrochemical H_2O_2 Generation

Oxygen Reduction

Electrochemical O_2 reduction to H_2O_2 is a two electron process and takes place according to the following redox reaction:

$O_2 + 2e^- + 2H^+ \rightarrow H_2O_2$ 0.7V vs SHE at standard conditions
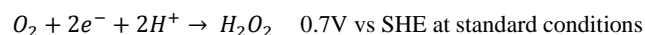
A wide variety of electrochemical catalysts have been found to reduce O_2 to H_2O_2 with a greater or lesser degree of specificity including TiO_2 particles[46], Platinum[47-49], manganese oxides[50], iron oxides[51], metal alloys such as Pd-Au[52] and Pt-Hg[53], copper complexes[54] and cobalt oxides[55-58]. The design of the electrocatalyst is important, as the competing 4-electron O_2 reduction to H_2O[59-61] :

$O_2 + 4e^- + 4H^+ \rightarrow 2H_2O$ -1.23V vs NHE
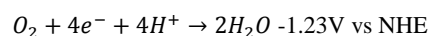
can cause efficiency losses. Bonakdapour *et al*. found that for non-noble metal catalysts the amount of H_2O_2 produced from oxygen reduction varied greatly depending on the catalyst loading on the surface of a rotating ring disk electrode[60]. In fact, by altering the catalyst loading from $20\mu gcm^2$ to $800\mu gcm^2$ the fraction of H_2O_2 observed at the ring from a Fe-N-C catalyst fell from 95% to as low as 5%. This was attributed to the lifetime of H_2O_2 in the bulk of the catalyst being shortened either by further oxidation to water or by a chemical reaction with itself to produce O_2 and water. By reducing the thickness of the electrode most H_2O_2 was produced at the surface and

was released to the electrolyte near the electrode before being further oxidised on the electrode.

In terms of mass electrochemical production of H_2O_2 from O_2 the surface area of a catalyst per unit area is a major limiting factor in production rates. Higher surface area means a higher number of catalytically active sites available for O_2 reduction at any one time. Some materials such as porous carbon have been used for O_2 reduction to H_2O_2 and have quite good activity, but poor faradaic efficiency[62-64]. Recently Liu *et al.* have reported very good H_2O_2 production rates from O_2 reduction as high as 2249.4 $mgL^{-1}h^{-1}$ using hierarchically porous carbon in a solution at pH 1[65]. These materials have a surface area of around $2000m^2g^{-1}$ which was considered to be one of the major contributing factors to their high activity. The faradaic efficiency of these materials, however, varied greatly with changes to the electrolyte pH. The highest efficiency of 85-90% was achieved in pH 1 electrolytes and the efficiency decreased with increasing pH, most likely due to the propensity for H_2O_2 to disproportionate at higher pHs.

In terms of pH, two electron reduction of O_2 to H_2O_2 has been found to be highly favoured on Ag(111) in acidic electrolytes when the overpotential applied is kept below a certain threshold[66]. As higher overpotentials were applied, the rate of complete, four electron water oxidation increased until only O_2 evolution was observed. In alkaline environments there was very little H_2O_2 produced at all overpotentials applied. This behaviour was hypothesised to be highly dependent on the interaction between the catalytic surface and the intermediate reactants and spectating species. As such certain catalysts are able to perform the two electron O_2 reduction only in alkaline environments[58].
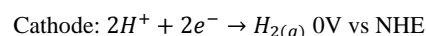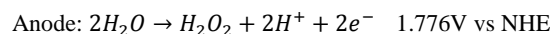
Photocatalytic H_2O_2 production has also been observed in water saturated with O_2. Graphitic carbon nitride[67], TiO_2 and zinc oxide[68, 69] catalysts have shown highly selective (in some cases greater than 90%), two electron O_2 reduction to H_2O_2 simply by irradiation with sunlight or even sonication reaching H_2O_2 concentrations of up to 350μM in 1 hour.

Water Oxidation

Water oxidation to H_2O_2 has been studied less thoroughly than O_2 reduction but nonetheless shows promise as an efficient electrochemical production method. The process was observed by Izgorodin *et al.*[70] in an ionic liquid-based electrolyte using a catalytic manganese oxide catalyst. The presence of free amine in the alkaline electrolyte was proposed to solvate the H_2O_2 by hydrogen bonding which limits the reaction to a 2-electron oxidation. Using chronoamperometry, the potential of the working electrode was kept at 0.59V vs Ag/AgCl a total of 0.08 μmol of H_2O_2 was produced with a faradaic efficiency of 77%. Further work elaborated on this by testing other cation and anion pairs for the electrolyte including secondary ammonium cations (diethylammonium) and longer chain alkylammonium cations (hexylammonium) as well as larger anions such as methanesulfonate and ethanesulfonate[71]. While it was found that none of these produced more H_2O_2 than butylammonium sulfate (BAS) the efficiency of the process was improved by identifying the
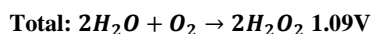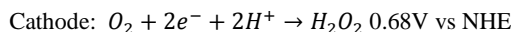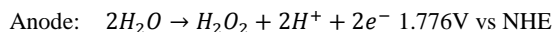
necessary applied potential at which H_2O_2 is produced but not further oxidised to $O_{2(g)}$. It was also found that H_2O_2 production from water oxidation occurs in a limited pH range starting at approximately pH9.0 and reaching a maximum at pH10.5.

By performing water oxidation to generate H_2O_2 rather than reducing O_2 an interesting synergy can be exploited. As a part of the conventional hydrogen evolution reaction (HER) to produce H_2 gas there are two reactions that usually take place; proton reduction to H_2 and water oxidation to O_2. The water oxidation process is generally the more energy intensive part of this water splitting process, but the O_2 is not considered to be an important by-product. Alternatively, Ando *et al.*[72] proposed a dual system in which H_2O_2 is produced simultaneously with H_2 according to the reaction shown below:

$$\text{Anode: } 2H_2O \rightarrow H_2O_2 + 2H^+ + 2e^- \quad 1.776\text{V vs NHE}$$

$$\text{Cathode: } 2H^+ + 2e^- \rightarrow H_{2(g)} \; 0\text{V vs NHE}$$

This system was hypothesised to be more cost effective as two products of value would be produced; H_2 as a fuel and H_2O_2 as an industrial oxidant.

Following the same reasoning it may be possible to combine both of the H_2O_2 production methods outlined above into one system where H_2O_2 is produced at the cathode (O_2 reduction to H_2O_2) and anode (H_2O oxidation to H_2O_2) simultaneously as shown below:

Anode: $\;\; 2H_2O \rightarrow H_2O_2 + 2H^+ + 2e^-$ 1.776V vs NHE

Cathode: $O_2 + 2e^- + 2H^+ \rightarrow H_2O_2$ 0.68V vs NHE

Total: $2H_2O + O_2 \rightarrow 2H_2O_2$ 1.09V

Given that water oxidation to H_2O_2 only occurs in alkaline electrolytes and O_2 reduction catalysts for H_2O_2 production generally perform better in acidic environments it is likely that such a system would need two different electrolytes separated by a conducting membrane. However such a set-up alters the half cell potential and also creates a membrane potential and therefore the voltage drop in the cell.

Hydrogen Peroxide in Fuel Cells

In general, fuel cells generate power because of the difference in electrochemical potential between the oxidative and reductive reactions spontaneously occurring on the electrodes. The power generated by a fuel cell is determined by the product of the current being drawn and the potential difference between the two electrodes at that current. As a larger current is drawn that potential difference is reduced and as such each fuel cell will have a current at which the power is at a maximum. Therefore this maximum power point is strongly influenced by the open circuit potential of the cell (which is the cell potential at which no current is being drawn from the cell) and the limiting current density (which is the total current density that can be drawn when the potential difference between the electrodes is biased to zero). When either the OCP or the limiting current density is increased the maximum achievable power density of the fuel cell generally trends upwards as well. The most obvious way to improve

both of these values is to alter the electrochemical catalyst that is used for both the oxidation and reduction on the cathode and anode.

These components of an H2O2 fuel cell are particularly important when it comes to improving the OCP. As mentioned previously, the theoretical potential difference between the H_2O_2 to H_2O reduction potential and the H_2O_2 to O_2 oxidation potential is 1.09V. Unfortunately, this value is not achievable in a real cell due to an additional energy input required to perform both redox reactions most commonly referred to as the overpotential. The overpotential is a result of the activation energy barrier that needs to be overcome for both reactions and it is influenced by the interaction between the fuel cell electrolyte and the surface of the anode or cathode. By coating the anode or cathode in an appropriate catalyst this overpotential can be reduced at both electrodes meaning that less energy is lost to overcome the activation barrier of the reduction or oxidation.

Hydrogen peroxide Reduction and Oxidation

As stated above the theoretical standard potentials for H_2O_2 oxidation and reduction are 0.68V and 1.77V respectively, but significant overpotentials associated with both reactions are typically required. This has been demonstrated by numerous studies, in particular by those who have attempted to incorporate H_2O_2 as an oxidant into other types of alternative fuel cells and semi-fuel cells[25-27, 73, 74]. One of the problems associated with using H_2O_2 as a reductant or an oxidant is that on many catalysts it is possible for H_2O_2 to be reduced and oxidised on the same surface[75-77] (Fig. 2), effectively causing the decomposition of the H_2O_2

Jing et al.[78] investigated this phenomenon by measuring the OCPs of H_2O_2 on various noble metals in an electrochemical cell with electrolytes containing H_2O_2. OCP is defined here as the potential applied to the electrode of interest at which there is zero current in the cell compared to an external reference electrode. The interpretation given by Jing et al. was that rather than defining the oxidation and reduction potentials of H_2O_2 it was more useful to observe the degree to which the OCP trended towards the theoretical oxidation and reduction potentials. For example, in both acidic and alkaline media they found that on Pt, Au, Pd and glassy carbon (GC) electrodes the OCP tended to be closer to the standard theoretical oxidation potential and concluded that this represented a mixed potential where both H_2O_2 reduction to H_2O and H_2O_2 oxidation to O_2 were taking place on the same electrode, but with a greater propensity towards the oxidation reaction. As these two processes are taking place simultaneously on the same electrode the total current being recorded will be the sum of both processes. This is problematic for fuel cells as not only is the maximum power of the cell diminished, but some fuel will be lost due to unproductive disproportionation of the H_2O_2 which lowers its overall fuel efficiency.

A number of studies have looked at reduction and oxidation catalysts for H_2O_2 for varying purposes such as fuel cells or H_2O_2 detectors[79-81]. In alkaline environments, perovskite[82, 83] and cobalt-based catalysts (particularly those based on Co_3O_4) have shown superior H_2O_2 reduction properties. Cathodes incorporating spinel structured Co_3O_4 nanoparticles were found to exhibit high activity towards H_2O_2 reduction in 3M NaOH[84]. The H_2O_2 reduction current remained steady over the course of 30 minutes of chronoamperometry (constant potentials of -0.2V to -0.4V) indicating that the Co_3O_4 cathode is reasonably stable in alkaline electrolytes. In work performed by Zhihao et al. three-dimensional gold-cobalt oxide cathodes were synthesised[85] and showed large reduction current peaks at -0.28V vs Ag/AgCl in highly alkaline, 3M KOH solutions. Catalysts based around the dye Prussian blue have also been found to reduce H_2O_2 with high faradaic efficiency in neutral to slightly acidic electrolytes[86].

The H_2O_2 oxidation catalyst on the anodic electrode has not been studied nearly as thoroughly in the context of fuel cells as the reduction catalysts, as the latter reaction is thought to be the major cause of energy loss through high overpotentials. Metals such as nickel or gold are often used as anodes in DHPFCs except in the case of some two-compartment fuel cell studies where the cathode and the anode can be the same material. For example, Yang et al. constructed a DHPFC[87] in which the cathode and the anode were both Pd particles electrodeposited onto carbon fibre cloth as discussed further below.

Direct Hydrogen Peroxide Fuel Cell Designs

Two-compartment fuel cells

The first DHPFC was designed by Hasegawa et al.[88] using two electrolytes, solutions of H_2SO_4 and NaOH containing H_2O_2, brought into contact with each other by a microfluidic flow cell. This cell achieves power generation by the reduction and oxidation of H_2O_2 in the acidic and alkaline electrolytes respectively.

$O_2 + 2H^+ + 2e^-$ $H_2O_2 + 2H^+ + 2e^-$
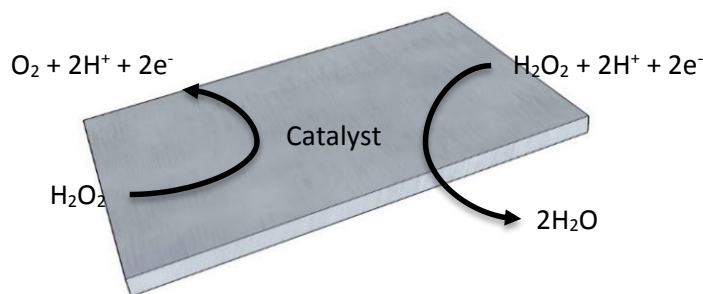
Catalyst

H_2O_2 $2H_2O$

Figure 1: Schematic of H2O2 disproportionation on a catalytic surface in an acidic environment.

As the electrolytes are not separated by a membrane the charge is balanced by the formation of a NaSO4 solution at the point of mixing. The maximum power density for this cell was found to be 23mWcm^{-2} at 300mV and 76mAcm^{-2}. As no membrane is required for this cell design the authors proposed that the cost and electrical resistivity are reduced making it superior in that respect to H_2 or methanol fuel cells. However, in a practical application of the technology this cell is limited by both the scalability of a microchannel design and critically by the consumption of the components of the electrolyte other than the fuel and the oxidant. Subsequent two-compartment fuel cell designs have included a membrane separating the acidic and the alkaline electrolytes. Fig. 2 describes a possible arrangement of such a two-compartment DHPFC.

Despite the drawbacks of fuel cells containing membranes they have been included in the majority of designs of two-compartment DHPFCs since 2005. The focus of the research into these types of fuel cells has been on the catalytic materials used for the cathode and anode, increasing the selectivity for H_2O_2 oxidation and reduction and improving the limiting current densities. Sanli *et al.* developed a two-compartment cell that utilised a Ni-carbon paper anode and a Pt cathode[2]. Nickel was used because in previous DHPFCs[89] it was found to have the lowest rate of unproductive H_2O_2 decomposition compared to other metals such as Au, Ag, Pt and Pd.

One of the major sources of inefficiency in a fuel cell is the membrane that separates the anodic and cathodic chambers. Membranes introduce resistance into the cell that results in loss of power density. They also complicate cell construction and limit its size, shape and the distance between electrodes. Some fuel cells can function without a membrane and these are usually based around the use of the laminar flow of electrolytes through microchannels. An example of this is given by Hasegawa *et al.* [88] as described above. However, as the two different electrolytes are in contact with each other there is usually going to be some degree of crossover of ions due to concentration gradients. The micro-channel design also limits the size and geometry of the cell if large-scale designs are necessary.

One-compartment DHPFCs

The unique operation of the H_2O_2 fuel cell also allows for the construction of a different membrane-less design called a "single-compartment DHPFC" (Fig. 3). Here, a single electrolyte is used in conjunction with two different catalysts. An open circuit potential is produced based on the selectivity that the catalysts have towards the oxidation and reduction of H_2O_2, rather than the pH difference at the surface of the cathode and anode. Thus, a membrane is not required to separate the cathode and anode and an entire resistive (and expensive) element can be eliminated from the fuel cell. Yamazaki *et al.*[89] were the first to design a one-electrolyte, one-compartment DHPFC using metals such as Ag, Au, Pt, Pd and Ni as catalysts. In that study an aqueous 1M NaOH solution containing 0.3M H_2O_2 was used as the fuel into which two different metals were immersed yielding an OCP of approximately 100mV. This OCP is obviously much lower than the theoretical 1.09V and this was ascribed to the problem of mixed potentials that was discussed above. In particular the high overpotential at the cathode was suggested to be the major
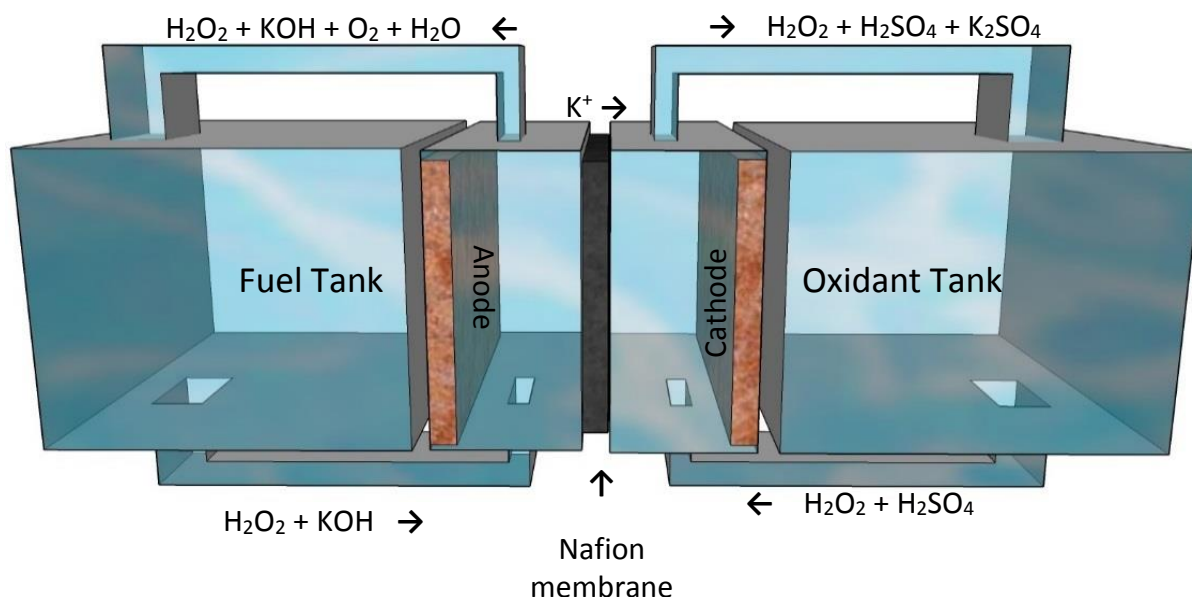

Figure 2: Schematic of a two-compartment direct H_2O_2 fuel cell containing a K^+ conducting Nafion membrane as a separator. This specific cell is designed as a flow cell where both oxidant and fuel are passed over the catalytic electrodes. The output of the fuel cell will reflect the concentrations of both the starting reactants as well as the products such as O_2 (g) and K_2SO_4 which will build up over time in the oxidant tank[2]. A K^+ conducting Nafion film is used as the membrane to facilitate charge transfer between the cathodic and anodic compartments. During the operation of the fuel cell K_2SO_4 is generated as a by-product meaning that regeneration of the electrolyte becomes more difficult. Developing a fuel generation system based on electrochemical H_2O_2 production for this type of cell will also require a source of H_2SO_4 and KOH which adds to the cost and logistical issues.
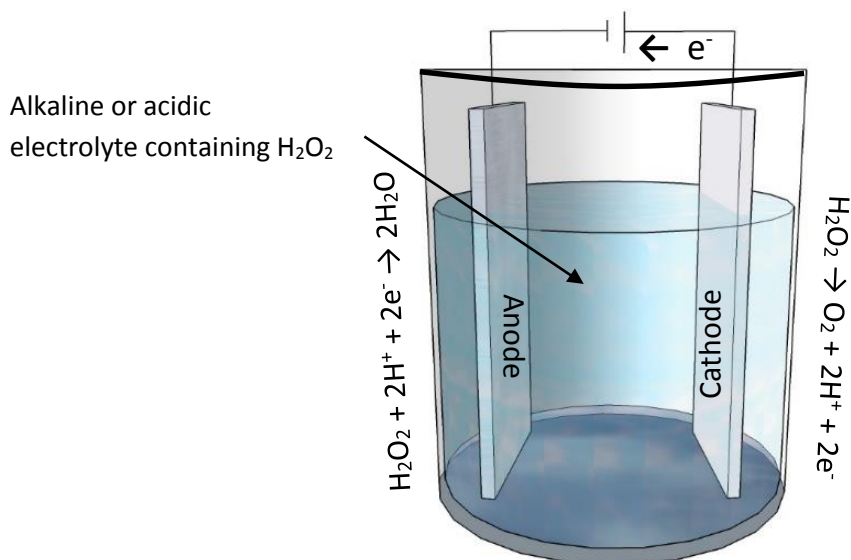
Figure 3: Schematic of a one-compartment DHPFC. The cathode and anode are different materials which have greater catalytic activity towards H₂O₂ reduction and oxidation respectively. The reactions presented at each electrode are representative of H₂O₂ oxidation and reduction taking place in an acidic environment, but the same principle applies in an alkaline electrolyte.

contributor to the poor performance of the cell. By modifying the surface of Ag metal with nanostructured Ag-Pb alloys, the total voltage produced by the cell was improved from 100mV to 150mV[90]. Here, the introduction of Ag and Ag-Pb nanoparticles was thought to increase the catalytic surface area of the cathode, thereby increasing the current generated by the cell. Interestingly, the introduction of small amounts of Pb to the alloy (Ag:Pb = 7:3 and Ag:Pb = 9:1) gave higher OCPs and limiting current densities than just Ag nanoparticles, or when the Pb ratio was too high (Ag:Pb = 6:4). These experiments were all conducted in a highly alkaline, 1M NaOH electrolyte, however, H_2O_2 is known to be unstable in most alkaline environments. An exception to this is aqueous, alkaline, ammonium-based solutions containing free amines which were discussed previously for their use in low overpotential water oxidation[70, 71].

Yamada *et al.* have used a number of metal-based complexes as H_2O_2 reduction catalysts for single-compartment fuel cells that make use of acidic electrolytes as the fuel medium. Complexes such as protonated iron-pthalocyanine[91], Fe^{II}_{3}-[2][92] and pyrazine-bridged $Fe[M^C(CN)_4]$ ($M^C = Pt^{2+}$ and Pd^{2+})[93] have been used as H_2O_2 reduction catalysts with great success. Fuel cells using these electrodes have achieved very high OCPs of around 0.8V along with high limiting current densities up to 15mAcm⁻² for total power densities up to 4mWcm⁻². Most recently Yamada *et al.* found that the presence of Sc^{3+} ions in the electrolyte solution inhibited the disproportionation of H_2O_2 and extended the time that a stable output potential could be maintained while a current was being produced by the cell. The stabilising effect was attributed to the trapping of $HO_2^•$ produced from the H_2O_2 by the Fe ions. Instead of acting as the initiator for further reaction, the presence of Sc^{3+} trapped the radical as Sc^{3+}-bound $O_2^{•-}$ as described by the authors. While stabilisation of the H_2O_2 solution may be important for improving the efficiency of these types of fuel cells, another important aspect to consider is the need to regenerate or treat the electrolyte between cycles of electrochemical H_2O_2 production and fuel cell operation. Given that the $O_2^{•-}$ radical is bound to the Sc^{3+}

ions the electrolyte may need to be regenerated or begin to lose effectiveness after several cycles of operation.

Prussian blue, another cyano-complex, has been used as a cathode catalyst[94] to produce reasonably high OCPs in acidic, one-compartment H_2O_2 fuel cells with a maximum power density of 1.55mWcm⁻².

Conclusions

H_2O_2 is a viable alternative to other 'green' fuels as it can be produced electrochemically from renewable feedstock such as O_2 or water. Given its importance as an oxidant in industrial applications the benefits of electrochemically producing H_2O_2 *via* renewable energy sources is two-fold. Compared to H_2 gas, it has a reasonably similar energy density per volume and can be stored without pressurisation or expensive and heavy solid state storage materials. Due to its unique properties as both an oxidant and reductant the H_2O_2 peroxide fuel cell is flexible in its design as either a two-compartment device with a membrane or a one-compartment device with only one electrolyte. Further work remains to bring these types of fuel cells to practical applications including improving the maximum power density and investigating the long term cyclabililty of a complete H_2O_2 fuel production and utilisation system. This can be done through investigating new catalysts that reduce the overpotential needed for both H_2O_2 oxidation and reduction and also have good stability in high concentrations of H_2O_2. Given that H_2O_2 can be produced electrochemically by both O_2 reduction and water oxidation an extremely efficient H_2O_2 generation system may be designed that produces both the fuel and oxidant simultaneously with no loss of energy to unneeded reactions. This, in combination with the H_2O_2 fuel cell, allows for a completely reversible fuel cell in which the electrogenerated H_2O_2 can be stored and transported to be utilised in a fuel cell later on. To make this practical both the electrolyte and catalysts must be stable for long-term cyclability. The concentration

of electrogenerated H_2O_2 must also be increased either during production or by post-processing through fractional distillation for example.

1. S. Shafiee and E. Topal, *Energy Policy*, 2009, **37**, 181-189.
2. A. E. Sanli and A. Aytaç, *International Journal of Hydrogen Energy*, 2011, **36**, 869-875.
3. T. Zielinski, J. Marcin Węsławski and K. Kuliński, *Impact of climate changes on marine environments*, Springer, New York, 2015.
4. N. V. Patel, *Foreign Policy*, 2015, 28-29.
5. J. Tollefson, *Nature*, 2010, **464**, 1262+.
6. B. G. Ram and K. K. Pant, in *Hydrogen Fuel*, CRC Press, 2008, pp. 2-32.
7. A. Szyszka, *International Journal of Hydrogen Energy*, 1998, **23**, 849-860.
8. S. Sharma and S. K. Ghoshal, *Renewable and Sustainable Energy Reviews*, 2015, **43**, 1151-1158.
9. R. Ortiz Cebolla, B. Acosta, P. Moretto, N. Frischauf, F. Harskamp, C. Bonato and D. Baraldi, *International Journal of Hydrogen Energy*, 2014, **39**, 6261-6267.
10. M. Royle and D. Willoughby, *Process Safety and Environmental Protection*, 2011, **89**, 452-462.
11. L. Ma, D. J. Mihalcik and W. Lin, *Journal of the American Chemical Society*, 2009, **131**, 4610-4612.
12. I. A. Ibarra, S. Yang, X. Lin, A. J. Blake, P. J. Rizkallah, H. Nowell, D. R. Allan, N. R. Champness, P. Hubberstey and M. Schroder, *Chemical Communications*, 2011, **47**, 8304-8306.
13. Y. Yan, S. Yang, A. J. Blake and M. Schröder, *Accounts of Chemical Research*, 2014, **47**, 296-307.
14. M. Lototskyy and V. A. Yartys, *Journal of Alloys and Compounds*, 2015, **645, Supplement 1**, S365-S373.
15. F. Schuth, B. Bogdanovic and M. Felderhoff, *Chemical Communications*, 2004, 2249-2258.
16. C. M. Rangel, V. R. Fernandes, Y. Slavkov and L. Bozukov, *International Journal of Hydrogen Energy*, 2009, **34**, 4587-4591.
17. I. P. Jain, *International Journal of Hydrogen Energy*, 2009, **34**, 7368-7378.
18. S. Niaz, T. Manzoor and A. H. Pandith, *Renewable and Sustainable Energy Reviews*, 2015, **50**, 457-469.
19. U. Suess Hans, *Pulp Bleaching Today*, 2010.
20. K. Sato and R. Noyori, *Science*, 1998, **281**, 1646+.
21. A. Aleboyeh, H. Aleboyeh and Y. Moussa, *Dyes and Pigments*, 2003, **57**, 67-75.
22. P. Blach, Z. Böstrom, S. Franceschi-Messant, A. Lattes, E. Perez and I. Rico-Lattes, *Tetrahedron*, 2010, **66**, 7124-7128.
23. H. Egami, T. Oguma and T. Katsuki, *Journal of the American Chemical Society*, 2010, **132**, 5886-5895.
24. L. Cui, S. Furuhashi, Y. Tachikawa, N. Tada, T. Miura and A. Itoh, *Tetrahedron Letters*, 2013, **54**, 162-165.
25. N. A. Choudhury, R. K. Raman, S. Sampath and A. K. Shukla, *Journal of Power Sources*, 2005, **143**, 1-8.
26. S. J. Lao, H. Y. Qin, L. Q. Ye, B. H. Liu and Z. P. Li, *Journal of Power Sources*, 2010, **195**, 4135-4138.
27. G. Agladze, P. Nikoleishvili, V. Kveselava, G. Tsurtsumia, G. Gorelishvili, D. Gogoli and I. Kakhniashvili, *Journal of Power Sources*, 2012, **218**, 46-51.
28. D. M. F. Santos, P. G. Saturnino, R. F. M. Lobo and C. A. C. Sequeira, *Journal of Power Sources*, 2012, **208**, 131-137.
29. M. A. Ak, A. Ulas, B. Sümer, B. Yazıcı, C. Yıldırım, L. O. Gönc and F. E. Orhan, *Fuel*, 2011, **90**, 395-398.
30. R. S. Disselkamp, *International Journal of Hydrogen Energy*, 2010, **35**, 1049-1053.
31. S. Haji, B. Benstaali and N. Al-Bastaki, *Chemical Engineering Journal*, 2011, **168**, 134-139.
32. V. M. Daskalaki, E. S. Timotheatou, A. Katsaounis and D. Kalderis, *Desalination*, 2011, **274**, 200-205.
33. S. Yang, P. Wang, X. Yang, L. Shan, W. Zhang, X. Shao and R. Niu, *Journal of Hazardous Materials*, 2010, **179**, 552-558.
34. D. Sloboda-Rozner, P. L. Alsters and R. Neumann, *Journal of the American Chemical Society*, 2003, **125**, 5280-5281.
35. K.-P. Ho, K.-Y. Wong and T. H. Chan, *Tetrahedron*, 2006, **62**, 6650-6658.
36. Y. Xu, N. R. B. J. Khaw and Z. Li, *Green Chemistry*, 2009, **11**, 2047-2051.
37. P. Jin, Z. Zhao, Z. Dai, D. Wei, M. Tang and X. Wang, *Catalysis Today*, 2011, **175**, 619-624.

38.   J. Kim, S. Jung, S. Park and S. Park, *Tetrahedron Letters*, 2011, **52**, 2866-2868.
39.   F. Nikbakht and A. Heydari, *Tetrahedron Letters*, 2014, **55**, 2513-2516.
40.   Q. Chen, *Journal of Cleaner Production*, 2006, **14**, 708-712.
41.   M. Giomo, A. Buso, P. Fier, G. Sandonà, B. Boye and G. Farnia, *Electrochimica Acta*, 2008, **54**, 808-815.
42.   G. Fioroni, F. Fringuelli, F. Pizzo and L. Vaccaro, *Green Chemistry*, 2003, **5**, 425-428.
43.   G. B. Payne, *Journal of the American Chemical Society*, 1959, **81**, 4901-4904.
44.   I. Oller, S. Malato and J. A. Sánchez-Pérez, *Science of The Total Environment*, 2011, **409**, 4141-4166.
45.   I. Yamanaka, T. Onisawa, T. Hashimoto and T. Murayama, *ChemSusChem*, 2011, **4**, 494-501.
46.   M. A. Ghanem, A. M. Al-Mayouf, M. N. Shaddad and F. Marken, *Electrochimica Acta*, 2015, **174**, 557-562.
47.   A. von Weber, E. T. Baxter, H. S. White and S. L. Anderson, *The Journal of Physical Chemistry C*, 2015, **119**, 11160-11170.
48.   M. Gara, E. Laborda, P. Holdway, A. Crossley, C. J. V. Jones and R. G. Compton, *Physical Chemistry Chemical Physics*, 2013, **15**, 19487-19495.
49.   A. Ohma, K. Fushinobu and K. Okazaki, *Electrochimica Acta*, 2010, **55**, 8829-8838.
50.   M. Gennari, D. Brazzolotto, J. Pécaut, M. V. Cherrier, C. J. Pollock, S. DeBeer, M. Retegan, D. A. Pantazis, F. Neese, M. Rouzières, R. Clérac and C. Duboc, *Journal of the American Chemical Society*, 2015, **137**, 8644-8653.
51.   W. R. P. Barros, Q. Wei, G. Zhang, S. Sun, M. R. V. Lanza and A. C. Tavares, *Electrochimica Acta*, 2015, **162**, 263-270.
52.   J. S. Jirkovský, I. Panas, E. Ahlberg, M. Halasa, S. Romani and D. J. Schiffrin, *Journal of the American Chemical Society*, 2011, **133**, 19432-19441.
53.   S. Siahrostami, A. Verdaguer-Casadevall, M. Karamad, D. Deiana, P. Malacrida, B. Wickman, M. Escudero-Escribano, E. A. Paoli, R. Frydendal, T. W. Hansen, I. Chorkendorff, I. E. L. Stephens and J. Rossmeisl, *Nature Materials*, 2013, **12**, 1137-1143.
54.   S. Kakuda, R. L. Peterson, K. Ohkubo, K. D. Karlin and S. Fukuzumi, *Journal of the American Chemical Society*, 2013, **135**, 6513-6522.
55.   M. Campos, W. Siriwatcharapiboon, R. J. Potter and S. L. Horswell, *Catalysis Today*, 2013, **202**, 135-143.
56.   I. Yamanaka, R. Ichihashi, T. Iwasaki, N. Nishimura, T. Murayama, W. Ueda and S. Takenaka, *Electrochimica Acta*, 2013, **108**, 321-329.
57.   K. Mase, K. Ohkubo and S. Fukuzumi, *Journal of the American Chemical Society*, 2013, **135**, 2800-2808.
58.   G. Göransson and E. Ahlberg, *Electrochimica Acta*, 2014, **146**, 638-645.
59.   C. Di Bari, S. Shleev, A. L. De Lacey and M. Pita, *Bioelectrochemistry*, 2016, **107**, 30-36.
60.   A. Bonakdarpour, M. Lefevre, R. Yang, F. Jaouen, T. Dahn, J.-P. Dodelet and J. R. Dahn, *Electrochemical and Solid-State Letters*, 2008, **11**, B105-B108.
61.   V. G. Khomenko, K. V. Lykhnytskyi and V. Z. Barsukov, *Electrochimica Acta*, 2013, **104**, 391-399.
62.   T.-P. Fellinger, F. Hasché, P. Strasser and M. Antonietti, *Journal of the American Chemical Society*, 2012, **134**, 4072-4075.
63.   T. Murayama and I. Yamanaka, *The Journal of Physical Chemistry C*, 2011, **115**, 5792-5799.
64.   I. Yamanaka and T. Murayama, *Angewandte Chemie International Edition*, 2008, **47**, 1900-1902.
65.   Y. Liu, X. Quan, X. Fan, H. Wang and S. Chen, *Angewandte Chemie International Edition*, 2015, **54**, 6837-6841.
66.   B. B. Blizanac, P. N. Ross and N. M. Markovic, *Electrochimica Acta*, 2007, **52**, 2264-2271.
67.   Y. Shiraishi, S. Kanazawa, Y. Kofuji, H. Sakamoto, S. Ichikawa, S. Tanaka and T. Hirai, *Angewandte Chemie International Edition*, 2014, **53**, 13454-13459.
68.   C. Kormann, D. W. Bahnemann and M. R. Hoffmann, *Environmental Science & Technology*, 1988, **22**, 798-806.
69.   N. Her, J.-S. Park and Y. Yoon, *Chemical Engineering Journal*, 2011, **166**, 184-190.
70.   A. Izgorodin, E. Izgorodin, D. R. MacFarlane, *Energy & Enviroonmental Science*, 2012, **5**, 9496-9501.

71. C. McDonnell-Worth and D. R. MacFarlane, *RSC Advances*, 2014, **4**, 30551-30557.
72. Y. Ando and T. Tanaka, *International Journal of Hydrogen Energy*, 2004, **29**, 1349-1354.
73. N. Luo, G. H. Miley, K.-J. Kim, R. Burton and X. Huang, *Journal of Power Sources*, 2008, **185**, 685-690.
74. R. R. Bessette, J. M. Cichon, D. W. Dischert and E. G. Dow, *Journal of Power Sources*, 1999, **80**, 248-253.
75. X. Li, D. Heryadi and A. A. Gewirth, *Langmuir*, 2005, **21**, 9251-9259.
76. I. Katsounaros, W. B. Schneider, J. C. Meier, U. Benedikt, P. U. Biedermann, A. A. Auer and K. J. J. Mayrhofer, *Physical Chemistry Chemical Physics*, 2012, **14**, 7384-7391.
77. R. J. Bowen, H. B. Urbach and J. H. Harrison, *Nature*, 1967, **213**, 592-593.
78. X. Jing, D. Cao, Y. Liu, G. Wang, J. Yin, Q. Wen and Y. Gao, *Journal of Electroanalytical Chemistry*, 2011, **658**, 46-51.
79. L. Shi, X. Niu, T. Liu, H. Zhao and M. Lan, *Microchim Acta*, 2015, **182**, 2485-2493.
80. Z. Yin, J. Wu and Z. Yang, *Biosensors and Bioelectronics*, 2011, **26**, 1970-1974.
81. C. Debiemme-Chouvy, *Biosensors and Bioelectronics*, 2010, **25**, 2454-2457.
82. G. Wang, Y. Bao, Y. Tian, J. Xia and D. Cao, *Journal of Power Sources*, 2010, **195**, 6463-6467.
83. T. Poux, A. Bonnefont, A. Ryabova, G. Kerangueven, G. A. Tsirlina and E. R. Savinova, *Physical Chemistry Chemical Physics*, 2014, **16**, 13595-13600.
84. D. Cao, J. Chao, L. Sun and G. Wang, *Journal of Power Sources*, 2008, **179**, 87-91.
85. Z. Li, Y. He, X. Ke, L. Gan, J. Zhao, G. Cui and G. Wu, *Journal of Power Sources*, 2015, **294**, 136-140.
86. R. Araminaitė, R. Garjonytė and A. Malinauskas, *Journal of Solid State Electrochemistry*, 2010, **14**, 149-155.
87. F. Yang, K. Cheng, X. Liu, S. Chang, J. Yin, C. Du, L. Du, G. Wang and D. Cao, *Journal of Power Sources*, 2012, **217**, 569-573.
88. S. Hasegawa, K. Shimotani, K. Kishi and H. Watanabe *Electrochemical and Solid-State Letters*, 2005, **8**, A119-A121.
89. S.-i. Yamazaki, Z. Siroma, H. Senoh, T. Ioroi, N. Fujiwara and K. Yasuda, *Journal of Power Sources*, 2008, **178**, 20-25.
90. Y. Yamada, Y. Fukunishi, S.-i. Yamazaki and S. Fukuzumi, *Chemical Communications*, 2010, **46**, 7334-7336.
91. Y. Yamada, S. Yoshida, T. Honda and S. Fukuzumi, *Energy & Environmental Science*, 2011, **4**, 2822-2825.
92. Y. Yamada, M. Yoneda and S. Fukuzumi, *Chemistry – A European Journal*, 2013, **19**, 11733-11741.
93. Y. Yamada, M. Yoneda and S. Fukuzumi, *Inorg. Chem.*, 2014, **53**, 1272-1274.
94. S. A. Mousavi Shaegh, N.-T. Nguyen, S. M. Mousavi Ehteshami and S. H. Chan, *Energy & Environmental Science*, 2012, **5**, 8225-8228.

Chapter 2

Ion Effects in Water Oxidation to Hydrogen Peroxide

2.1 Specific Declaration for Chapter 2.3 & 2.4

Monash University

Declaration for Thesis Chapter 2.3 & 2.4

Declaration by candidate

In the case of Chapter 2.3 & 2.4, the nature and extent of my contribution to the work was the following:

Nature of contribution	Extent of contribution (%)
Experimental design, data collection and interpretation, manuscript writing and preparation	85%

The following co-authors contributed to the work. If co-authors are students at Monash University, the extent of their contribution in percentage terms must be stated:

Name	Nature of contribution	Extent of contribution (%) for student co-authors only
Douglas R. MacFarlane	Initiation, key ideas, manuscript editing and preparation	10
Alexey Izgorodin	Initiation, key ideas	5

The undersigned hereby certify that the above declaration correctly reflects the nature and extent of the candidate's and co-authors' contributions to this work*.

Candidate's Signature	███████████	Date 25/02/2016

Main Supervisor's Signature	███████████	Date 25/02/2016

*Note: Where the responsible author is not the candidate's main supervisor, the main supervisor should consult with the responsible author to agree on the respective contributions of the authors.

2.2 General Overview

The following chapter is a paper titled "Ion Effects in Water Oxidation to Hydrogen Peroxide" published in RSC Advances in 2014. In this Chapter the production of H_2O_2 *via* electrochemical water oxidation in various electrolytes was studied. Chronoamperometric methods were employed to observe the relationship between applied electrochemical potential, H_2O_2 production and faradaic efficiency for electrolytes containing different ammonium-based salts at varying pHs. It was hypothesised that changes to the cation and anion of the electrolyte would affect the amount of H_2O_2 produced as this would alter the hydrogen bonding environment which is thought to be integral to the water oxidation to H_2O_2 process[1]. Changing the pH by increasing the amount of free amine in these alkaline electrolytes was also expected to have a dramatic impact on the performance of these cells for the same reason.

Comparisons were made between 1M, pH 10 solutions of butylammonium sulfate, butylammonium methanesulfonate, diethylammonium sulfate and butylammonium ethanesulfonate and while all were found to produce H_2O_2, butylammonium sulfate produced the most and produced it with the highest faradaic efficiency for a certain range of applied potentials. H_2O_2 production generally began at 600mV vs Ag/AgCl and reached a maximum rate of production at 800mV vs Ag/AgCl. As the potential was increased the faradaic efficiency of H_2O_2 production tended to decrease which coincided with the beginning of the oxygen evolution reaction (OER), a competing four electron water oxidation process.Significant H_2O_2 production was found to only occur above pH9.5 and plateaued above pH 10.5. This pH range coincides with the buffer region of butylamine suggesting that the action of the amine in absorbing protons produced by the water oxidation reaction may be aiding the process by keeping the electrolyte at the surface of the catalyst at a stable pH.

The production of H_2O_2 over long term chronoamperometry was also investigated using both a counter electrode separated from the working electrode with a glass frit and one that was not. Over the course of two hours the amount of H_2O_2 produced increased linearly with time in the fritted cell but reached a maximum after one hour in the other indicating that H_2O_2 was migrating to the counter electrode and being reduced.

A possible mechanism for H_2O_2 production *via* water oxidation was discussed that attempted to explain the low oxidation potentials observed in this system. It has been suggested that during one of the intermediate electrochemical steps required for the oxygen evolution reaction -OH is adsorbed on a catalytically active site on the electrode[2]. Hydrogen bonding to the free amine near the surface of the catalyst may lower the energy required to break this bond with the catalyst and allow the formation of H_2O_2 following the reaction below:

$$\Sigma - OH + OH^- \rightarrow \Sigma + H_2O_2 + e^-$$
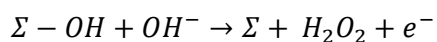
1. A. Izgorodin, E. Izgorodin, D. R. MacFarlane, *Energy & Enviroonmental Science*, 2012, **5**, 9496-9501.
2. H. Dau, C. Limberg, T. Reier, M. Risch, S. Roggan and P. Strasser, *ChemCatChem*, 2010, **2**, 724-761.

Chapter 2.3

Ion effects in water oxidation to hydrogen peroxide†

Ciaran McDonnell-Worth* and Douglas. R. MacFarlane

We investigate the effect of pH, potential and electrolyte ions in the electrochemical oxidation of water to produce hydrogen peroxide. This process has the potential to provide a low energy-cost route to the generation of hydrogen peroxide, either for *in situ* use as a "green" oxidant or as part of a water splitting process for the generation of oxygen and hydrogen. Electrodeposited manganese oxide films were used as the working electrode along with aqueous solutions of various ammonium-based cations as the electrolyte. Oxidation of water was carried out at potentials as low as 0.6 V *vs.* Ag/AgCl at pH 10. Hydrogen peroxide production was found to be highly sensitive to pH, only occurring above pH 9.5, in solutions where the pH had been adjusted by the addition of excess amine. Highly efficient, approaching 100% Faradaic efficiency, production of hydrogen peroxide was observed the range pH 10–10.5. Faradaic efficiency of hydrogen peroxide formation decreased at applied potentials higher than 1 V *vs.* Ag/AgCl where direct, or further, oxidation to oxygen begins to dominate. Investigation of a number of alkylammonium cations and alkyl sulphate anions of different alkyl chain length indicated that the optimum system is butylammonium sulphate at concentrations around 1 M.

Introduction

Water oxidation is a vital process, in natural systems as part of both carbon and nitrogen fixation in plants, and also in a variety of important chemical processes. Water oxidation has the potential to offer an energy efficient route to the important and well known oxidant, hydrogen peroxide, which has strong green credentials among oxidants and would be used more widely and efficiently if it could be made more readily on-site or *in situ*. Equally, water oxidation to oxygen is a key part of efforts to produce hydrogen in large scale from water splitting as an energy storage medium or fuel. Hydrogen is a promising in this regard, as it has a relatively high gravimetric energy density and it can be produced and utilised cleanly by water electrolysis and hydrogen fuel cells respectively.[1] An outstanding problem with the electrolysis of water, however, is the high energy cost of producing hydrogen gas, relative to the energy released by using it as fuel,[2] *i.e.*, the round-trip energy efficiency is <50%. This is, in part, caused by the high overpotential required in the four-electron, four proton electrochemical oxidation of water to oxygen, (eqn (1)), which is also known as the Oxygen Evolution Reaction (OER).

ARC Centre of Excellence for Electromaterials Science, School of Chemistry, Monash University, Clayton, Victoria 3800, Australia. E-mail: ciaran.mcdonnell-worth@monash.edu

† Electronic supplementary information (ESI) available: Cyclic voltammograms of low performance electrolytes and description of catalytic MnO_x films. See DOI: 10.1039/c4ra05296j

$$2H_2O = O_2 + 4H^+ + 4e^-, \quad E^0 = 1.23 \text{ V } vs. \text{ NHE} \quad (1)$$
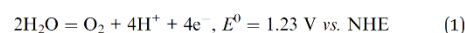
The same issue arises with concepts involving electrochemical reduction of carbon dioxide to fuels, as the only practical oxidation reaction to couple to this process in large scale is water oxidation.

The utilisation of electrocatalysts to lower this water oxidation overpotential has been widely researched in recent years and has focused on the development and understanding of a number of different catalytic materials. Some of the best known electrocatalysts are metal oxides, the most common and highest efficiency being ruthenium[3,4] and iridium oxides.[5] Such catalysts that rely on rare and expensive elements are unsuitable for large scale water oxidation, so catalysts that make use of cheaper and more abundant materials[6] such as cobalt,[7–11] manganese,[12–15] titanium,[16] iron[17] or nickel[18] oxides have been under intense investigation. The influence that chemical composition, crystal structure and nanostructure has on the efficiency of these metal oxide catalysts has also been heavily scrutinised,[16] along with the effects of mixing the metal ions in the oxide.[19–23] However, to date none of these candidates have been able to match the catalytic performance of the precious metal oxides at fundamental turnover frequency and efficiency level.

O_2 is not the only possible product of water oxidation given the complex intermediate steps involved.[26] Hydrogen peroxide formation *via* a two electron, two proton process is an alternative outcome (eqn (2)).

$$2H_2O \rightarrow HOOH + 2H^+ + 2e^-, \quad E^0 = 1.776 \text{ V } vs. \text{ NHE} \quad (2)$$

25

In fact, detailed studies of the water oxidation centre in Photo-system II, which involves a manganese–oxo cluster, have been instructive in this respect. These have deepened the understanding of the mechanisms of water oxidation, providing some insight into the details of the four, distinct oxidation and proton transfer steps.[24] Theoretical modelling shows that the formation of the first O–O bond, i.e., to form a per-oxy species via the loss of the first two electrons and two protons, is a key step in the overall process[25] and that the loss of the third electron may present the greatest energy barrier.

Similarly, Ando et al. have also suggested that a 2-electron reaction of water oxidation to H_2O_2,[27] may be possible in vitro. Since E^0 for hydrogen peroxide production is substantially higher than that for oxygen, the ideal catalyst/electrolyte combination for this process will be one that lowers the overpotential, and possibly also the $E^0(H_2O/H_2O_2)$, of eqn (2), thereby promoting the preferential formation of hydrogen peroxide over oxygen. However, in practical water oxidation research, less emphasis has been placed on the interaction between the catalysts and the electrolyte surrounding the catalytic site. Clearly proton activity and proton activity (pH) buffering are key aspects of the role of the electrolyte, both from thermodynamic and kinetic points of view. There is also a potential for specific chemical interaction aspects of the electrolyte to influence the mechanism of the reaction. In this direction, evidence was found by Izgorodin et al.[28] that suggests that direct oxidation of water to hydrogen peroxide preferentially occurs when alkylammonium cation based electrolyte solutions are used in conjunction with a manganese oxide electro-catalyst.[28] It was hypothesised that the process involved preferential solvation of the hydrogen peroxide product by the alkylammonium cation and/or its conjugate base, lowering the free energy of the solvated species and thereby lowering the potential at which it is formed. Hydrogen peroxide efficiencies as high as 77% at 0.59 V vs. Ag/AgCl were demonstrated in an electrolyte that consisted of 1 M of a butylammonium sulfate salt/base mixture at pH 10. These are relatively low potentials for a water oxidation process compared to the potentials typically required for direct water oxidation to oxygen at the same pH. It was suggested that this process could be used as a means of direct production of hydrogen peroxide for use as an oxidant. Alternatively, if combined with a subsequent decomposition to form oxygen (eqn (3)), the process appears to offer a potentially low energy-cost alternative to the traditional 4-electron oxidation oxygen evolution reaction.

$$2HOOH \rightarrow H_2O + O_2 \tag{3}$$
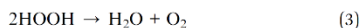
Hydrogen peroxide is used as a strong oxidant and bleaching agent and is most commonly produced using the anthroquinone auto-oxidation process, which is energy intensive and can have environmentally unfriendly byproducts.[29] Small scale H_2O_2 production is an active area of research[30–39] as it could eliminate the need for expensive handling and transportation of H_2O_2 from the relatively small number of production facilities world-wide. It also opens up possibilities for electro-generated H_2O_2 to be generated in situ for important chemical processes[40]

or even as an alternative standalone fuel in a hydrogen peroxide fuel cell.[41–44]

Based on the original hypothesis of Izgorodin et al.[28] that solvated hydrogen peroxide complexes were responsible for their observation of preferential formation of H_2O_2 we investigate in the present work the role of the electrolyte cations and anions involved. The organic salts examined include a number that originate from the protic ionic liquid family of salts, being those that in their pure state have melting points below 100 °C; in the present work this ionic liquid nature serves to increase solubility in the 1 M aqueous solutions that are used. We also investigate the proton activity dependence of the amount and efficiency of H_2O_2 produced in these electrolytes, with the ultimate goal of further optimising the features of this process.

Experimental

Catalytic film deposition

Manganese oxide catalyst films were electrodeposited using the method described by Zhou et al.[45] Films were electrodeposited on gold in a 2 mL solution of 1 M ethylammonium nitrate and 10 mM manganese acetate. The electrodeposition was conducted at room temperature using chronopotentiometry at a constant current density of 200 µA cm^{-2} over 10 minutes. The films were then heat-treated at 90 °C for 30 minutes by placing the electrode on a hotplate. Manganese acetate tetrahydrate 99.99% was purchased from Sigma-Aldrich. 70% nitric acid was purchased from Univar.

Electrolyte preparation

Electrolyte solutions were made by dissolving a sufficient amount of the relevant acid in each case to achieve 1 M acid in water. The required amine was added to adjust the pH using a TPS smartCHEM-pH meter to the desired value in the range between 9 and 11. This is considerably beyond the simple 1 : 1 salt mole ratios in each case and in fact is approximately the buffer region of the base in each case. This approach to the electrolyte preparation, using the glass electrode based pH measurement ensures that constant proton activity is obtained across all of the systems.

The amines used were 99.5% butylamine and diethylamine and 99% hexylamine purchased from Sigma-Aldrich. The acids used were 98.08% sulphuric acid purchased from Unilever, 99.5% methanesulfonic acid and 99% ethanesulfonic acid and toluenesulfonic acid monohydrate purchased from Sigma-Aldrich.

Electrochemistry

All electrochemical measurements were carried out using a multi-channel potentiostat (VMP2, Princeton Applied Research). Electrochemical cells consisted of the MnO_x film as the working electrode, a Ag/AgCl reference electrode and a titanium mesh counter electrode. When measuring cyclic voltammograms of the different electrolytes with various ions and pHs, 0.5 mL of the electrolyte and a scan rate of 1 mV s^{-1} was used. Conductivity was determined by potentio-electrochemical

26

impedance spectroscopy (PEIS). The solution resistance of the electrolytes between two flat gold electrodes 1 cm apart was used to calculate the conductivity.

The measurements of H_2O_2 production were carried out using potentiostatic coulometry where a constant potential was applied to the cell and the current was measured over a known time. In these measurements a fritted compartment was used to contain the counter-electrode in order that back reduction of the H_2O_2 could not take place at the cathode. The total charge that passed through the cell was then calculated using the VMP software by integrating the area under the current *vs.* time curve. The electrolyte was then transferred to a separate vessel for chemical determination of the H_2O_2 content. The number of moles of H_2O_2 in solution was determined using a standard titration of the electrolyte using $KMnO_4$ according to the reaction:

$$2MnO_4^- + 5H_2O_2 + 6H^+ \rightarrow 2Mn^{2+} + 5O_2 + 8H_2O \qquad (4)$$
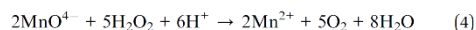
For this titration 250 µL of 1 M sulphuric acid was added to 250 µL of the electrolyte. A 7.55×10^{-3} M potassium permanganate solution was used as the titrant and added to the analyte in volumes of 10 µL. Additions were separated by 20 minutes to allow the absorption reading to stabilise. A UV-Vis spectrometer measured absorption at 565 nm wavelength. The Faradaic efficiency of H_2O_2 production was then determined using the total charge passed through the cell during the experiment. An efficiency <100% in this respect reflected the competing production of oxygen in the oxidation reaction. Errors in calculations were estimated from repetitions ($n = 4$–5) in selected cases using the same film. A single film was used to carry out each series of experiments (*i.e.* a different film for each electrolyte, one film used for all of the comparisons of pH and one film used for time measurements). This was done to maintain consistency within the experiments and allow for any degradation of the films with use. The potassium permanganate was purchased from Sigma-Aldrich and the concentration of the $KMnO_4$ solution was determined by titration with sodium oxalate. The total amount of H_2O_2 produced was divided by the total amount of Mn in the film to determine the turn over number of an experiment and this number was then divided by the length time of applied potential to determine the turn over frequency. The total amount of Mn in the film was estimated by calculating the charge used in the deposition and equivocating each mole of Mn deposited to 2 moles of electrons. This represents an upper bound on the amount of Mn in the film as some charge is lost during deposition to other processes.

Results

The cyclic voltammograms in Fig. 1 show an oxidation peak beginning at around 0.6 V *vs.* Ag/AgCl at pH > 10, before the main water oxidation to oxygen peak appears at 1.3 V *vs.* Ag/AgCl. A clear correlation is revealed in Fig. 2 between this oxidation peak at 0.6 V *vs.* Ag/AgCl and the start of H_2O_2 production in the butylammonium sulfate (BAS), electrolytes. This is consistent with the previously reported oxidation
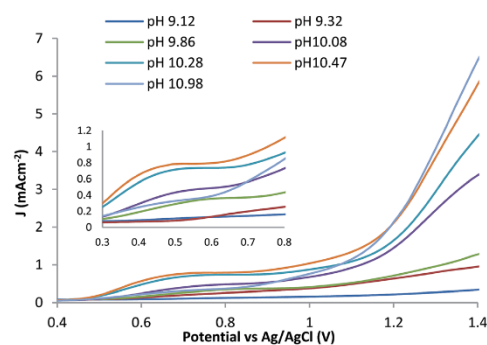

Fig. 1 Cyclic voltammograms during water oxidation in 1 M BAS electrolyte, at various pHs on a MnO_x electrode. The scan rate was 1 mV s^{-1}.

potential using this type of electrolyte.[28] This indicates that the water oxidation to hydrogen peroxide reaction starts to occur at potentials considerably lower than that for oxygen production and that the hydrogen peroxide produced is sufficiently stable in the solution for subsequent determination by the chemical means used. Fig. 1 also shows the influence that the pH of the electrolyte has on the performance of the water oxidation processes. From the cyclic voltammograms in Fig. 1, the first oxidation peaks start to appear when using electrolytes with a pH higher than ~9.5. When the pH approaches 11 this peak disappears while the second peak (*i.e.* the OER process) shows the highest current of all of these electrolytes, indicating the strong influence that pH has on the OER reaction on this electrocatalyst.

In the controlled potential electrolysis runs in Fig. 2, detectable H_2O_2 production begins around pH 9 and tends to increase as the pH is increased. (Note that Fig. 1 shows that the current is relatively constant around 0.8 V *vs.* Ag/AgCl in all cases; therefore the shift in E^0 due to pH changes in Fig. 2 is not a significant factor in determining the current). The Faradaic
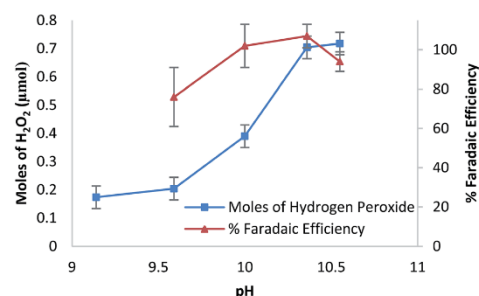

Fig. 2 H_2O_2 production at 0.8 V *vs.* Ag/AgCl during controlled potential electrolysis for 10 minutes on an MnO_x electrocatalyst in 1 M BAS electrolyte at various pH values. (0.8 V *vs.* Ag/AgCl over 10 min).

efficiency with respect to H_2O_2 production reaches 100% in the pH region between 10 and 10.4. At higher pH, Faradaic efficiency decreases as a result of further oxidation on the electrode to generate oxygen. Experiments were not conducted at even higher pH values because the addition of more amine caused the electrolyte to become too volatile to maintain a constant pH. At the lower pHs, when the electrolyte is closer to neutral, the MnO_x films are known to lose their effectiveness as catalysts.[15,28] Thus, it appears that this particular process of water oxidation to H_2O_2 occurs most readily within a specific pH range around 10–11. Referring to the pK_a data in Table 1, this corresponds approximately to the buffer region in each case, suggesting that a buffering action in absorbing the protons produced in the reaction may be a factor in the efficiency of this process. However, as was shown by Izgorodin et al.,[28] inorganic buffer solutions do not support H_2O_2 production and therefore buffering action and/or pH alone are not the origins of this mechanism.

Fig. 3(a)–(d) show cyclic voltammograms and the associated trends in H_2O_2 production and efficiency from the potentiostatic coulometry experiments, for a range of electrolytes, including butylammonium methanesulfonate (BAMeS) and butylammonium ethanesulfonate (BAEthS), as the potential applied to the cell is increased. The pH of the solution is maintained at 10 in each case and the concentration of the electrolyte is 1 M (with respect to the anion). Cyclic voltammograms of 1 M butylammonium tosylate, diethylammonium tosylate and hexylammonium sulfate electrolyte solutions (pH 10) were also measured, but were found to have relatively low currents at the expected potentials for water oxidation (see ESI Fig. A†). A hexylammonium tosylate electrolyte was also tested but upon addition of the amine to acid a solid formed that was insoluble in water.

In the BAS and BAMeS systems the amount of H_2O_2 produced seems to plateau around 1 V vs. Ag/AgCl before increasing again at higher potentials when the second oxidation process occurs. This tends to follow the current density in the cyclic voltammograms such that a higher current in this region means more H_2O_2 generated. In the BAEthS system there is a more significant drop in the amount of H_2O_2 as the applied potential is increased from 0.8 V to 1.0 V vs. Ag/AgCl. The cell using the 1 M BAS electrolyte shows twice the amount of H_2O_2 produced at all potentials, as compared to the BAMeS and DEAS cells.

Fig. 3d shows the production and efficiency of the cell when the secondary amine based electrolyte, DEAS, is used. In this case the cyclic voltammogram shows two oxidation peaks that occur at higher potentials than the other cells, at 0.7 and 1.0 V vs. Ag/AgCl respectively, before the main water oxidation to oxygen (OER) peak at 1.3 V vs. Ag/AgCl. This additional process may be the appearance of the amine oxidation process to the N-oxide which occurs more readily in secondary and tertiary amines than in primary amines. It has been demonstrated previously that the butylammonium sulphate systems are not oxidised under these conditions.[28]

Also shown in Fig. 3 in each case is the apparent Faradaic efficiency calculated as described in the experimental section (the uncertainty in the efficiency measurement at the lower applied potentials, 0.7 V and below, makes further analysis difficult in these cases). In the BAS electrolyte, the H_2O_2 production efficiency reaches 100% within error around 1.0 V vs. Ag/AgCl, while in the other electrolytes the efficiency is lower. The BAS result achieved here is somewhat higher than previously reported by Izgorodin et al.,[28] due to the different potential range studied in that work; it appears from the present work that potentials around 0.9–1.0 V vs. Ag/AgCl are optimum for efficient H_2O_2 production.

Generally the efficiency of hydrogen peroxide production drops as the potential rises above 1.2 V vs. Ag/AgCl. This is as expected due to the consumption of current by the competing OER that begins to occur at these higher potentials. It is also possible that the further 2 electron oxidation of the H_2O_2 begins to occur at these potentials.

Table 1 compares the data from Fig. 3 at 0.8 V vs. Ag/AgCl showing the current density, the quantity of H_2O_2 produced and the Faradaic efficiency at this potential for each electrolyte. It can be seen that BAS and BAEthS have the highest Faradaic efficiency. It also appears, comparing the butylammonium and diethylammonium cations, that the former produces a significantly larger amount of H_2O_2. The variation in efficiency across the salts in Fig. 3 indicates an involvement of the cation and/or anion in promoting the high efficiency H_2O_2 formation route. To explore this further we list in Table 1 the conductivities of the electrolytes; it appears that, although there are significant differences between them, the conductivity of the electrolyte does not seem to have a strong influence over the amount of H_2O_2 produced. Although the BAS electrolyte has the highest conductivity and also produces the most H_2O_2 at 0.8 V vs. Ag/AgCl, the BAEthS electrolyte has a low conductivity, but produces the second highest amount of H_2O_2 at the same potential. Higher conductivity may result in higher current densities at a particular potential (as shown in the third column of Table 1). However, it is likely that other factors such as the

Table 1 H_2O_2 production data for 1 M ammonium-based electrolytes at pH 10 for

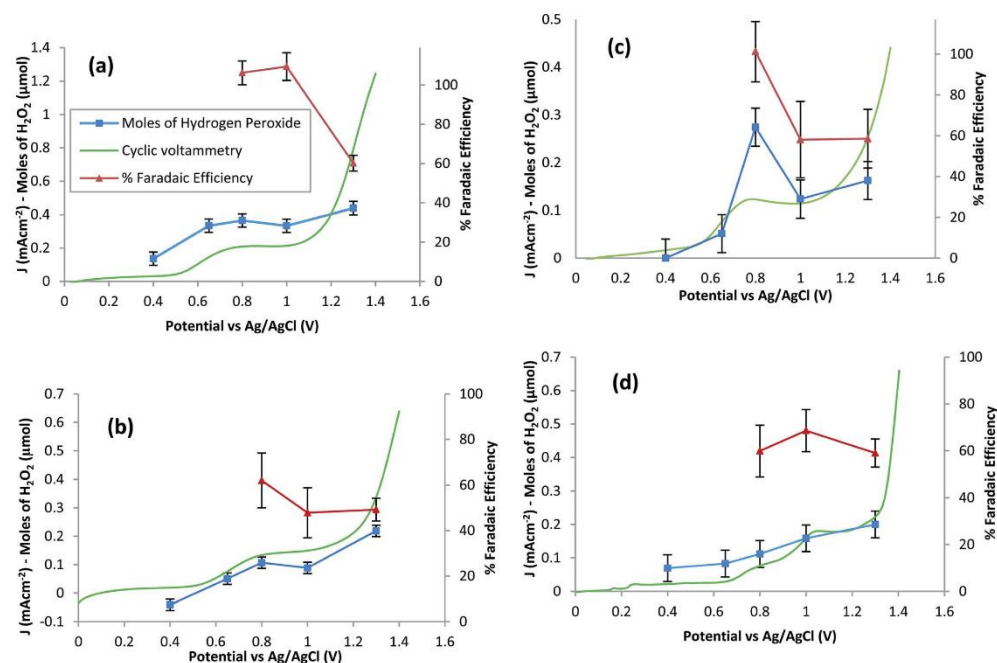| Electrolyte	Conductivity (S cm^{-1})	Current density at 0.8 V vs. Ag/AgCl (mA cm^{-2})	Moles H_2O_2 produced (10 min, at 0.8 V vs. Ag/AgCl) (µmol) (±0.04)	% Faradaic efficiency of H_2O_2 production (10 min, at 0.8 V vs. Ag/AgCl) (±6%)	pK_a (base)
BAS	0.11	0.2	0.37	106	10.77
BAMeS	0.06	0.13	0.11	62	10.77
BAEthS	0.04	0.12	0.27	101	10.77
DEAS	0.04	0.07	0.11	60	11.2

28

Fig. 3 (a–d): H_2O_2 production during 10 minutes constant potential electrolysis in (a) BAS, (b) BAMeS, (c) BAEthS and (d) DEAS electrolytes at 1 M pH 10 in each case. The scan rate for the cyclic voltammetry was 1 mV s^{-1}.

rate of H_2O_2 disproportionation in the different electrolytes have a greater influence over the detected H_2O_2.

Fig. 4 shows the change in the amount of H_2O_2 produced as the water oxidation is conducted over different lengths of time. This experiment has been carried out both with and without a separator isolating the working and counter electrodes in the cell. In the two compartment cell, an almost linear increase in the amount of H_2O_2 produced is observed over two hours.
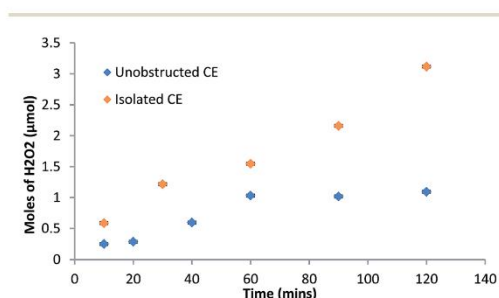
Fig. 4 Production of H_2O_2 in 1 M pH 10 BAS electrolyte when potential is applied to the cell for various lengths of time (cell volume 500 µL of 1 M electrolyte).

A clear limit of about 1 µmol is reached after one hour of applied potential in a cell without a separator, indicating reduction on the counter electrode of the H_2O_2 produced and that therefore compartment separation is important in respect of the efficiency of this process at longer electrolysis times. However, flow through type cells that might be used in an *in situ* application of this process may not require separation because of the relatively shorter residence time. While it is likely that only manganese species located on the surface of the film are catalytically active it is nonetheless instructive to calculate the turnover number (TON) and turnover frequency (TOF) on the basis of total manganese in the film. On this basis, the maximum TON observed thus far in our experiments without any serious sign of degradation is 20 over 2 hours. It is important to note that this represents a lower bound on the real number since some of the manganese is likely to be inactive. The TOF calculated on the same basis can be as high as 0.378 mol (H_2O_2) mol (Mn)$^{-1}$ min^{-1} (from experiments where pH = 10).

Discussion

The results shown above indicate that the pathway to hydrogen peroxide lowers the potential of water oxidation in this electrolyte. Energy calculations performed by Rossmeisl *et al.*[16] for a

rutile-type oxide catalyst examined the following water oxidation reaction mechanism:

$$2H_2O \xrightarrow{\Delta G_1} OH_{(ad)} + H^+ + e^- + H_2O \tag{5}$$

$$OH_{(ad)} \xrightarrow{\Delta G_2} O_{(ad)} + H^+ + e^- \tag{6}$$

$$O_{(ad)} + H_2O \xrightarrow{\Delta G_3} OOH_{(ad)} + H^+ + e^- \tag{7}$$

$$OOH_{(ad)} \xrightarrow{\Delta G_4} O_2 + H^+ + e^- \tag{8}$$
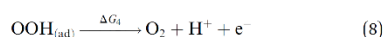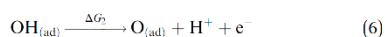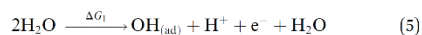
The calculations suggest that the third step, which produces the HOO˙ species, is the least thermochemically favourable step (*i.e.* highest potential required) and is thus thought to be the potential-limiting reaction. This is believed to not depend upon the type of catalytic surface. Dau *et al.*[26] described a related series of reactions that can instead lead to the formation of hydrogen peroxide in the second step in an alkaline electrolyte (where $\sum$ is a catalytically active surface site):

$$\sum + OH^- \rightarrow \sum-OH + e^- \tag{9}$$

$$\sum-OH + OH^- \rightarrow \sum + H_2O_2 + e^- \tag{10}$$
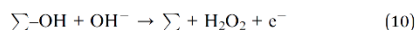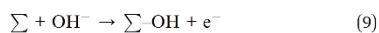
As was demonstrated in energetic calculations by Izgorodin *et al.*[28] the H_2O_2 formed in this reaction (eqn (10)) is likely to be hydrogen bonded to the free amine in the electrolyte. This may aid the breaking of the $\sum$-OH bond in this reaction scheme, leading to the net formation of solvated H_2O_2 at low potentials without further oxidation to O_2. This is also consistent with the observation of a lower H_2O_2 production rate seen when the 1 M DEAS electrolyte is used, since a secondary amine would offer more limited hydrogen bonding.

Examining the pH effect on these reactions, Takashima *et al.*[15] hypothesised that the presence of Mn^{3+} in MnO_x catalytic films is a precursor for water oxidation. Their work focused on the dramatic effect that pH has on electrochemical water oxidation on MnO_2 films, and showed that the reaction was unfavourable at pHs at which Mn^{3+} is unstable. For pH values >9, the com-proportionation of Mn^{2+} and Mn^{4+} in the film stabilises the Mn^{3+} centre on which water oxidation occurs. Thus there may be multiple origins of the pH effects seen in the present work; nonetheless the presence of the organic cation/amine appears to be strongly implicated in the mechanism involved.

Summary and conclusions

The interactions of various ammonium-based, free amine containing salt solutions with electrocatalytic MnO_x films in a water oxidation cell have been examined. A correlation between the oxidation peaks in the cyclic voltammograms of these cells and the production of H_2O_2 was shown, beginning at 0.6 V *vs.* Ag/AgCl which yields a relatively low potential of 0.2 V compared to the equilibrium potential of a standard OER. The production of H_2O_2 was found to be sensitive to the cation and anion of the

salt as well as the pH of the electrolyte. The amount of H_2O_2 produced was found to increase linearly with time when the counter electrode is isolated from the rest of the cell over a period of several hours. This creates clear potential for the H_2O_2 to be used as an *in situ* generated oxidant. Further work in this demonstrating such applications are underway and will be reported in due course.

References

1 A. Szyszka, *Int. J. Hydrogen Energy*, 1998, **23**, 849–860.
2 J. O. M. Bockris, B. Dandapani, D. Cocke and J. Ghoroghchian, *Int. J. Hydrogen Energy*, 1985, **10**, 179–201.
3 L. Wang, L. L. Duan, L. P. Tong and L. C. Sun, *J. Catal.*, 2013, **306**, 129–132.
4 Y. M. Badiei, D. E. Polyansky, J. T. Muckerman, D. J. Szalda, R. Haberdar, R. F. Zong, R. P. Thummel and E. Fujita, *Inorg. Chem.*, 2013, **52**, 8845–8850.
5 M. G. Walter, E. L. Warren, J. R. McKone, S. W. Boettcher, Q. Mi, E. A. Santori and N. S. Lewis, *Chem. Rev.*, 2010, **110**, 6446–6473.
6 A. Singh and L. Spiccia, *Coord. Chem. Rev.*, 2013, **257**, 2607–2622.
7 J. D. Blakemore, H. B. Gray, J. R. Winkler and A. M. Muller, *ACS Catal.*, 2013, **3**, 2497–2500.
8 F. Jiao and H. Frei, *Energy Environ. Sci.*, 2010, **3**, 1018–1027.
9 Y.-H. Lai, C.-Y. Lin, Y. Lv, T. C. King, A. Steiner, N. M. Muresan, L. Gan, D. S. Wright and E. Reisner, *Chem. Commun.*, 2013, **49**, 4331–4333.
10 G. Mattioli, P. Giannozzi, A. A. Bonapasta and L. Guidoni, *J. Am. Chem. Soc.*, 2013, **135**, 15353–15363.
11 D. Wang and J. T. Groves, *Proc. Natl. Acad. Sci. U. S. A.*, 2013, **110**, 15579–15584.
12 U. Maitra, B. S. Naidu, A. Govindaraj and C. N. R. Rao, *Proc. Natl. Acad. Sci. U. S. A.*, 2013, **110**, 11704–11707.
13 M. M. Najafpour, M. Kompany-Zareh, A. Zahraei, D. Jafarian Sedigh, H. Jaccard, M. Khoshkam, R. D. Britt and W. H. Casey, *Dalton Trans.*, 2013, **42**, 14603–14611.
14 H.-Y. Su, Y. Gorlin, I. C. Man, F. Calle-Vallejo, J. K. Norskov, T. F. Jaramillo and J. Rossmeisl, *Phys. Chem. Chem. Phys.*, 2012, **14**, 14010–14022.
15 T. Takashima, K. Hashimoto and R. Nakamura, *J. Am. Chem. Soc.*, 2011, **134**, 1519–1527.
16 Q.-Q. Meng, J.-G. Wang, Q. Xie, H.-Q. Dong and X.-N. Li, *Catal. Today*, 2011, **165**, 145–149.
17 A. Abbaspour and E. Mirahmadi, *Electrochim. Acta*, 2013, **105**, 92–98.
18 W. J. Zhou, X. J. Wu, X. H. Cao, X. Huang, C. L. Tan, J. Tian, H. Liu, J. Y. Wang and H. Zhang, *Energy Environ. Sci.*, 2013, **6**, 2921–2924.
19 M.-R. Gao, Y.-F. Xu, J. Jiang, Y.-R. Zheng and S.-H. Yu, *J. Am. Chem. Soc.*, 2012, **134**, 2930–2933.
20 M. Gong, Y. Li, H. Wang, Y. Liang, J. Z. Wu, J. Zhou, J. Wang, T. Regier, F. Wei and H. Dai, *J. Am. Chem. Soc.*, 2013, **135**, 8452–8455.
21 M. Busch, E. Ahlberg and I. Panas, *Catal. Today*, 2013, **202**, 114–119.

22 R. D. L. Smith, M. S. Prevot, R. D. Fagan, S. Trudel and C. P. Berlinguette, *J. Am. Chem. Soc.*, 2013, **135**, 11580–11586.

23 Y. Zhang, B. Cui, C. Zhao, H. Lin and J. Li, *Phys. Chem. Chem. Phys.*, 2013, **15**, 7363–7369.

24 M. Wiechen, H.-M. Berends and P. Kurz, *Dalton Trans.*, 2012, **41**, 21–31.

25 N. Cox, D. A. Pantazis, F. Neese and W. Lubitz, *Acc. Chem. Res.*, 2013, **46**, 1588–1596.

26 H. Dau, C. Limberg, T. Reier, M. Risch, S. Roggan and P. Strasser, *ChemCatChem*, 2010, **2**, 724–761.

27 Y. Ando and T. Tanaka, *Int. J. Hydrogen Energy*, 2004, **29**, 1349–1354.

28 A. Izgorodin, E. Izgorodin and D. R. MacFarlane, *Energy Environ. Sci.*, 2012, **5**, 9496–9501.

29 Q. Chen, *J. Cleaner Prod.*, 2006, **14**, 708–712.

30 M. Giomo, A. Buso, P. Fier, G. Sandonà, B. Boye and G. Farnia, *Electrochim. Acta*, 2008, **54**, 808–815.

31 T. Inoue, Y. Kikutani, S. Hamakawa, K. Mawatari, F. Mizukami and T. Kitamori, *Chem. Eng. J.*, 2010, **160**, 909–914.

32 L. Shengli, H. Sheng and Z. Han, *IEEE Transactions on Plasma Sciences*, 2012, **40**, 63–67.

33 S. Robl, M. Worner, D. Maier and A. M. Braun, *Photochem. Photobiol. Sci.*, 2012, **11**, 1041–1050.

34 S. Maehara, M. Taneda and K. Kusakabe, *Chem. Eng. Res. Des.*, 2008, **86**, 410–415.

35 E. Ntainjua, J. K. Edwards, A. F. Carley, J. A. Lopez-Sanchez, J. A. Moulijn, A. A. Herzing, C. J. Kiely and G. J. Hutchings, *Green Chem.*, 2008, **10**, 1162–1169.

36 T. Kinumoto, J. Nakamura, K. Kikuchi and Z. Ogumi, *Tanso*, 2010, 143–146.

37 T.-P. Fellinger, F. Hasché, P. Strasser and M. Antonietti, *J. Am. Chem. Soc.*, 2012, **134**, 4072–4075.

38 M. Campos, W. Siriwatcharapiboon, R. J. Potter and S. L. Horswell, *Catal. Today*, 2013, **202**, 135–143.

39 E. S. Bobkova, T. G. Shikova, V. I. Grinevich and V. V. Rybkin, *High Energy Chem.*, 2012, **46**, 56–59.

40 W. Li, A. Bonakdarpour, E. Gyenge and D. P. Wilkinson, *ChemSusChem*, 2013, **6**, 2137–2143.

41 S. Hasegawa, K. Shimotani, K. Kishi and H. Watanabe, *Electrochem. Solid-State Lett.*, 2005, **8**, A119–A121.

42 A. E. Sanli and A. Aytaç, *Int. J. Hydrogen Energy*, 2011, **36**, 869–875.

43 F. Yang, K. Cheng, X. Liu, S. Chang, J. Yin, C. Du, L. Du, G. Wang and D. Cao, *J. Power Sources*, 2012, **217**, 569–573.

44 S. Fukuzumi, Y. Yamada and K. D. Karlin, *Electrochim. Acta*, 2012, **82**, 493–511.

45 F. Zhou, A. Izgorodin, R. K. Hocking, V. Armel, L. Spiccia and D. R. MacFarlane, *ChemSusChem*, 2013, **6**, 643–651.

46 J. Rossmeisl, Z. W. Qu, H. Zhu, G. J. Kroes and J. K. Nørskov, *J. Electroanal. Chem.*, 2007, **607**, 83–89.

31

Ion Effects in Water Oxidation to Hydrogen Peroxide

Ciaran McDonnell-Worth[a], Douglas. R. MacFarlane[a]
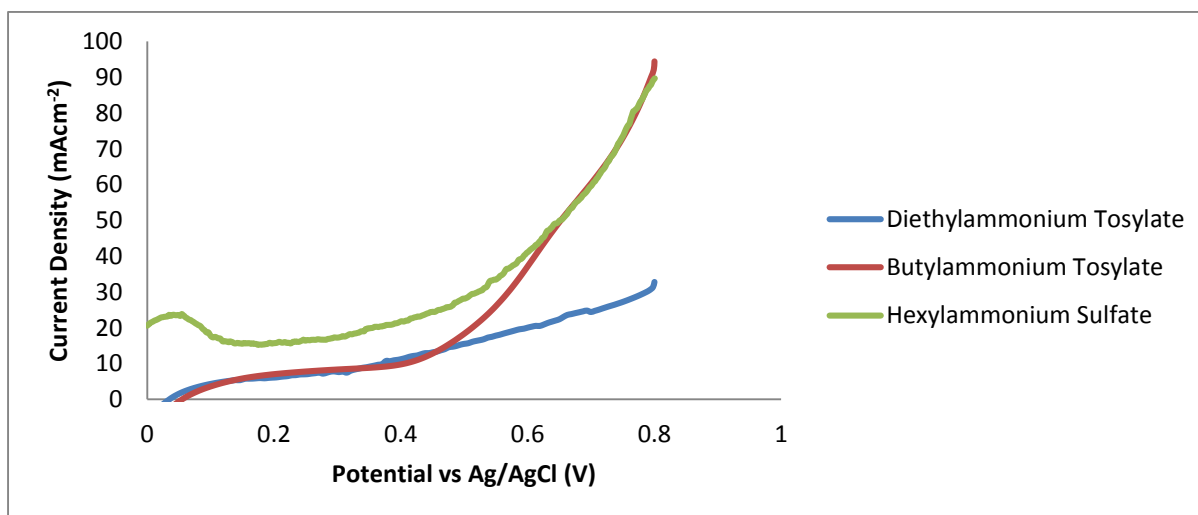
Supplementary Figure A: Cyclic voltammograms of 1M pH10 diethylammonium tosylate, butylammonium tosylate and hexylammonium sulfate electrolytes with a catalytic MnOx film. Scan rate of 1mVs⁻¹.

Supplementary section B:

This supplementary section provides information about the catalytic manganese oxide films used in the experiments. The technique for making the films and their characterisation were reported by Zhou *et al.*[1] . To summarise briefly, by examining EXAFS spectra the films were found to have a birnessite-like structure. Heat treatment of the films (as was performed in this paper) produced a small amount (3-10% of the total manganese) of reduced Mn (Mn^{II} or Mn^{II}) within the film. SEM images of the heat treated films showed a porous and fibrous structure on the surface of the film. Heat treatment was found to reduce the amount of water in the films and cause an 8% weight loss in the films when heat treated at 90°C for 30 minutes. Improvement in the catalytic activity for water oxidation to O_2 in aqueous, inorganic electrolytes over non-heat treated films was attributed to the increase in carrier density and surface mobility caused by the loss of water and hydroxyl groups on the surface of the film.

1.   F. Zhou, A. Izgorodin, R. K. Hocking, V. Armel, L. Spiccia and D. R. MacFarlane, *ChemSusChem*, 2013, **6**, 643-651.

Chapter 3

Catalysts and Electrolytes for One-Compartment, Direct H_2O_2 Fuel Cells

3.1 Specific Declaration for Chapter 3.3 & 3.4

Monash University

Declaration for Thesis Chapter 3.3 & 3.4

Declaration by candidate

In the case of Chapter 3.3 & 3.4, the nature and extent of my contribution to the work was the following:
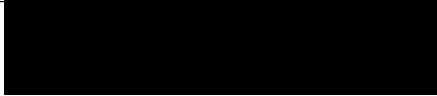
Nature of contribution	Extent of contribution (%)
Initiation, key ideas, experimental design, data collection and interpretation, manuscript writing and preparation	75%

The following co-authors contributed to the work. If co-authors are students at Monash University, the extent of their contribution in percentage terms must be stated:
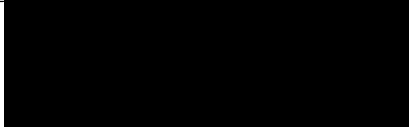
Name	Nature of contribution	Extent of contribution (%) for student co-authors only
Douglas R. MacFarlane	Initiation, key ideas, manuscript editing and preparation	10%
Fengling Zhou	Initiation, key ideas	5%
Kun Chen	Scanning electron microscopy (SEM) measurements and data analysis	10%

The undersigned hereby certify that the above declaration correctly reflects the nature and extent of the candidate's and co-authors' contributions to this work*.

Candidate's Signature		Date 25/02/2016

Main Supervisor's Signature		Date 25/02/2016

*Note: Where the responsible author is not the candidate's main supervisor, the main supervisor should consult with the responsible author to agree on the respective contributions of the authors.

3.2 General Overview

This Chapter investigates direct, one-compartment H_2O_2 fuel cells (DHPFCs) including the use of new catalysts for the oxidation and reduction of H_2O_2. Although the theoretical open circuit potential of these cells is 1.09V in practice the actual OCP will always be lower and is dependent on the catalytic ability of the anode and cathode for H_2O_2 oxidation and reduction respectively.

The selectivity of the catalysts for either H_2O_2 reduction or oxidation is integral to reducing this gap and thus reducing energy inefficiencies in DHPFCs. Given that H_2O_2 reduction and oxidation may occur simultaneously on the same electrode the loss of H_2O_2 through spontaneous and unproductive disproportionation is also a source of inefficiency in these cells. This Chapter discusses the relationship between these sources of inefficiencies and the individual open circuit potentials of each catalyst.

Cobalt oxides were investigated as the cathodic catalyst in these fuel cells as they have been proven to be good H_2O_2 reduction catalysts previously. These catalysts, combined with a novel, heat-treated Ni foam anode for H_2O_2 oxidation, showed relatively high open circuit potentials and reasonably good stability.

This research is presented in Section **3.3** in the format of a paper ready to be submitted including a Supplementary Section (**3.4**) of SEM results discussed in the paper. Section **3.5** is an Extended Supplementary that includes additional results and discussion that increase the scope of the research presented in **3.3** but were excluded to narrow the focus of the paper.

Cobalt and Nickel Oxide Catalysts for One-Compartment, Direct Hydrogen Peroxide Fuel Cells (DHPFCs) in Ammonium-based Electrolytes

Ciaran McDonnell-Worth[a], Kun Chen[a], Douglas. R. MacFarlane[a]

[a]ARC Centre of Excellence for Electromaterials Science, School of Chemistry, Monash University, Clayton, Victoria 3800, Australia. E-mail: ▮▮▮▮▮▮▮▮▮▮▮▮▮▮

We investigate the catalytic performance of cobalt and nickel oxide electrodes for the electrochemical reduction and oxidation of H_2O_2 for use in one-compartment, direct H_2O_2 fuel cells (DHPFCs). H_2O_2 fuel cells have the potential to provide a low-cost, renewable and "green" alternative to fossil fuels and are advantageous over H_2 fuel cells due to the easy storage and transportability of H_2O_2. It was found that both electrodeposited Co_2O_3 films and films made by a mixture of Co_3O_4 and carbon black provid good catalytic activity for H_2O_2 reduction. Heat treating Ni foam at 400°C for 40 minutes reduced the potential for H_2O_2 oxidation on Ni by 30mV. Fuel cells were constructed from these catalysts and tested using an aqueous, alkaline, ammonium cation based electrolytes, which have previously been used for highly efficient, electrochemical H_2O_2 production *via* water oxidation. This provides the possibility of a fully reversible fuel cell system. The maximum power achieved from these fuel cells was $25\mu Wcm^{-2}$. The general effects of the catalysts in one-compartment DHPFCs is also discussed as to how it affects both the open-circuit potential of the fuel cell and the unproductive disproportionation of H_2O_2 on the surface of the catalyst. The longer-term stability of the best performing fuel cells were also measured over the course of two hours operation.

Introduction

Clean fuels are necessary for the effective storage of energy harvested from renewable sources such as wind and solar. Hydrogen peroxide is an interesting alternative to hydrogen and methanol as a clean fuel for energy storage. Hydrogen peroxide can be both oxidised and reduced which means that within the operation of a direct hydrogen peroxide fuel cell (DHPFC) it acts as both the oxidant and the fuel[1, 2]. Much like hydrogen gas, hydrogen peroxide can be produced electrochemically[3-9] to easily make use of surplus renewable electricity supplies, but has the added advantage of being in a liquid/solution state, i.e. without the need for pressurisation or refrigeration which is an inevitable cost for H_2 fuel[10-12].

The potential that can be achieved using hydrogen peroxide is also, in principle, comparable to conventional hydrogen fuel cells. Taking the expected oxidation and reduction reactions of hydrogen peroxide:

$$H_2O_2 \rightarrow O_2 + 2H^+ + 2e^- \quad 0.68\text{V vs SHE} \qquad \text{Eq. (1)}$$

$$H_2O_2 + 2H^+ + 2e^- \rightarrow 2H_2O \ 1.77\text{V vs SHE} \qquad \text{Eq. (2)}$$
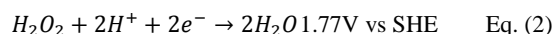
The theoretical maximum potential that these cells can produce is 1.09V, compared to 1.23V from a hydrogen – air fuel cell.

One of the major points of loss for most fuel cell designs is the membrane that is required to separate the cathode and anode. Contamination of reactant or product species from one side to the cell to the other can cause inefficiency in the cell and can also degrade the performance of the catalysts over time; the membrane needs to be highly efficient in allowing transport of only target species (usually protons and water) but no other reactive species. However, the membrane lowers efficiency by adding resistance to the cell. Thus, the unique chemistry of the DHPFC, in which H_2O_2 acts as both the oxidant and the fuel, allows for a one-compartment design[13] needing no membrane These cells operate on the principle that by immersing two different catalysts in a single electrolyte a potential difference is generated across the cell that is based on the selectivity of each catalyst towards H_2O_2 oxidation or reduction.

Yamazaki *et al.*[13] designed a one-compartment DHPFC with metal catalysts in an alkaline electrolyte (1M NaOH) and determined that silver metal was the most effective cathode material in conjunction with a gold, nickel, palladium or platinum anode. Unfortunately this

cell design is limited in that the practical open circuit potential achieved ($0.1V$[13]) was well below the theoretical value of $1.09V$. This loss was attributed to the high overpotential required to reduce H_2O_2 at the cathode; this has subsequently been improved (by approx. $50mV$) through the use of deposited Ag and Ag-Pb alloy nanoparticles as the cathode[14]. A further issue found when using metals as selective catalysts is that H_2O_2 is spontaneously decomposed at the catalytic surfaces (observable as bubble formation) at open circuit. This produces a loss of H_2O_2 without power generation and therefore loss of fuel cell efficiency. In this study we show further improvement in the OCP of DHPFCs in alkaline electrolytes through the use of selective catalytic metal oxide films, as well as low spontaneous H_2O_2 decomposition at the catalyst surface.

Metal oxides such as cobalt, manganese and iron oxides have been shown to be good catalysts for electrochemical reactions such as the oxygen evolution reaction (OER)[15-19]. Compared to metal catalysts such as platinum or palladium they can be produced cheaply and the materials are relatively abundant and in that sense are ideal for mass production. Cobalt oxides are of particular interest because they have already been used as the catalyst for H_2O_2 reduction in Al-H_2O_2 fuel cells[20] and are advantageous over previously reported Pd-Ir catalysts[21] because they are cheaper and more abundant materials.

Further improvements can also be made to the performance of these fuel cells by finding better anode materials. In particular, nickel oxides (NiO) in various forms have been applied as H_2O_2 oxidation catalysts in peroxide sensors[22, 23]. These materials also have the advantage of being non-noble metal catalysts (which have been used in previous one- and two-compartment DHPFCs[2, 13, 14]) making them cheaper to produce. Additionally, impressive results have been achieved for one-compartment DHPFCs in acidic electrolytes[24] however, H_2O_2 is not so efficiently generated at low pHs. Electrocatalytic production of H_2O_2 in acidic electrolytes is generally achieved through the 2 electron reduction of O_2. The maximum faradaic efficiency of these cells is around 70-90%[25]. This is an issue since the ideal source for H_2O_2 in these fuel cells is electrochemical production which can make use of surplus renewable energies.

In our previous work we have reported on a highly efficient water oxidation method to electrochemically produce H_2O_2 in alkaline solutions at relatively high yields using an ammonium salt based alkaline electrolyte; 100% faradaic efficiency can be achieved in these systems[26]. Additionally, it was found that the water to H_2O_2 reaction took place at low overpotentials providing an opportunity to integrate it with electrochemical $H_{2(g)}$ production[4]. Here we report on DHPFC characteristics under a variety of alkaline conditions including these ammonium salt electrolytes, towards the eventual goal of designing a fully reversible fuel cell system.

Experimental

Electrochemical

All electrochemical testing was performed using a VMP-2 (variable multichannel potentiostat) from Princeton Applied Research. Cyclic voltammograms were performed in a standard three electrode set-up with a Pt wire counter electrode and a saturated calomel reference electrode. Standard fuel cell measurements were conducted using a two electrode set up with the anode designated as the working electrode and the cathode acting as both the counter and reference electrode. The electrodes (which had defined surface areas) were immersed in 2mL of electrolyte. I-V curves were plotted by step-chronoamperometry where the potential was held constant for five seconds for each step and increased towards a cell potential of 0V starting at the open circuit potential. 1M butylammonium sulfate (BAS) was prepared by adding butylamine to 1M sulfuric acid until the pH of the solution reached the required value. 0.05M borate solutions were prepared by dissolving sodium borate in deionised water and pH was adjusted with 1M NaOH. pH was measured using TPS smartChem-pH meter. All chemicals were purchased from Sigma-Aldrich with the exception of Co_3O_4 powder which was synthesised and characterised within our group.

Catalyst Preparation

Heat-treated nickel foam was prepared by heating nickel foam in a furnace under atmospheric conditions at 400°C for 40 minutes. The Co_2O_3 catalyst was prepared by electrodeposition onto fluorine-doped tin oxide (FTO) from an aqueous solution of 0.05M cobalt acetate tetrahydrate and 0.5M sodium acetate following the method described by Yih-Wen *et al*[16]. A three-electrode cell was used for the deposition with a Pt wire counter electrode and a Ag/AgCl reference electrode. A potential of -1V was applied to the working electrode for 30 minutes and the film produced was subsequently washed with distilled water and left to dry. The Co_3O_4/C65 film was prepared by making a paste of Co_3O_4 powder, C65 conductive Carbon Black and polyvinylidene fluoride (binder) in a ratio of approximately 8:1:1 with N-methyl-2-pyrrolidone as a solvent. The paste was then spread onto aluminium foil and left to dry overnight before being heated in an oven at 100°C for one day. Before electrochemical experiments the silver plates were scoured using sandpaper and then polished with AlO_2 powder before being rinsed with distilled water. Scanning electron microscopy was conducted by Kun Chen at the Monash Centre for Electron Microscopy (MCEM).

Results and Discussion

H_2O_2 reduction and oxidation on metal and metal oxide catalysts

Cyclic voltammetry was used in order to examine the selectivity towards H_2O_2 reduction and oxidation of various metals and metal oxides. For all catalysts, cyclic voltammograms were first recorded without H_2O_2 added to the electrolyte as a control experiment and no significant oxidative or reductive currents were observed in the potential region of interest between -0.5 and 0.5V vs SCE, indicating that the catalysts and electrolytes were electrochemically stable.

Fig.1 shows cyclic voltammograms of both a nickel foam and a heat-treated nickel foam in a 0.05M borate buffer at pH 9.2 with 300mM H_2O_2 added to the electrolyte. For both catalysts there are oxidative and reductive currents observed above approximately 0.1V vs SCE and below -0.2V vs SCE respectively, which are not present without H_2O_2 addition. The oxidative current for the heat-treated Ni foam is

much larger and appears to start at lower potentials than the plain Ni foam indicating that it has better catalytic activity for H_2O_2 oxidation. H_2O_2 reduction begins at approximately -0.3mV vs SCE for both the Ni and heat-treated Ni foam. The reductive current for the untreated Ni foam is approximately twice as large as that of the heat-treated Ni. For the heat-treated foam the potential difference between the onsets of the oxidation and reduction reactions (as determined arbitrarily from the potentials where I= +/-0.25mA) was 0.82V compared to 0.63V for the untreated Ni.
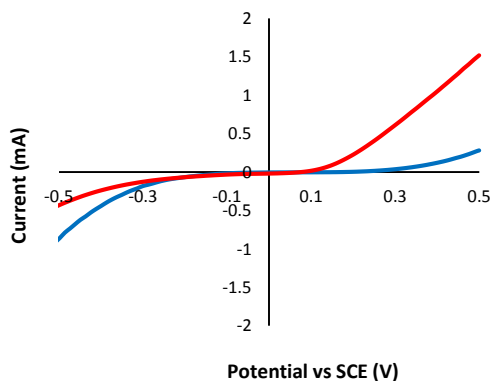
Figure 1: Cyclic voltammograms of Nickel foam (blue) and Heat-treated Nickel foam (red) in 0.05M borate buffer (pH9.2) with 300mM H_2O_2 added. Scan rate 20mVs^{-1}.

Fig. 2 shows slow scan polarisation curves obtained at 1mV/s for these two electrodes. Here the logarithm of the current is plotted against the potential. This is a common way of interpreting the corrosion activity of metals where the metal is being oxidised and some species in solution is being reduced; in this case it is presumed that H_2O_2 can being oxidised and reduced at the catalyst surface (this will be discussed on more depth later in the paper). As the current approaches 0 the logarithm of the current approaches -∞ and the intersection point derived by plotting two straight lines extrapolated from the linear ("Tafel") portions of the plot on either side gives an approximation of the open circuit potential, E_{OC}. E_{OC} is the potential at which the electrochemical process on the working electrode changes from oxidative to reductive (ie. where the net, measureable current is zero). This plot is useful as changes in the redox potentials is more easily observable with the E_{OC} value than by looking at the cyclic voltammogram of the same system. Fig. 2 shows that the oxidative process of the heat-treated Ni foam begins 30mV lower than that of the untreated electrode indicating that the activation energy of H_2O_2 oxidation on Ni foam is lowered by heat treatment. This makes it more

suitable as the anode in a single compartment, alkaline DHPFC, because the overpotential to oxidise H_2O_2 is lower at this electrode.
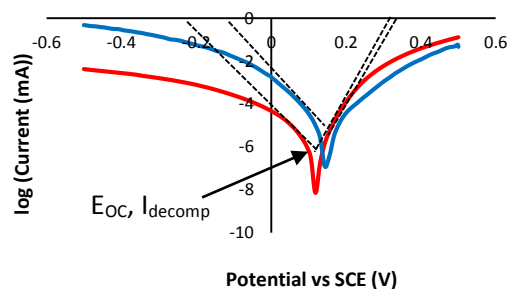
Figure 2: Polarisation curves of Ni foam (blue) and heat-treated Ni foam (red) in 0.05M borate buffer (pH 9.2). Construction shown indicates method of estimating I_{decomp}

Figure 2 also shows an estimation of the effective rate of the decomposition reaction ($2H_2O_2 = 2H_2O + O_2$) that occurs at E_{OC}, corresponding to Eqs. (1) and (2) happening simultaneously and spontaneously on the electrode. This rate is obtained as a current, I_{decomp} being a nonzero current determined from the polarisation curves at E_{OC} where the *measured* current (I_{meas}) is equal to zero and is the sum of the oxidative currents (labelled I_{ox}) and the reductive currents (I_{red}) being produced by redox processes on the surface of the electrode (Eq. (3)):

$$I_{meas} = I_{ox}(E) + I_{red}(E) = 0 \qquad \text{Eq. (3)}$$

In the context of this system the I_{decomp} value is directly proportional to the rate of oxidation *and* reduction of H_2O_2 at the point of zero current. Thus, when I_{decomp} is lower this occurs when the rate of oxidation *and* reduction of H_2O_2 at E_{OC} are lower.

The lower E_{OC} value for heated treated Ni in Fig 2 is accompanied by a drop in I_{decomp}. This indicates that less H_2O_2 is spontaneously disproportionated at the surface of the electrode in this case. This is advantageous, as it has been hypothesized that this spontaneous disproportion of H_2O_2 is one of the main challenges in improving the energy efficiency of a DHPFC catalyst[13].

Fig. 3 shows a comparison between the I-V and I-P curves of two DHPFCs, one using a Ni foam anode and one using a heat-treated Ni foam anode. Both have a Ag plate cathode and a 0.05M borate buffer solution (pH 9.2) with 300mM H_2O_2 added to it as an electrolyte. The circular points represent the I-V curve which is plotted as the measured steady state current density of the fuel cell when various potentials are applied between the two electrodes. The open circuit potential (OCP) of the cell is defined in this curve as the cell potential when the current is zero. The maximum current that can be achieved by the cell (the limiting current) is determined to be the measured current when the cell potential is biased to zero. These two values are important as, in general, a fuel cell with a higher OCP and limiting current density will have a larger maximum power density output. The power density generated by the cell is calculated by multiplying the steady state current density and the cell potential at that point and is represented by the triangles in Fig. 3. In the I-V curves in Fig. 3 the

fuel cell using the heat-treated anode has a higher OCP of 0.17V, as expected given the difference in H_2O_2 oxidation potentials of the two electrodes seen in Fig 1. The heat-treated anode shows an improvement in the limiting current density as well, which is increased by approximately $30\mu Acm^2$ with heat treatment. As expected, when we compare at the I-P curve of two fuel cells, the use of a heat-treated Ni foam almost doubles the maximum power density of the cell from $3.5\mu Wcm^{-2}$ to $6\mu Wcm^{-2}$.
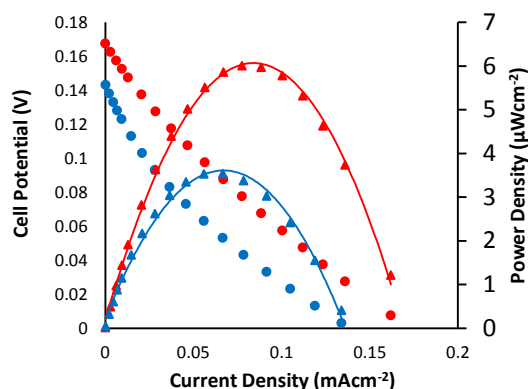
Figure 3: I-V and I-P curves of DHPFCs with a Ag plate cathode and a Ni foam (blue) or heat-treated Ni foam (red) anode with a Ag cathode in a 0.05M borate buffer (pH 9.2)/300mM H_2O_2 electrolyte

Moving to the Cobalt oxide cathode catalysts, Fig. 4 shows cyclic voltammograms of a $Co_3O_4/C65$ film and an electrodeposited Co_2O_3 film immersed in 0.05M borate buffer (pH 9.2) to which 300mM of H_2O_2 was added. For comparison the same experiment was performed using a polished silver cathode. It is clear that, as opposed to the CVs of the Ni anode catalysts in Figure 1, the cathodes investigated below do not have well defined or noticeable onset of large oxidative or reductive currents. Instead, the measured voltammograms are almost linear as the potential is swept from quite negative to positive potentials.
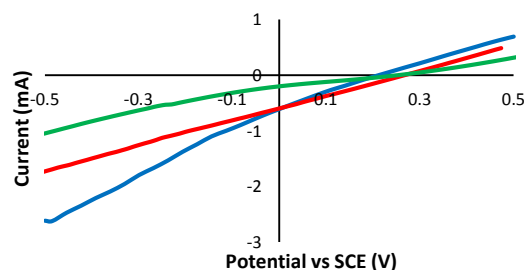
Figure 4: CVs of Ag plate (blue), $Co_3O_4/C65$ film (red) and electrodeposited Co_2O_3 film (green) in 0.05M borate buffer (pH 9.2) with a Pt wire counter electrode. Scan rate of $20mVs^{-1}$.

The polarisation curves of these cobalt and silver catalysts shown in Fig. 5 reveals the anodic and cathodic regions more clearly. Here, H_2O_2 reduction begins at more positive potentials for the cobalt

catalyst than for the polished silver electrode. As in the case of the Ni foam oxidation catalysts the E_{OC} values can be approximated from these curves (Ag plate – 200mV, Electrodeposited Co_2O_3 film – 250mV and $Co_3O_4/C65$ film – 270mV). As such it is expected that the OCP of a DHPFC with a $Co_3O_4/C65$ or electrodeposited Co_2O_3 catalyst as a cathode will be higher, compared to that of a polished silver cathode.
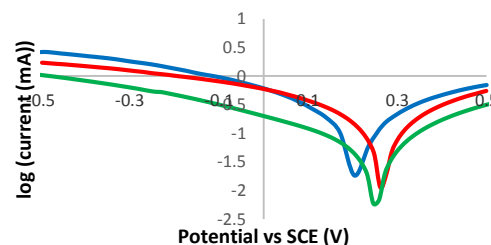
Figure 5: Polarisation curves of Ag plate (blue), $Co_3O_4/C65$ film (red) and electrodeposited Co_2O_3 film (green) in 0.05M borate buffer (pH 9.2).

For both cobalt electrodes the I_{decomp} value is also lower (significantly in the case of the electrodeposited film) which indicates that the rate of spontaneous H_2O_2 decomposition at zero current is lower for these catalysts compared to the Ag plate. This was observed qualitatively as fewer bubbles were seen to be produced on the cobalt catalysts especially on the electrodeposited Co_2O_3 film.

The improved performance of the cobalt catalysts is confirmed in Fig. 6 which shows the I-V and I-P curves for fuel cells constructed with a heat-treated Ni foam anode and different cathodes in a 0.05M borate buffer electrolyte (pH 9.2) with 300mM H_2O_2 added. Cells with two types of cobalt oxide catalysts are shown; the electrodeposited Co_2O_3 film on FTO and the film made from a slurry of powdered Co_3O_4 and carbon black powder (C65). A cell with a polished, silver metal cathode is shown for comparison.
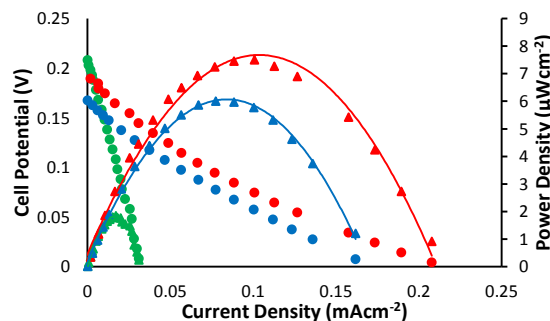
Figure 6: I-V and I-P curves of DHPFCs with a Ag plate(blue), $Co_3O_4/C65$ film (red) or electrodeposited Co_2O_3 film (green) cathode and a heat-treated Ni foam anode in a 0.05M borate buffer (pH 9.2)/300mM H2O2 electrolyte.

Both cobalt cathodes show an improvement in the OCP of the fuel cell over the silver cathode by approximately 30-50mV. The cell with the electrodeposited Co_2O_3 film has a low limiting current density compared to the others, most likely due to electrical resistance in the

FTO substrate of the film. The cell with a Co_3O_4/C65 cathode has a relatively high limiting current density of $0.21mAcm^{-2}$ and also the highest maximum power density out of the three cells ($7.5\mu Wcm^{-2}$). The high porosity of the mixed carbon and cobalt oxide film may provide a larger catalytic surface area than the silver metal and electrodeposited Co_2O_3 and therefor increase the oxidation rate of H_2O_2 when the fuel cell is in operation.

Origins of Mixed Potential

The behaviour exhibited by the cathodes shown above (and to a lesser extent the Ni foam anodes) is most likely due to each catalyst exhibiting a mixed potential at open circuit as a result of the oxidation and reduction processes occurring simultaneously (Equations 1 and 2). To illustrate this, Fig. 7 shows the two possible redox reactions that can take place on the surface of an electrode immersed in an aqueous solution of H_2O_2. The curves have been generated using a simplification of the Butler-Volmer equation[27] using the literature reversible potentials of each redox reaction under standard conditions. These equations for the H_2O_2/H_2O redox couple (Eq. (4)) and the O_2/H_2O_2 redox couple (Eq. (5)) are shown below:

$$I_{H_2O_2/H_2O} =$$
$$i_{0_{H2O2/O2}}[e^{-\alpha_{H2O/H2O2}f(E-E_{H2O2/H2O})} - e^{(1-\alpha_{H2O/H2O2})f(E-E_{H2O2/H2O})}]$$

Eq. (4)

$$I_{H_2O_2/O_2} =$$
$$i_{0_{H2O2/O2}}[e^{-\alpha_{O2/H2O2}f(E-E_{H2O2/O2})} - e^{(1-\alpha_{O2/H2O2})f(E-E_{H2O2/O2})}]$$

Eq. (5)

Where I is the total current of the redox reaction, E is the applied potential, $E_{H2O2/H2O}$ and $E_{H2O2/O2}$ are the equilibrium potentials for each redox couple, i is the exchange current, α is the charge transfer coefficient (assumed to be 0.5 in these calculations) and f is the constant term $\frac{nF}{RT}$ calculated at standard conditions. Both redox reactions may take place in this environment on the same electrode each with a different equilibrium potential. In Fig. 7 the blue curves represent the H_2O_2/H_2O redox couple and the red lines represent the

O_2/H_2O_2 redox couple. The total current (black line) is calculated as the sum of all the currents and can be written as Eq. (6):

$$I_{total} = I_{H_2O_2/H_2O} + I_{H_2O_2/O_2}$$

Eq. (6)
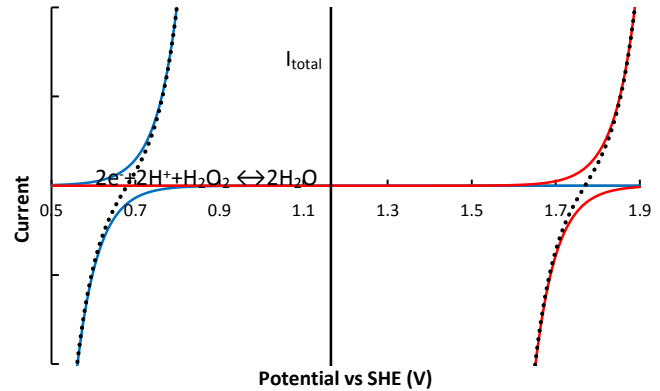
Figure 7: Schematic of the currents of H_2O_2 (red) and O_2 (blue) reduction processes that occur on an electrode in an electrolyte containing H_2O_2. Thick dashed lines indicate the H_2O_2 oxidative (blue) and reductive (red) currents while thin dotted lines indicate O_2 reductive currents (blue) and H_2O oxidative currents (red). The black line represents the sum of all currents.

The point at which the black line crosses the line of zero current represents the open circuit potential of all of the redox reactions at the electrode or the E_{OC}. In the context of a fuel cell the OCP *of the entire cell* (V_{OC}) is determined by the E_{OC} at both the anode ($E_{OC (a)}$) and the cathode ($E_{OC (c)}$) as shown in Fig. 8.
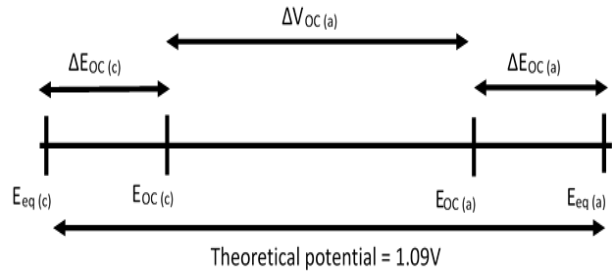

Figure 8: Effect of the overpotential on the total cell voltage of a H_2O_2 fuel cell

The E_{OC}, in turn, is determined by the catalytic selectivity of the anode and cathode for H_2O_2 oxidation and reduction.

Fig. 9 illustrates the role that the oxidative selectivity of the catalyst has on the E_{OC} of the anode as well as the disproportionation of H_2O_2 at its surface. The blue, dotted line in Fig. 9 represents the H_2O_2 oxidation current of a poor oxidation catalyst for the O_2/H_2O_2 redox couple. The solid blue line shows the oxidative current of a very good oxidation catalyst where the ΔE_{OC} for the O_2/H_2O_2 is close to zero. As expected, the total current produced by the good catalyst as a function

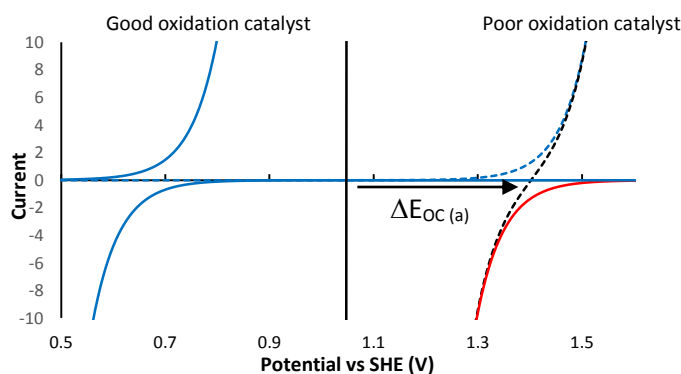of potential (calculated from Eq. (6)) begins to be oxidative at lower potentials than the poor catalyst.

Figure 9: Schematic of the effect of H_2O_2 oxidation selectivity on the mixed potential of a catalyst. The dotted blue line shows the oxidation and reduction currents of the H_2O_2/O_2 redox couple for a poor H_2O_2 oxidation catalyst. The solid blue line represents the H_2O_2/O_2 currents of a good H_2O_2 oxidation catalyst. The black lines give the total current of both the H_2O_2/H_2O and O_2/H_2O_2 redox couples for a good catalyst (solid) and a bad catalyst (dotted). ΔE_{OC} is the difference in the open circuit potential for both systems.

Additionally, in this case the good oxidation catalyst has a large oxidative current relative to the reductive current (red dotted line) at low values of $potential$. For the poor catalyst the oxidative and reductive currents are relatively equal at those low potentials resulting in the disproportionation of H_2O_2 on the catalyst surface, with little productive current contributed to the cell (as the two reactions produce a net zero charge) and causes a loss in efficiency[13]. In the case of the good oxidation catalyst the total current curve closely follows the oxidative curve meaning that largely only the desired redox reaction is taking place.

Of course, the same reasoning applies when examining a reduction catalyst where the total I value is composed of mostly reductive current.

Organic salts for single compartment reversible fuel cells

H_2O_2 may be electrochemically produced *via* a highly efficient water oxidation reaction performed in electrolytes containing certain organic salts[5, 26]. For a reversible DHPFC to be viable, efficiency and long-term stability must be high in both its operation as a fuel cell (i.e. discharging) and during electrochemical H_2O_2 production (charging). To demonstrate that the fuel cell of Fig. 10 could operate with these electrolytes, one was constructed with a $Co_3O_4/C65$ cathode, heat-treated Ni foam anode and an aqueous, 1M butylammonium sulfate (pH 9.7) solution with 300mM H_2O_2 added to it as an electrolyte. In

these alkaline electrolytes the H_2O_2 oxidation and reduction reactions (Eqs. (1) and (2)) become:

$$2OH^- + H_2O_2 \rightarrow O_2 + 2H_2O + 2e^- \quad \text{Eq. (7)}$$

$$H_2O_2 + e^- \rightarrow 2OH^- \quad \text{Eq. (8)}$$
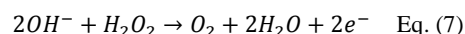
The resulting I-V and I-P curves are shown in Fig. 10 (blue) and are compared to fuel cells constructed with the same electrodes but a 0.05M borate buffer (pH 9.7) electrolyte and a mixed 0.05M borate buffer/1M NaSO4 electrolyte, both with 300mM H_2O_2 added. This was done to observe the impact that ion concentration in the electrolyte has on the overall performance of the fuel cell.
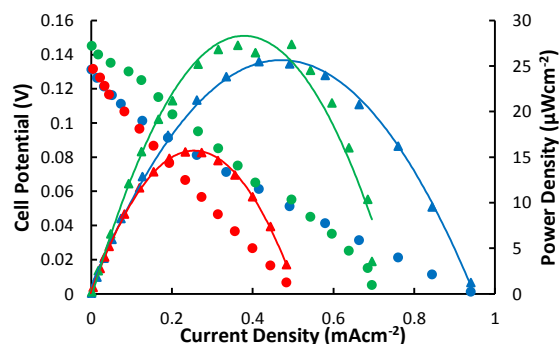

Figure 10: I-V and I-P curves of a fuel cell with a heat-treated Ni foam anode and $Co_3O_4/C65$ cathode. 1M BAS (pH 9.7)/300mM H_2O_2 electrolyte (blue), 0.05M borate buffer (pH9.7)/300mM H_2O_2 (red) or mixed 0.05M borate buffer/1M NaSO4 (pH 9.7)/300mM H_2O_2 electrolyte (green).

The OCP of the $Co_3O_4/C65$ system in 1M BAS was found to be 0.13V with a limiting current density of 0.94mAcm^{-2} and a maximum power of 25uWcm^{-2} which puts it on par with other single-cell alkaline H_2O_2 fuel cells[13, 14]. Compared to the same electrodes running in a borate buffer adjusted to the same pH, the OCP remains the same but the limiting current is improved greatly, no doubt due to the increased conductivity of the 1M BAS electrolyte (0.11Scm^{-1} for 1M BAS and approximately 2mScm^{-1} for the borate buffer). The OCP of the cell using the 0.05M borate/1M NaSO4 electrolyte was slightly higher (approximately 15mV) at 145mV but the limiting current was lower at 0.7mAcm^{-2} with a maximum power density that is approximately equivalent to the maximum power density achieved when using the 1M BAS electrolyte.

The BAS electrolyte result is promising as it demonstrates that the use of ammonium-based electrolytes are not deleterious to the performance of this type of fuel cell with these catalysts. Also, further increasing the conductivity of the electrolyte solution could improve the limiting current of the cell as demonstrated by the increase in current between the 0.05M borate buffer solution and the 0.05M borate buffer/1M NaSO4 solution.

Fig. 11 shows two direct hydrogen peroxide fuel cells using a BAS electrolyte running over an extended period of time (more than two hours) where the cell potential was held constant at 70mV (approximately the maximum power point) and the resulting current was measured. One fuel cell (red) used a $Co_3O_4/C65$ catalytic film as

the cathode and the other used a polished Ag plate. Both had a heat-treated Ni foam anode and the electrodes were immersed in a 1M BAS (pH9.7) electrolyte with 300mM H_2O_2 added. Both fuel cells show a sharp drop in current during the first 10 minutes of operation. The cell using the Ag cathode drops from approximately 0.45mA to 0.3mA in this period while the Co_3O_4/C65 cathode shows a much shorter decline from 0.45mA to 0.38mA. After this period the rate of decline in current is slower for both cells. These two different regions may be attributed to two different processes. During the long term experiments bubble generation was also observed on the surface of both cathodes (no bubbles were observed on the Ni anodes) and it was apparent that the Ag cathode generated bubbles at a faster rate than the Co_3O_4/C65 cathode. The efficiency of a DHPFC is partly limited by the decomposition of H_2O_2 at the surface of the electrodes; H_2O_2 can be completely decomposed to H_2O and O_2 in the presence of many metals and metal oxides. H_2O_2 disproportionation can be observed by noting the evolution of bubbles at the cathode (as only water is formed in the reduction of H_2O_2). No power is produced by this reaction and it competes with the reduction and oxidation of H_2O_2 at the cathode and anode of a DHPFC which results in a drop in fuel efficiency. This process even occurs in acidic media where H_2O_2 is more stable (around pH3.5-4.5). However, the generation of bubbles can also cause a drop in current over long term operation by the bubbles becoming attached to the surface of the electrode and lowering the effective catalytic area. This could be a reason for the first region of rapid current drop in the chronoamperometry of Fig. 11. After the first few minutes of bubble generation the area covered in bubbles on both electrodes would reach a maximum as bubbles start to be liberated from the surface and the current loss from this phenomenon would also plateau.
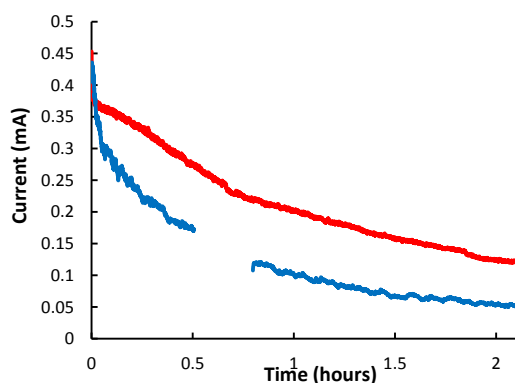
Figure 11: Long-term chronoamperometry of DHPFCs with a Ag plate (blue) or Co_3O_4/C65 film (red) cathode and a heat-treated Ni foam anode in 1M BAS (pH 9.7)/300mM H_2O_2 electrolyte. Cell potential was held at 0.06V for the duration.

Thereafter, a continued slow decline in current is seen over the two period of the experiment. Over the course of two hours the total current being generated is approximately 0.1mA higher when using the cobalt catalyst. This indicates that the Co_3O_4/C65 film performs better in long-term fuel cell operation despite the initial current being approximately equal for the two cells. The potential during this measurement corresponds to that at approximately half the initial limiting current density. This should mean that the fuel cells are

operating in the region of ohmic losses rather than where mass transport losses dominate at higher currents.

The total amount of charge consumed during the long term running of either of the cells tested in Fig. 11 equates to approximately 8.8μmol of H_2O_2 consumed due to power generation in the fuel cell. This is a very small amount in comparison to the total amount of H_2O_2 in the electrolyte at the beginning of the experiment (900umol) and so current loss due to lower fuel concentrations should not be an issue. However, after testing, the Ag electrode had developed a patina which indicates that during fuel cell operation some other reaction was occurring between the surface of this electrode and the electrolyte, most likely the formation of $AgSO_4$. This could explain the faster drop in current over the course of the long term fuel cell test using the polished Ag plate as a cathode. In the case of the Co_3O_4/C65 cathode, Energy dispersive X-ray spectroscopy (EDX) in conjunction with scanning electron microscopy (SEM) was performed on the films before and after several days of fuel cell testing with the same electrode (Supp. Fig. 1 and 2). It was found that the Co that was present in the 'before' film was almost completely absent in the 'after' film. This indicates that over the course of fuel cell testing most of the Co_3O_4 in the film had leeched out into the electrolyte, or was washed out when the film was rinsed with distilled water between experiments. Loss of catalyst in this way could contribute to the loss in current over the two hours of fuel cell operation shown in Fig. 11. There was no coloration evident in the solution that might suggest dissolution as Co(II), therefore the most likely explanation for the loss is due to disintegration of the binder.

Conclusion

We have shown the operation of a DHPFC in an alkaline, organic salt electrolyte with a maximum power density of 25μWcm^{-2} using a CoOx/C65 cathode and a heat-treated Ni foam anode. The long-term stability of this system has been shown to be relatively good compared to silver metal which has previously been used in similar alkaline DHPFCs. The electrolyte used for fuel cell operation is also suitable for high efficiency H_2O_2 production *via* water oxidation. Combining these two processes will allow for a fully reversible, one-compartment DHPFC.

1.   R. S. Disselkamp, *International Journal of Hydrogen Energy*, 2010, **35**, 1049-1053.

2.   A. E. Sanli and A. Aytaç, *International Journal of Hydrogen Energy*, 2011, **36**, 869-875.

3.   M. Giomo, A. Buso, P. Fier, G. Sandonà, B. Boye and G. Farnia, *Electrochimica Acta*, 2008, **54**, 808-815.

4.   Y. Ando and T. Tanaka, *International Journal of Hydrogen Energy*, 2004, **29**, 1349-1354.

5.   A. Izgorodin, E. Izgorodin, D. R. MacFarlane, *Energy & Enviroonmental Science*, 2012, **5**, 9496-9501.

6.   W. R. P. Barros, R. M. Reis, R. S. Rocha and M. R. V. Lanza, *Electrochimica Acta*, 2013, **104**, 12-18.

7.	M. Campos, W. Siriwatcharapiboon, R. J. Potter and S. L. Horswell, *Catalysis Today*, 2013, **202**, 135-143.

8.	K. Mase, K. Ohkubo and S. Fukuzumi, *Journal of the American Chemical Society*, 2013, **135**, 2800-2808.

9.	M. A. Ghanem, A. M. Al-Mayouf, M. N. Shaddad and F. Marken, *Electrochimica Acta*, 2015, **174**, 557-562.

10.	R. K. Ahluwalia, T. Q. Hua, J. K. Peng, S. Lasher, K. McKenney, J. Sinha and M. Gardiner, *International Journal of Hydrogen Energy*, 2010, **35**, 4171-4184.

11.	N. de Miguel, R. Ortiz Cebolla, B. Acosta, P. Moretto, F. Harskamp and C. Bonato, *International Journal of Hydrogen Energy*, 2015, **40**, 6449-6458.

12.	Z. Li, X. Pan, K. Sun and J. Ma, *International Journal of Hydrogen Energy*, 2013, **38**, 11174-11180.

13.	S.-i. Yamazaki, Z. Siroma, H. Senoh, T. Ioroi, N. Fujiwara and K. Yasuda, *Journal of Power Sources*, 2008, **178**, 20-25.

14.	Y. Yamada, Y. Fukunishi, S.-i. Yamazaki and S. Fukuzumi, *Chemical Communications*, 2010, **46**, 7334-7336.

15.	R. Brimblecombe, A. M. Bond, G. C. Dismukes, G. F. Swiegers and L. Spiccia, *Physical Chemistry Chemical Physics*, 2009, **11**, 6441-6449.

16.	Y. W. D. Chen and R. N. Noufi, *Journal of The Electrochemical Society*, 1984, **131**, 731-735.

17.	M. M. Najafpour, F. Rahimi, M. Amini, S. Nayeri and M. Bagherzadeh, *Dalton Transactions*, 2012, **41**, 11026-11031.

18.	K. Sun, N. Park, Z. Sun, J. Zhou, J. Wang, X. Pang, S. Shen, S. Y. Noh, Y. Jing, S. Jin, P. K. L. Yu and D. Wang, *Energy & Environmental Science*, 2012, **5**, 7872-7877.

19.	M. Gao, W. Sheng, Z. Zhuang, Q. Fang, S. Gu, J. Jiang and Y. Yan, *Journal of the American Chemical Society*, 2014, **136**, 7077-7084.

20.	D. Cao, J. Chao, L. Sun and G. Wang, *Journal of Power Sources*, 2008, **179**, 87-91.

21.	R. R. Bessette, J. M. Cichon, D. W. Dischert and E. G. Dow, *Journal of Power Sources*, 1999, **80**, 248-253.

22.	H. Li, W. Hao, J. Hu and H. Wu, *Biosensors and Bioelectronics*, 2013, **47**, 225-230.

23.	S. Jana, S. Samai, B. C. Mitra, P. Bera and A. Mondal, *Dalton Transactions*, 2014, **43**, 13096-13104.

24.	S. A. Mousavi Shaegh, N.-T. Nguyen, S. M. Mousavi Ehteshami and S. H. Chan, *Energy & Environmental Science*, 2012, **5**, 8225-8228.

25.	Y. Liu, X. Quan, X. Fan, H. Wang and S. Chen, *Angewandte Chemie International Edition*, 2015, **54**, 6837-6841.

26.	C. McDonnell-Worth and D. R. MacFarlane, *RSC Advances*, 2014, **4**, 30551-30557.

27.	A. J. Bard, *Electrochemical methods : fundamentals and applications*, New York : Wiley, New York, 1980.

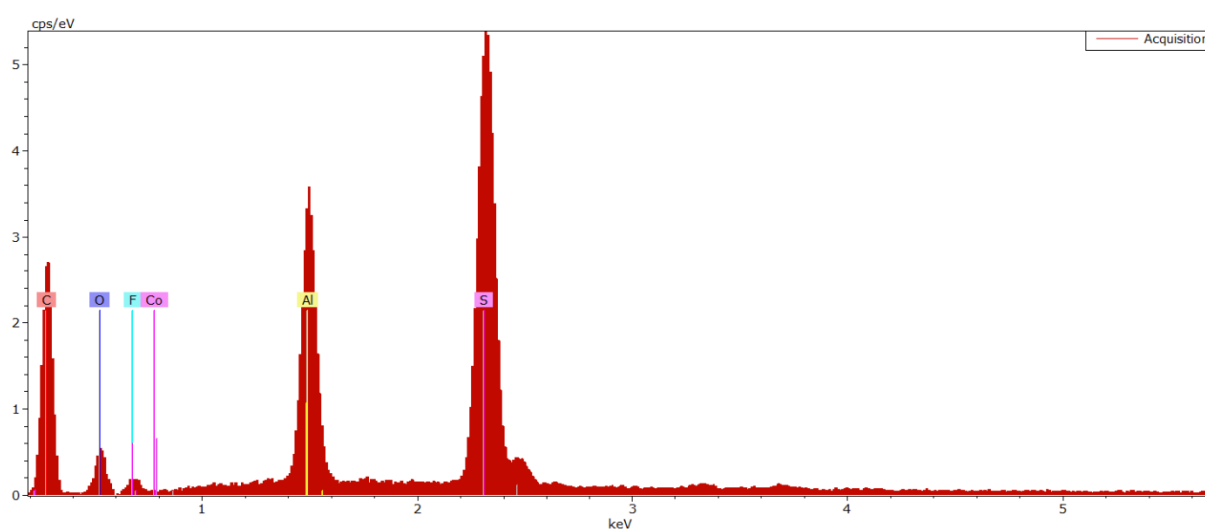# Chapter 3.4 – Supplementary Information for Chapter 3.3
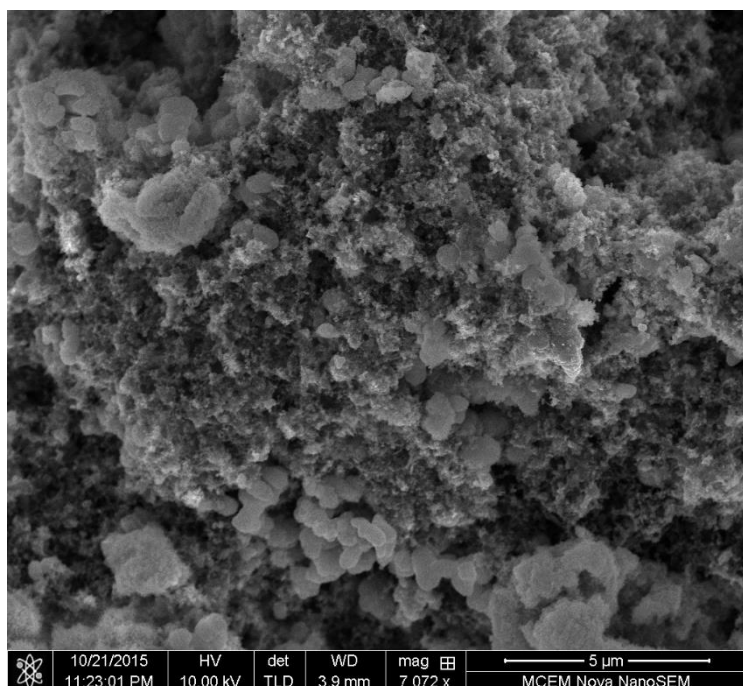
Supp Fig. 1a: SEM image of a Co$_3$O$_4$/C65 catalyst before fuel cell testing
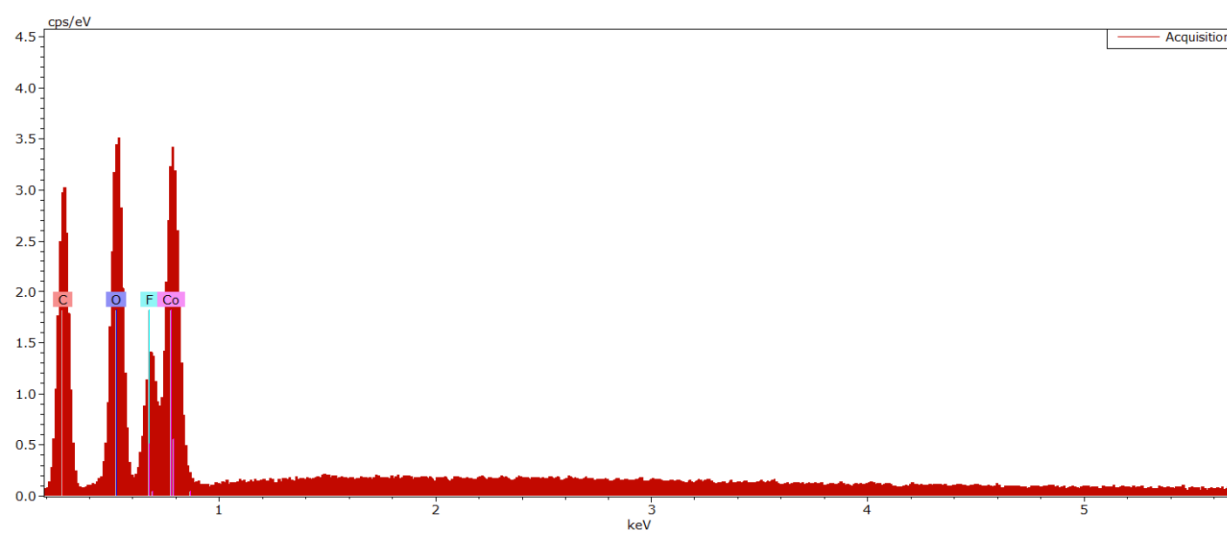
Supp Fig. 1b: EDX of a Co$_3$O$_4$/C65 catalyst before fuel cell testing
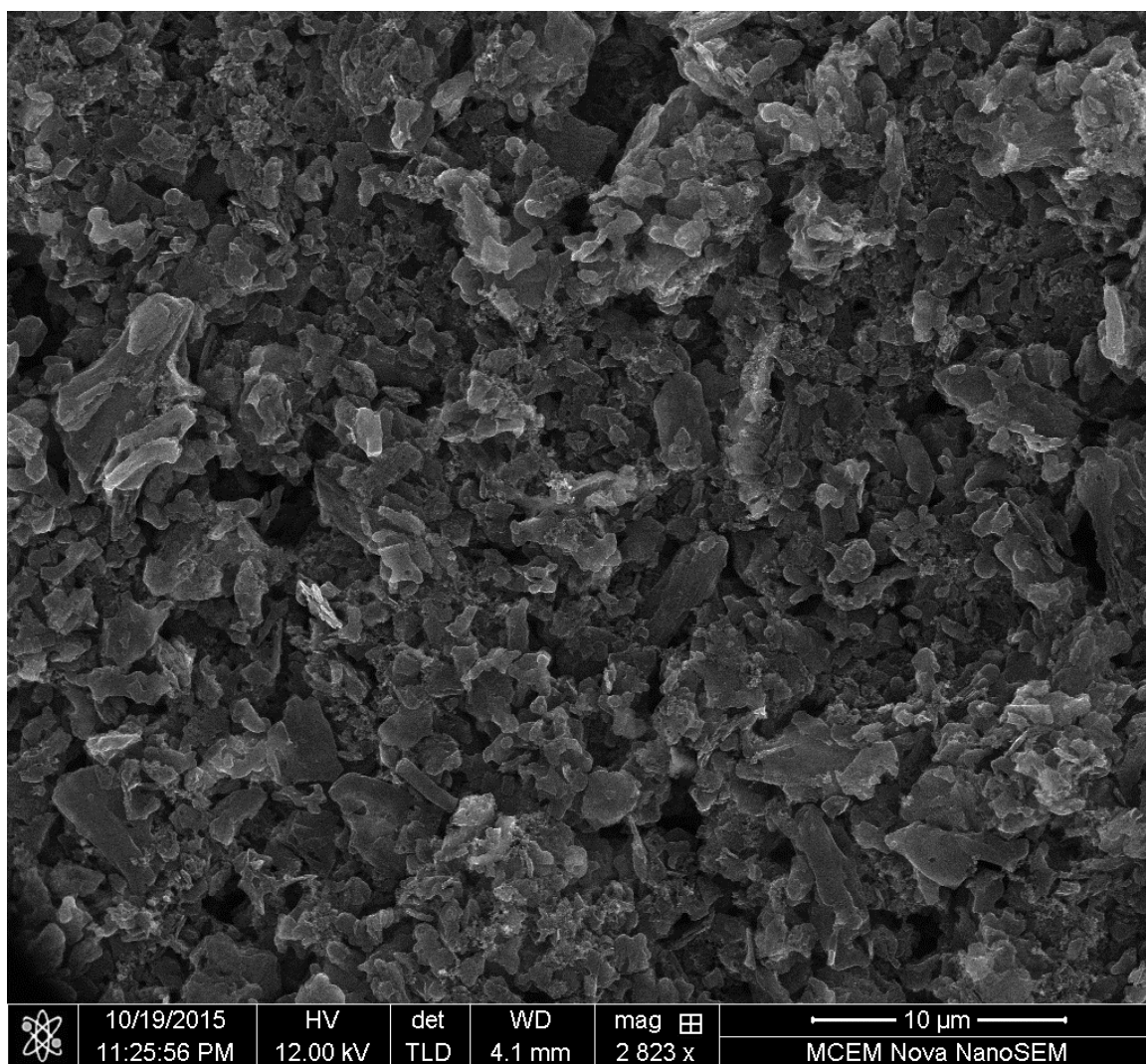
Supp. Fig. 2a: SEM image of a Co_3O_4/C65 catalyst after extensive fuel cell testing

Supp. Fig. 2b: EDX of a Co_3O_4/C65 catalyst after extensive fuel cell testing

3.5 Extended Supplementary Information

A number of fuel cell test were performed with combinations of catalysts as part of a screening process for the results presented in **Chapter 3**. Some of the results of these tests are shown in this Supplementary Section to demonstrate a wider picture of the catalysts and electrolytes available for these fuel cells.

Iron Oxide

Iron complexes have been used as catalysts in DHPFCs and as part of the investigation into cathodic and anodic catalysts shown in **Chapter 3**. Two different forms of iron oxide were tested (mainly as the anodic catalyst). One was a screen-printed FeOx film on FTO glass produced by Fengling Zhou. The other was a film of Fe_2O_3 electrodeposited on FTO glass using the deposition method described by Tamboli *et al*[1].

Cyclic voltammograms were performed in a three electrode cell of each of the iron oxide catalysts and are shown below in Figs. 1 and 2.
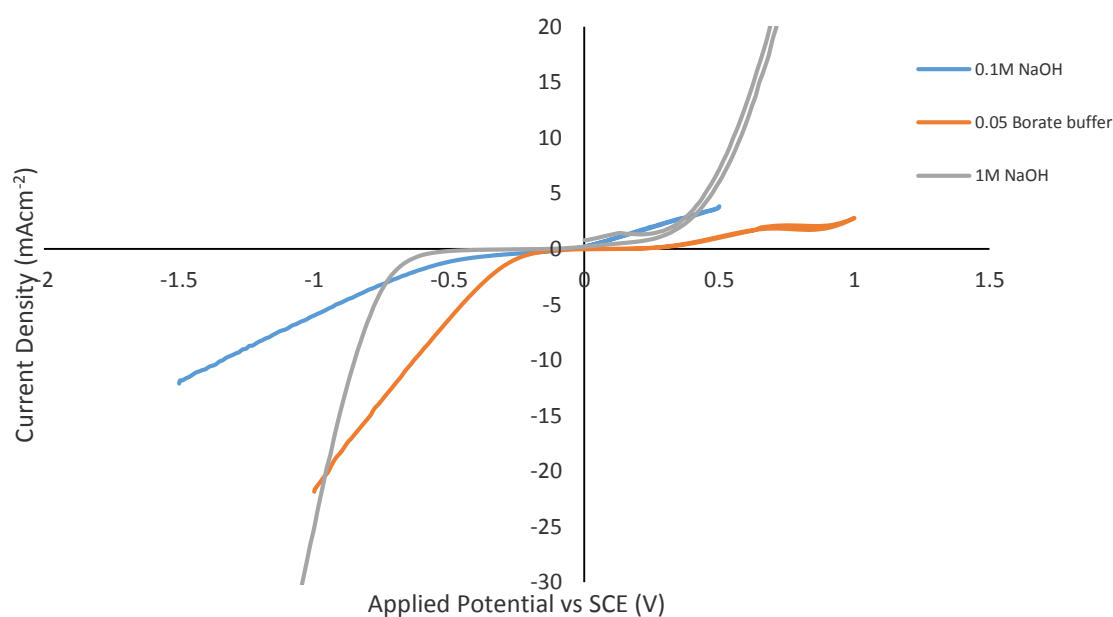
Figure 1: Cyclic voltammogram of a screen-printed FeOx film on FTO in various electrolytes with 300mM H_2O_2 added to each. Scan rate 20mVs^{-1}.
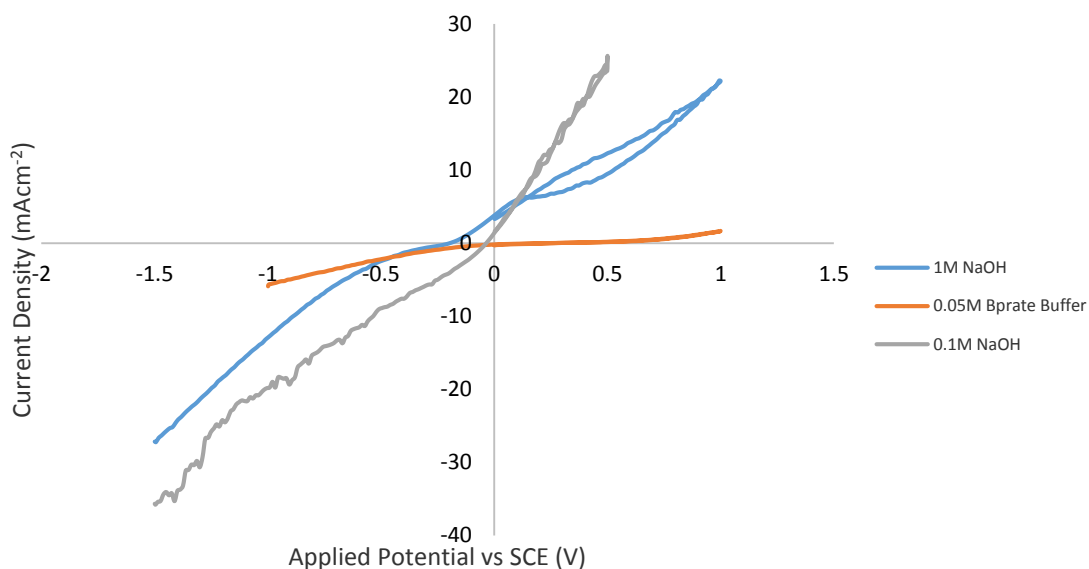
Figure 2: Cyclic voltammogram of an electrodeposited Fe$_2$O$_3$ film on FTO in various electrolytes with 300mM H$_2$O$_2$ added to each. Scan rate 20mVs^{-1}.

The screen printed FeOx electrode (Fig. 1) showed much higher currents than the electrodeposited Fe$_3$O$_3$ film for H$_2$O$_2$ reduction at potentials below -0.5V vs SCE in 0.5M borate buffer. However, they behaved very similarly for H$_2$O$_2$ oxidation above 0.5V vs SCE. In solutions of 1M NaOH and 0.1M NaOH their oxidative and reductive behaviour changes dramatically. H$_2$O$_2$ oxidation begins to occur much earlier and with much higher currents for both catalysts. On the screen printed FeOx film H$_2$O$_2$ reduction begins to occur at higher reductive potentials (above 0.5V vs SCE) whereas it occurs around the same potential in 1M NaOH on the electrodeposited film. The high oxidative and reductive currents that occur around the same potential (0V vs SCE) on the electrodeposited film in 0.1M NaOH indicates that the rate of H$_2$O$_2$ disproportionation on that electrode is high as discussed in **Chapter 3**.

Iron Oxide as an Anode in DHPFCs

Screen Printed Iron Oxide

Screen printed iron oxide films were tested primarily as an anode in direct H_2O_2 fuel cells. Fig. 3 shows the I-V and I-P curves of a fuel cell constructed with a screen-printed FeOx anode and an electrodeposited Co_3O_4 anode in a pH 9.2 borate buffer. Compared to the same cell using a heat-treated Ni foam (shown in Chapter 3) the open-circuit potential (OCP) is approximately equal. However, the limiting current and maximum power density achieved is even lower when using the screen-printed FeOx film. This may be because of the low conductivity of the film which is contributed to by both the FTO backing of the electrode and the screen printing process.
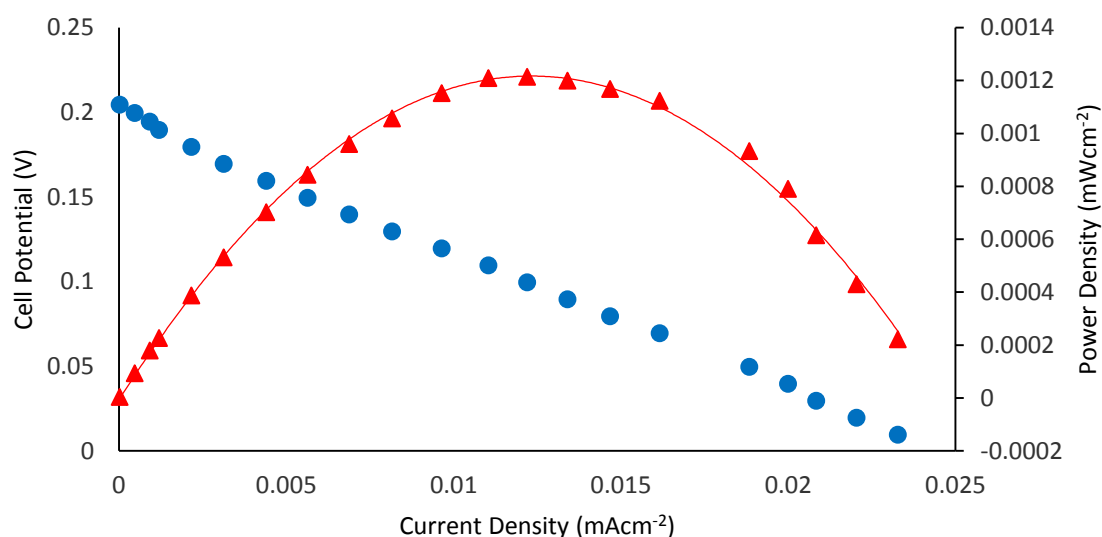
Figure 3: I-V (blue) and I-P (red) curves of a fuel cell constructed with a screen-printed FeOx anode and an electrodeposited Co_2O_3 cathode in a 0.05M borate buffer at pH 9.2.

The combination of a screen-printed FeOx anode and a polished Ag plate cathode (Fig. 4) shows a dramatic drop in OCP in comparison to using an electrodeposited Co_2O_3 film cathode (Fig. 3).
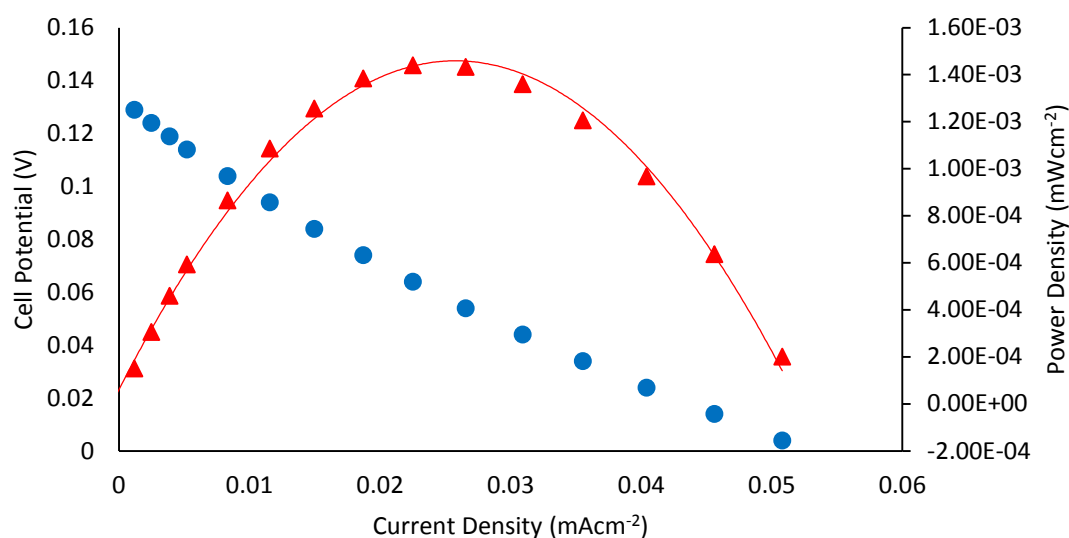
Figure 4: I-V (blue) and I-P (red) curves of a fuel cell constructed with a screen-printed FeOx anode and a polished Ag plate cathode in a 0.05M borate buffer at pH 9.2.

Fig. 5 shows the same electrodes in a borate buffer electrolyte adjusted to pH 10 with the addition of 1M NaOH. The OCP falls dramatically which is expected with the increase in pH and the limiting current density increases.
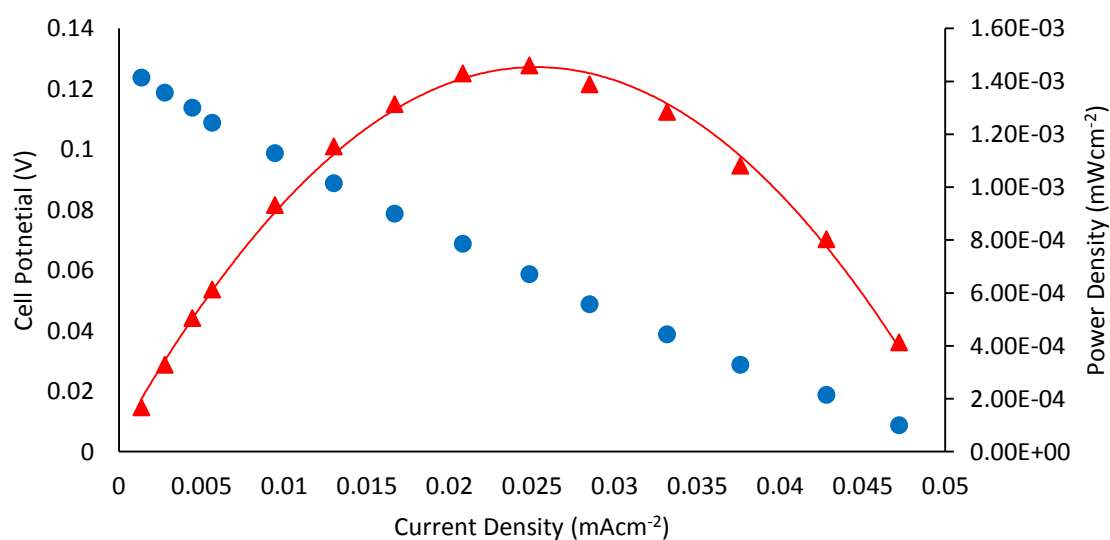
Figure 5: I-V (blue) and I-P (red) curves of a fuel cell constructed with a screen-printed FeOx anode and an electrodeposited Co_2O_3 cathode in a 0.05M borate buffer adjusted to pH 10 with NaOH

The combination of a screen-printed FeOx cathode and a Ni foam anode was tested in a H_2O_2 fuel cell with a 0.05M borate buffer electrolyte at pH 9.2 (Fig. 6). The OCP of this cell (shown in Figs. 6 and 7) was only 0.035V which demonstrates that the electrochemical potentials of H_2O_2 reduction and

oxidation on these two catalysts are too close to each other to provide a sizeable potential difference between them when they are immersed in a H_2O_2 solution.
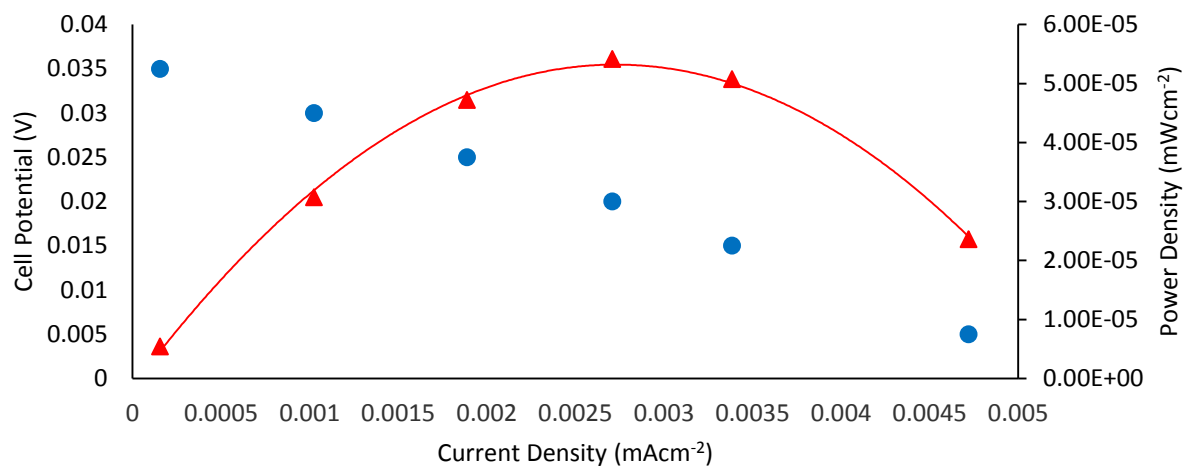
Figure 6: I-V (blue) and I-P (red) curves of a fuel cell constructed with a Ni foam anode and a screen-printed FeOx on FTO cathode in a 0.05M borate buffer at pH 9.2.

Fig. 7 shows the same electrodes (Ni foam and screen printed FeOx) in a 0.05M borate buffer electrolyte with 1M KCl added to improve the conductivity of the solution with the aim of increasing

the limiting current density of the fuel cell. However, the limiting current density was lowered dramatically with the addition of KCl in this particular cell.
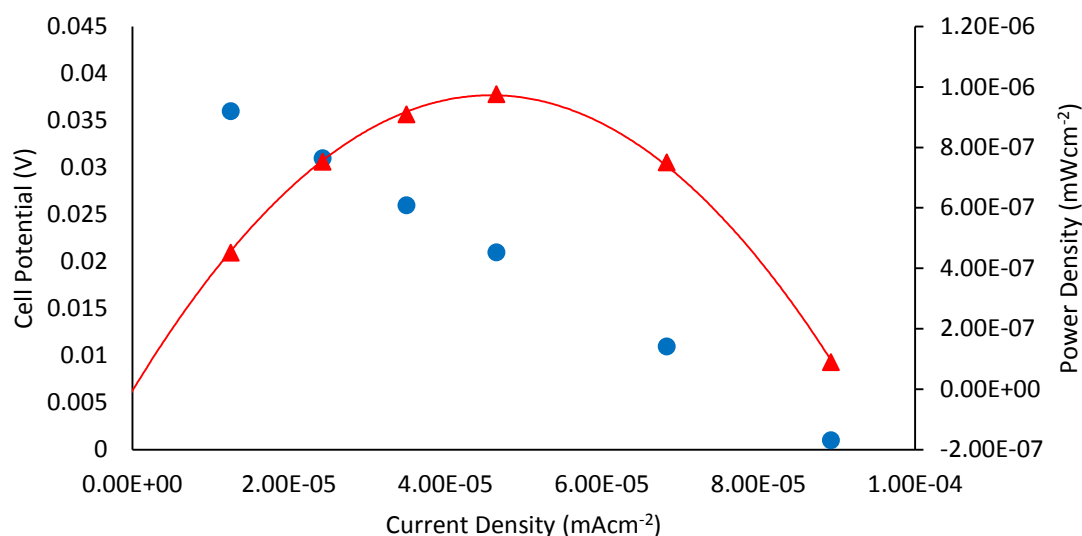
Figure 7: I-V (blue) and I-P (red) curves of a fuel cell constructed with a Ni foam anode and a screen-printed FeOx on FTO cathode in a 0.05M borate buffer/1M KCl electrolyte at pH 9.2.

Electrodeposited Fe_2O_3

Electrodeposited FeOx showed reasonable potential as a H_2O_2 oxidation catalyst in direct H_2O_2 fuel cells but was abandoned as the heat-treated Ni foam electrodes shown in **Chapter 3** produced both a higher OCP and also had the benefit of a higher surface area due to its porous structure. Some fuel cells tested are shown below that include an electrodeposited Fe_2O_3 film.

Fig. 8 and 9 shows the I-V and I-P curves of a fuel cell constructed with an electrodeposited Fe_2O_3 anode and an electrodeposited Co_2O_3 or polished Ag plate cathode respectively. The OCP is reasonably high at around 200mV but the limiting current density is quite low. Interestingly, here the addition of 1M KCl to the electrolyte has appeared to increase the limiting current density by about a factor of

five. This suggests that such a dramatic increase to the ionicity of the electrolyte does effect the achievable currents of this type of cell.
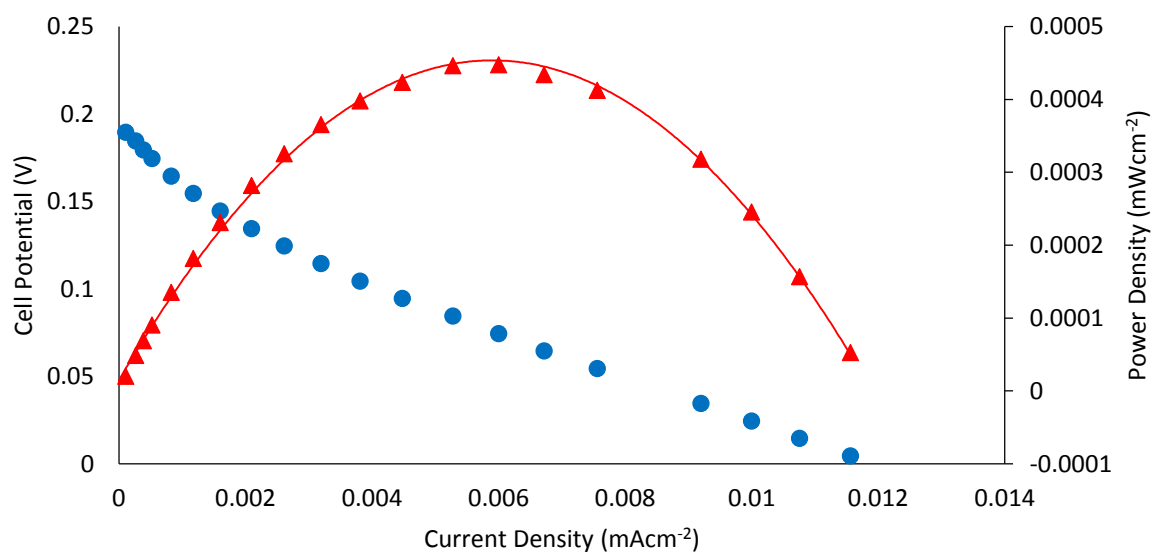
Figure 8: I-V (blue) and I-P (red) curves of a fuel cell constructed with an electrodeposited Fe_2O_3 anode and an electrodeposited Co_2O_3 on FTO cathode in a 0.05M borate buffer/1M KCl electrolyte at pH 9.2 with 300mM H_2O_2 added.
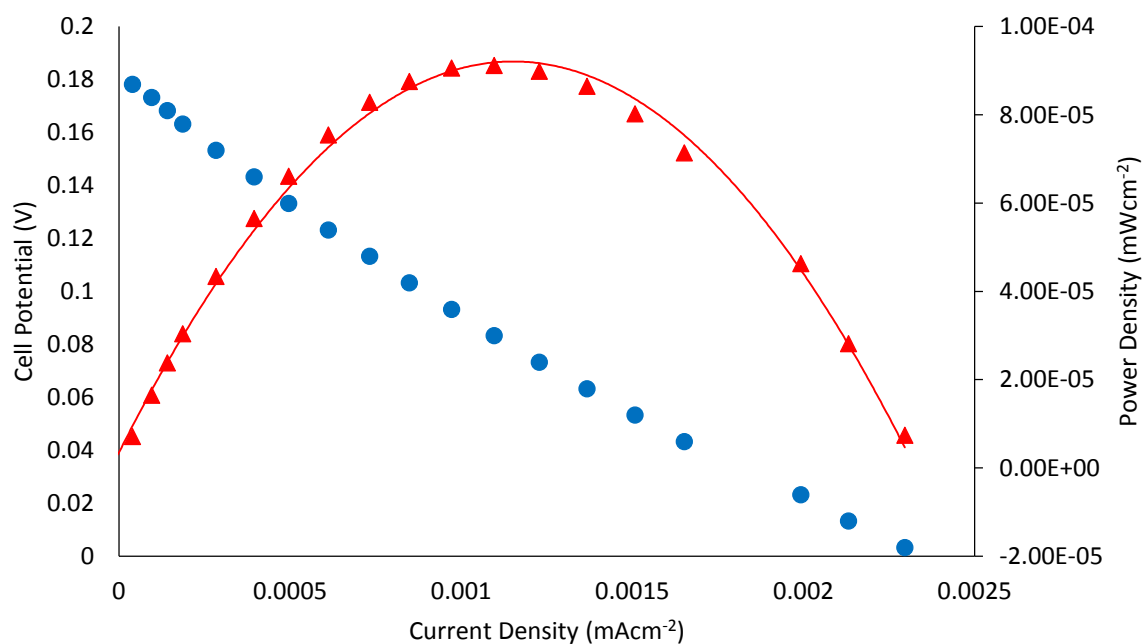

Figure 9: I-V (blue) and I-P (red) curves of a fuel cell constructed with a electrodeposited Fe_2O_3 anode and a polished Ag plate cathode in a 0.05M borate buffer at pH 9.2 with 300mM H_2O_2 added.

Fig. 10 shows a fuel cell operating with a combination of a screen-printed FeOx film as an anode and an electrodeposited Fe_2O_3 cathode in a pH 9.2 solution of 0.05M borate buffer and 300mM H_2O_2. The OCP of this cell is relatively low at approximately 45mV which is expected given that the two catalysts are both suited to H_2O_2 oxidation (ie. working as an anode).
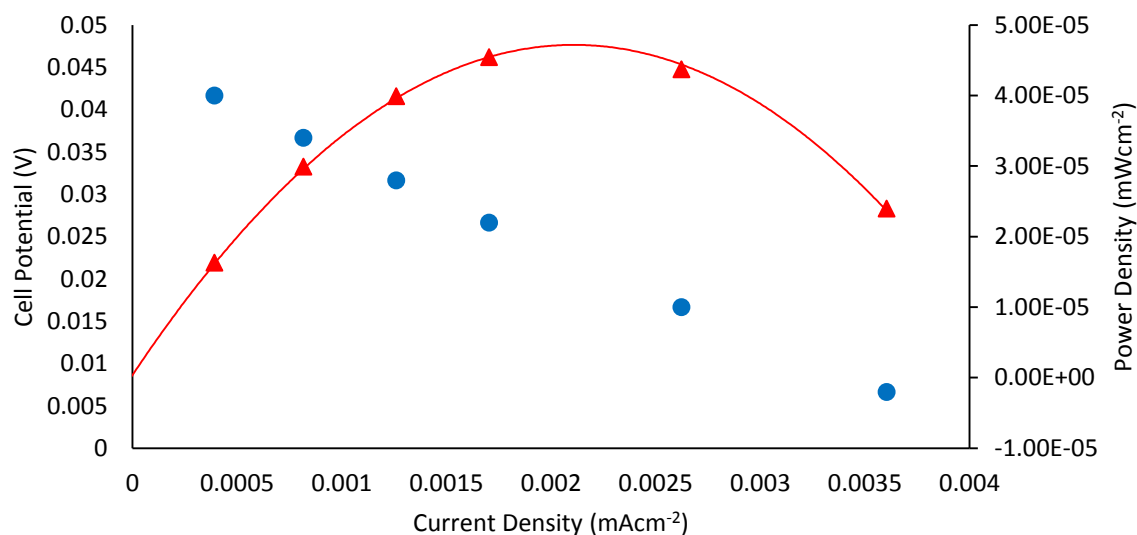
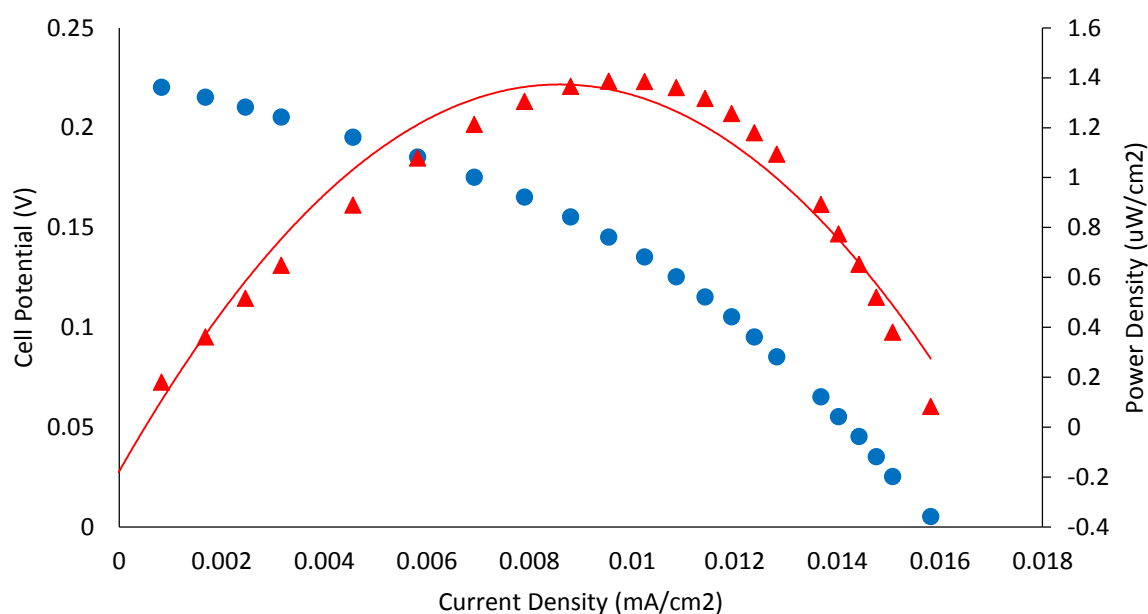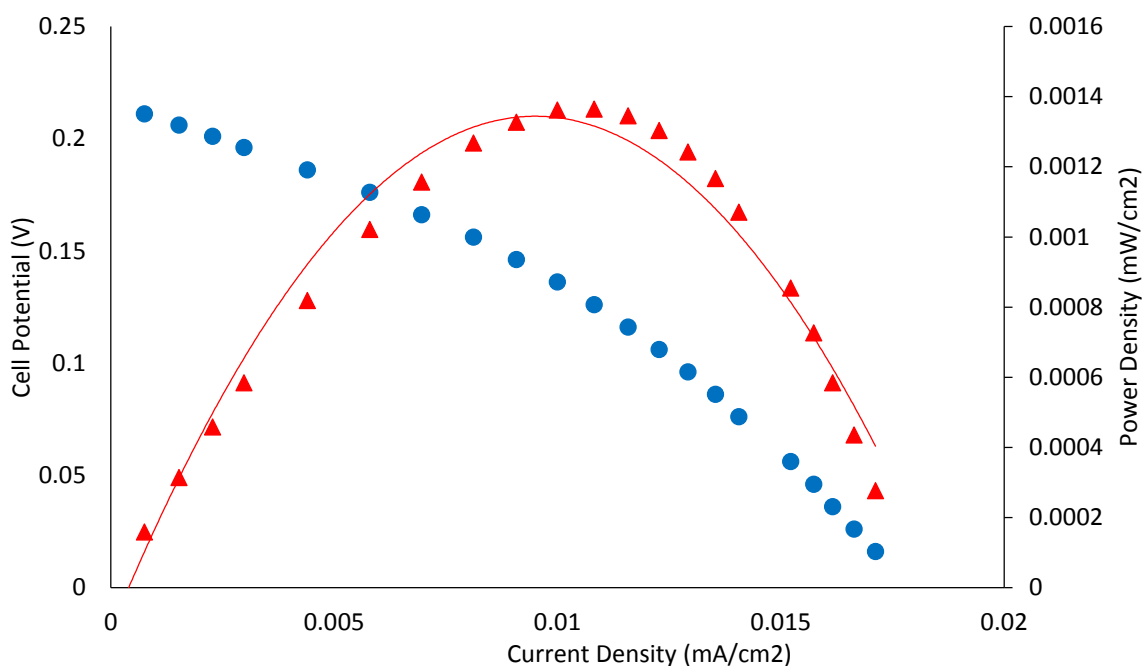*Figure 10: I-V (blue) and I-P (red) curves of a fuel cell constructed with a screen-printed FeOx on FTO anode and an electrodeposited Fe_2O_3 on FTO cathode in a 0.05M borate buffer at pH 9.2 with 300mM H_2O_2 added.*

Electrodeposited Co$_2$O$_3$ films in DHPFCs

Fuel cell tests using electrodeposited Co$_2$O$_3$ were carried out in addition to that shown in **Chapter 3** that showed the catalyst operating under various conditions. Although the low limiting current density achievable by fuel cells using this catalyst was low the relatively high overpotentials produced may make other types of catalysts including this material viable. Figs. 11 and 12 show DHPFCs with an electrodeposited Co$_2$O$_3$ cathode and a heat-treated Ni foam anode. The OCP of these cells is relatively high at around 220mV. The cell was tested in two different electrolytes, a 0.05M borate buffer in Fig. 11 and a mixed 0.05M borate buffer/0.1M KCl electrolyte in Fig. 12 (both at pH 9.2). The limiting current was unchanged in the different electrolytes.

Figure 11: I-V (blue) and I-P (red) curves of a fuel cell constructed with a heat-treated Ni foam anode and an electrodeposited Co2O3 cathode in a 0.05M borate buffer at pH9.2 with 300mM H2O2 added.
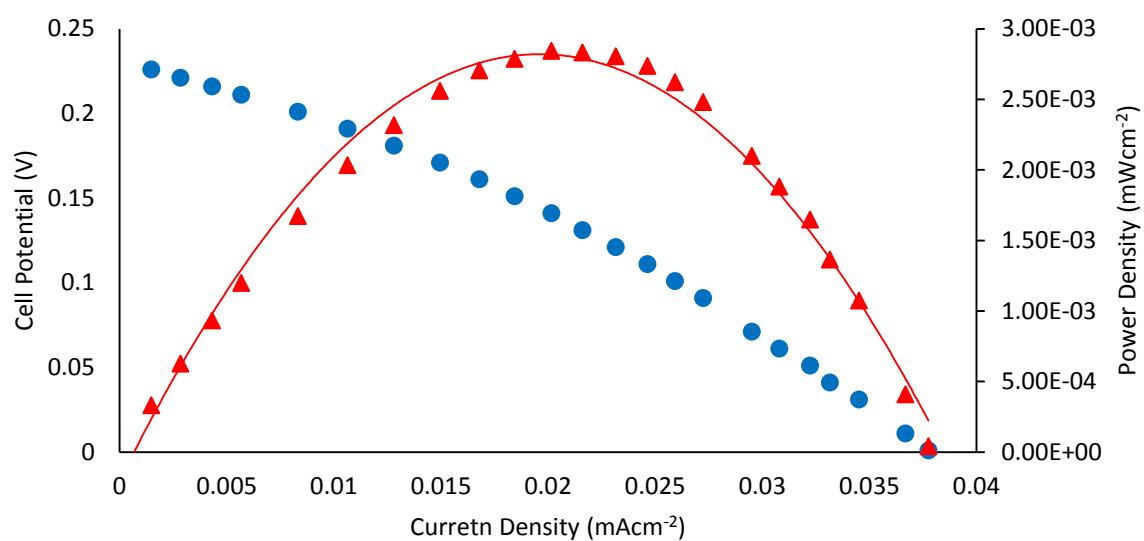
Figure 12: I-V (blue) and I-P (red) curves of a fuel cell constructed with a heat-treated Ni foam anode and an electrodeposited Co₂O₃ cathode in a 0.05M borate buffer/0.1M KCl electrolyte at pH9.2 with 300mM H₂O₂ added.

Fig. 13 shows a DHPFC operating with a Co_2O_3 cathode and a heat-treated Ni foam anode in 0.05M borate buffer. Here, the effect of shining simulated sunlight on the cell was observed. A Xenon lamp was used to direct a beam of light (roughly with an intensity roughly equivalent to that of direct sunlight at ground level) onto the surface of the cathode through the glass container of the cell and the electrolyte. No change to the OCP was observed in the I-V curve compared to that shown in Fig. 11 (which is the same cell with no sun) however the limiting current density was more than doubled indicating that the rate of H_2O_2 oxidation and reduction was increased. However, light is known to

cause H_2O_2 to decompose more rapidly which may be detrimental to the long-term operation of the fuel cell.

Figure 13: I-V (blue) and I-P (red) curves of a fuel cell constructed with a heat-treated Ni foam anode and an electrodeposited Co_2O_3 cathode in a 0.05M borate buffer at pH 9.2 with 300mM H_2O_2 added under light (intensity equivalent of 1 sun. Produced by Xenon lamp).

Combining an electrodeposited Co_2O_3 film on FTO cathode and a polished Ag plate anode showed only a very small open circuit potential which is expected given that they are both more suited to H_2O_2 reduction (ie. working as a cathode).
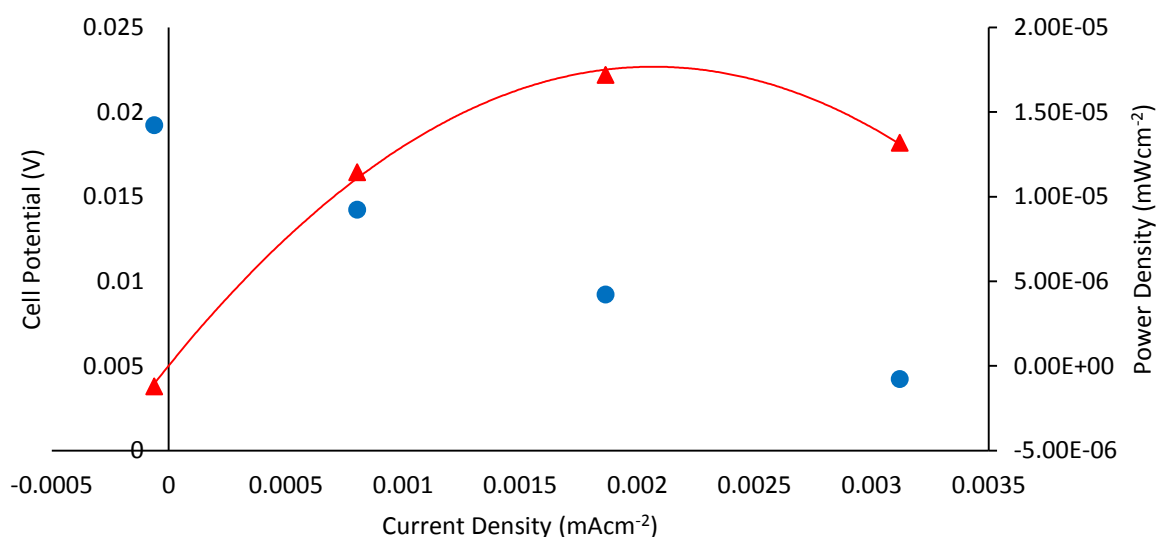
Figure 14: I-V (blue) and I-P (red) curves of a fuel cell constructed with an electrodeposited Co_2O_3 on FTO cathode and a polished Ag plate anode in a 0.05M borate buffer/0.1M KCl electrolyte at pH9.2 with 300mM H_2O_2 added.

In order to increase the surface area of the electrodeposited Co_2O_3 film the electrodeposition was performed on a Ni foam electrode rather than FTO. The electrode was then heat-treated at 400°C for 40 minutes. Fig. 15 shows a fuel cell operating with this electrode in conjunction with an electrodeposited Co_2O_3 film on FTO. The OCP of this cell was found to be the same as if the electrodeposition of Co_2O_3 had not occurred. However, a film was observed on the Ni foam surface so it was suspected that the surface of the anode exposed to the electrolyte was both Co_2O_3 and the original Ni. When the electrode was placed in a fuel cell with a good cathode (Co_2O_3 on FTO) the H_2O_2

was preferentially oxidised on the Ni foam. This behaviour was replicated when the Co_2O_3 on Ni foam electrode was used in conjunction with other catalysts as demonstrated in Fig. 16.
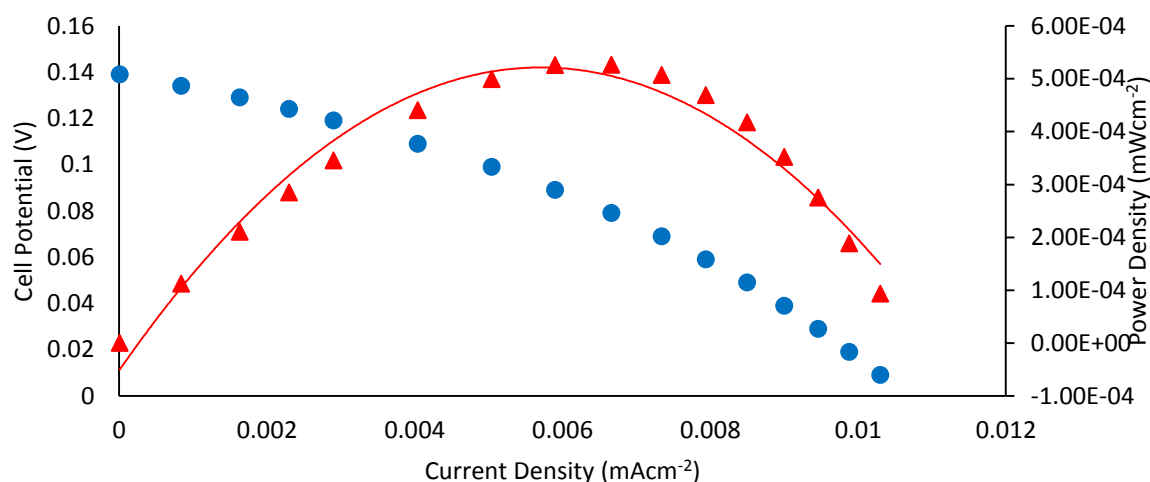

Figure 15: I-V (blue) and I-P (red) curves of a fuel cell constructed with an electrodeposited Co2O3 film on a heat-treated Ni foam anode and an electrodeposited Co_2O_3 on FTO cathode in 1M NaOH with 300mM H_2O_2 added.
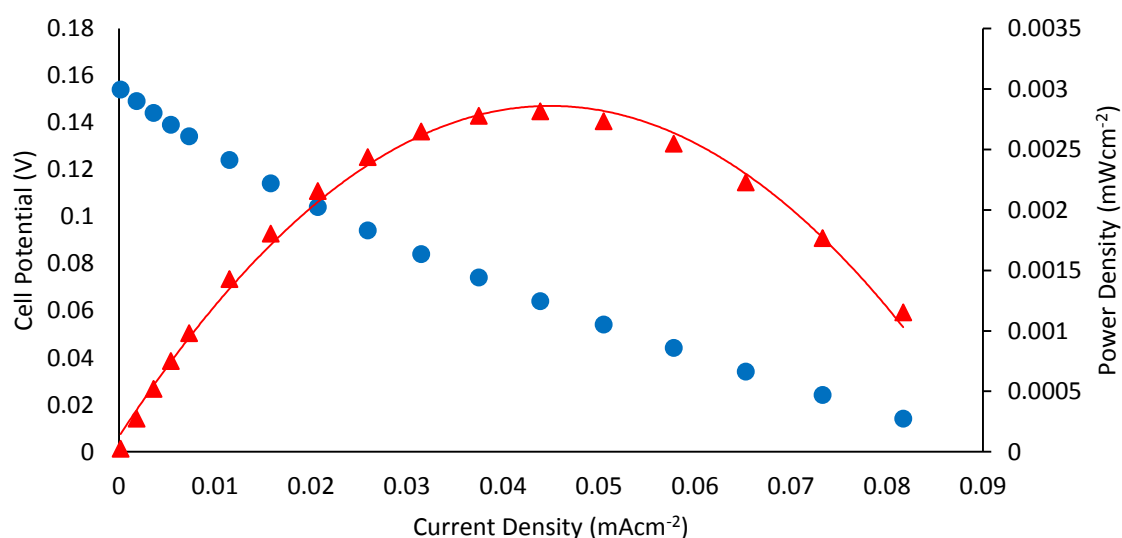

Figure 16: I-V (blue) and I-P (red) curves of a fuel cell constructed with an electrodeposited Co_2O_3 film on Ni foam anode and polished Ag plate cathode in a 0.05M borate buffer at pH9.2 with 300mM H_2O_2 added.

Figs. 17 and 18 show the effect that different concentrations of NaOH in the electrolyte have on the performance of the fuel cell when using an electrodeposited Co_2O_3 cathode. When the concentration of NaOH is higher (1M) the OCP is reduced by approximately 30mV but the limiting current density is more than double. It has been observed previously in **Chapter 3** that the OCP of these fuel cells tends to increase when the pH of the electrolyte is lower.
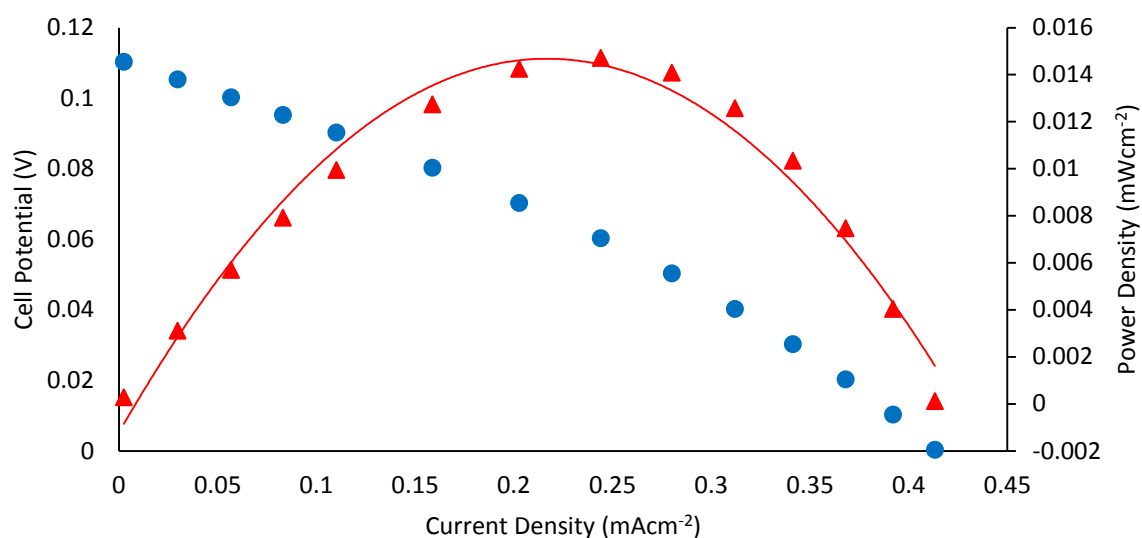
Figure 17: I-V (blue) and I-P (red) curves of a fuel cell constructed with a Ni foam anode and an electrodeposited Co_2O_3 on FTO cathode in a 1M NaOH electrolyte with 300mM H_2O_2 added.
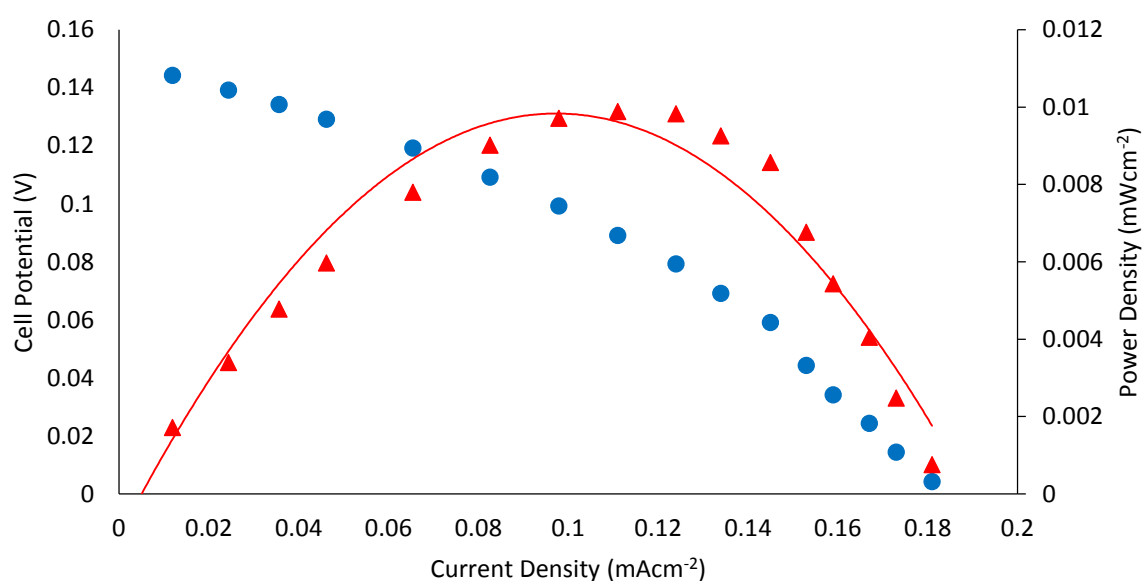

Figure 18: I-V (blue) and I-P (red) curves of a fuel cell constructed with a Ni foam anode and an electrodeposited Co_2O_3 on FTO cathode in 0.1M NaOH with 300mM H_2O_2 added.

A similar trend is observed in Figs. 19 and 20 where the limiting current density is greatly improved by increasing the concentration of NaOH in the electrolyte while slightly reducing the OCP of the cell. The OCP in this case is relatively low because both electrodes used, the electrodeposited Co_2O_3 film and the polished Ag plate, are poor H_2O_2 oxidation catalysts.
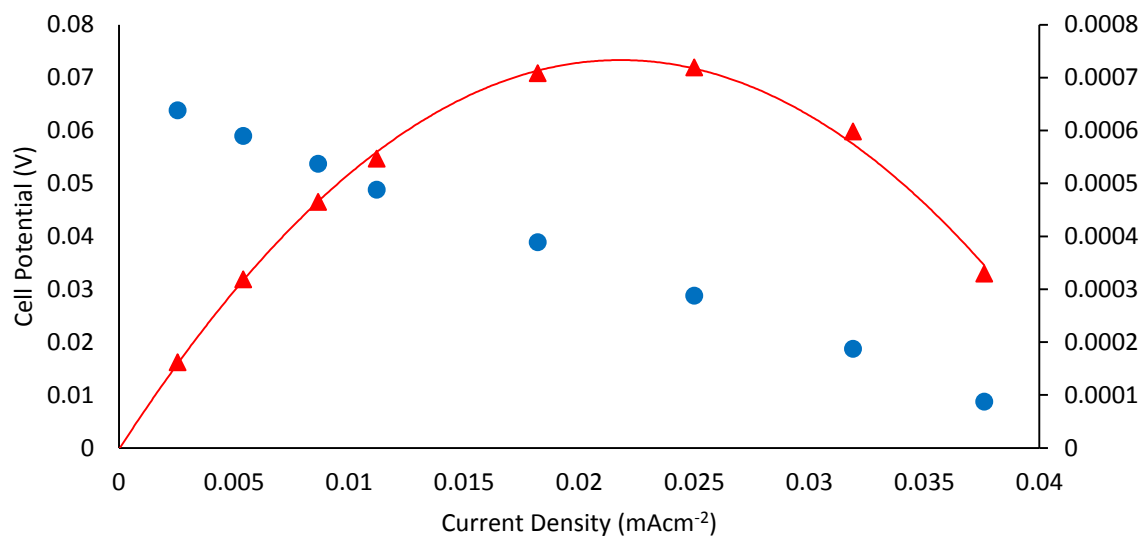
Figure 19: I-V (blue) and I-P (red) curves of a fuel cell constructed with a Co_2O_3 film electrodeposited on FTO cathode and a polished Ag plate anode in 0.1M NaOH with 300mM H_2O_2 added.
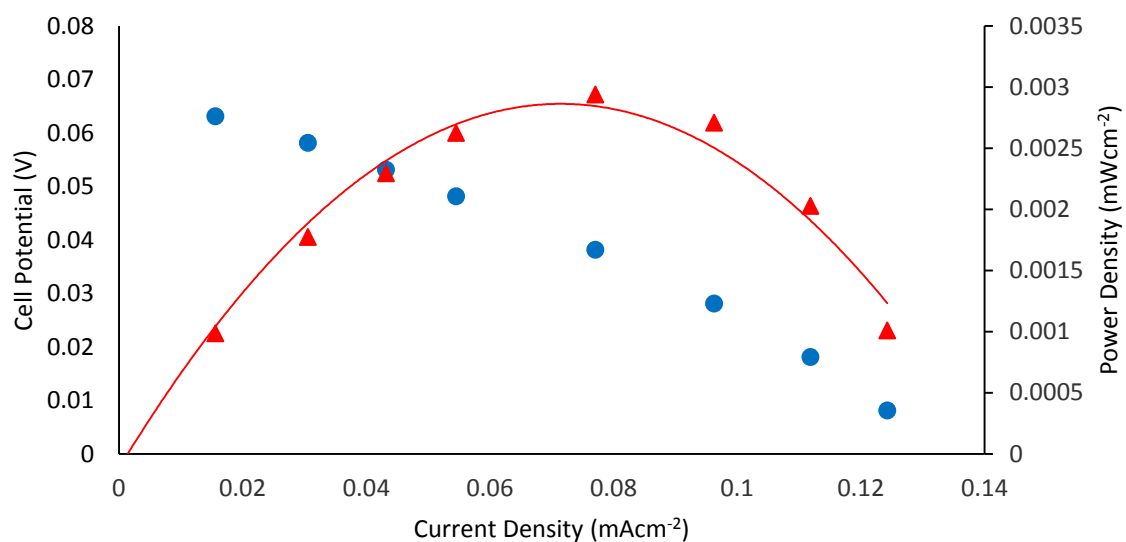

Figure 20: I-V (blue) and I-P (red) curves of a fuel cell constructed with a polished Ag plate anode and an electrodeposited Co_2O_3 on FTO cathode in 1M NaOH with 300mM H_2O_2 added.

Alternative electrolytes

Mixtures of organic and inorganic species in the fuel cell electrolyte were also tested to try to achieve greater OCPs and power densities. It was known that for the water oxidation to H_2O_2 process to take place the presence of free amine was required in the electrolyte. The intention of this project was to eventually integrate the H_2O_2 production process into a H_2O_2 fuel cell so testing fuel cells containing free amine was important. Figs. 21 and 22 show direct H_2O_2 fuel cells operating with an electrolyte containing a mixture of organic (butylamine) and inorganic (KOH) species. Here, a Ni foam anode and polished Ag plate cathode were used to give an OCP of approximately 0.12V for both the concentrated (1M KOH/1M butylamine) and less concentrated (0.1M KOH/0.1M butylamine) electrolytes. This OCP is expected for these catalysts and the doubling of the limiting current density between the less concentrated and more concentrated electrolytes has been seen previously. However, when these fuel cells were in operation a very large amount of bubbles were observed to evolve from both the anode and the cathode. The system with the 0.1M KOH/0.1M butylamine electrolyte showed the lowest amount of bubbling. This is indicative of the disproportionation of H_2O_2 at the surface of the catalyst.
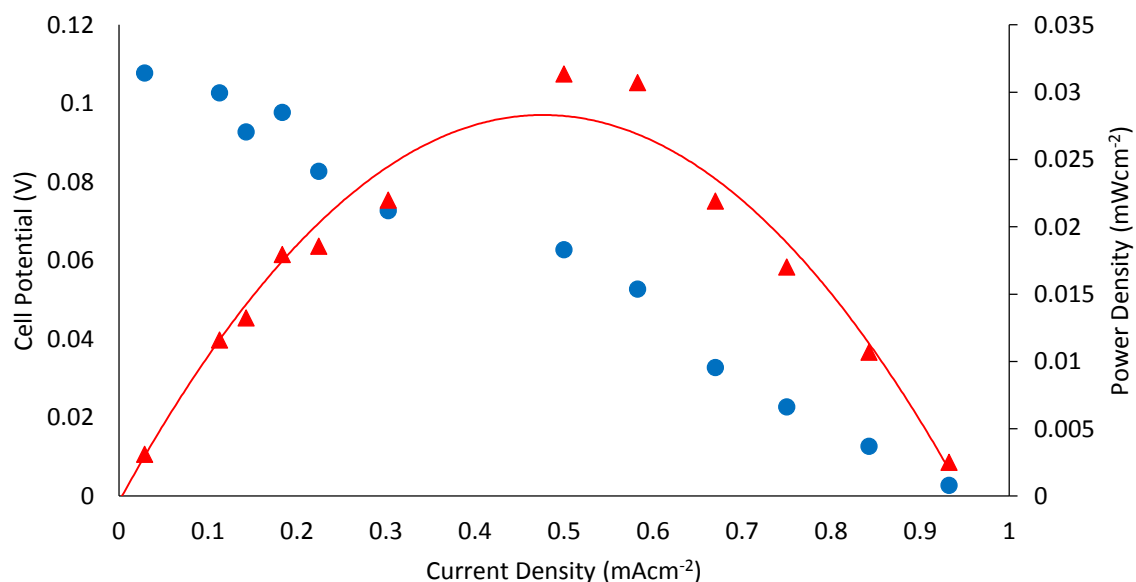

Figure 21: I-V (blue) and I-P (red) curves of 0.1M KOH/0.1M butylamine electrolyte at pH with 300mM H2O2 added. Nickel foam anode and silver plate cathode
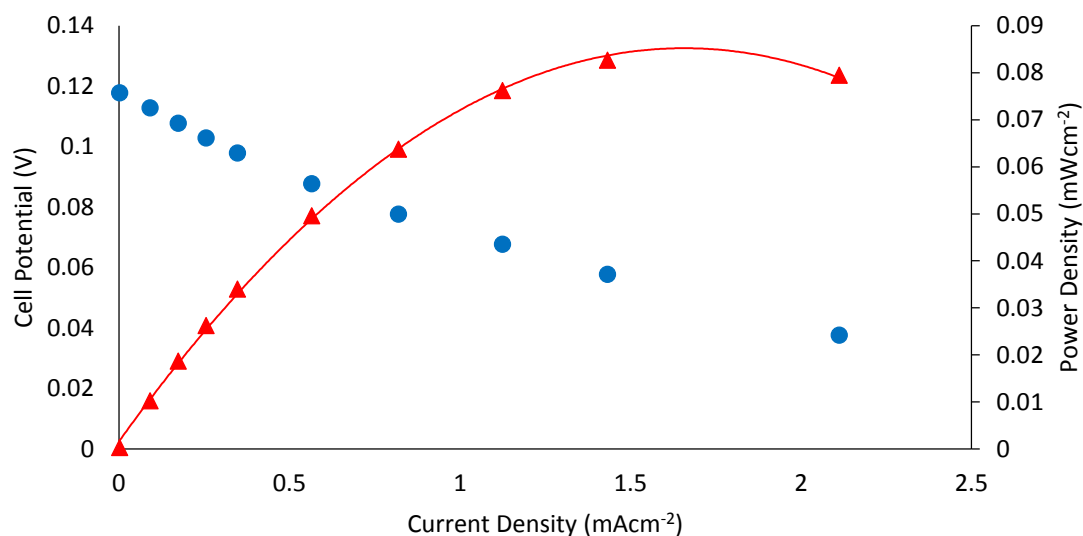
Figure 22: I-V (blue) and I-P (red) curves of 1M KOH/1M butylamine electrolyte at pH with 300mM H2O2 added. Nickel foam anode and silver plate cathode

Fig. 23 shows a similar system with an aqueous mixture of 1M ethylenediamine and 1M NaOH as the electrolyte. This system demonstrates a reasonably high OCP of 0.16V as well as a limiting current density of almost 4.5mAcm^{-2} and a maximum power density of 0.14mWcm^{-2}. This is a very high power density compared to other electrolytes tested in this project. Unfortunately this mixture of electrolytes was not found to produce H_2O_2 in noticeable quantities when it was used in the water oxidation cell described later in **Chapter 4**.
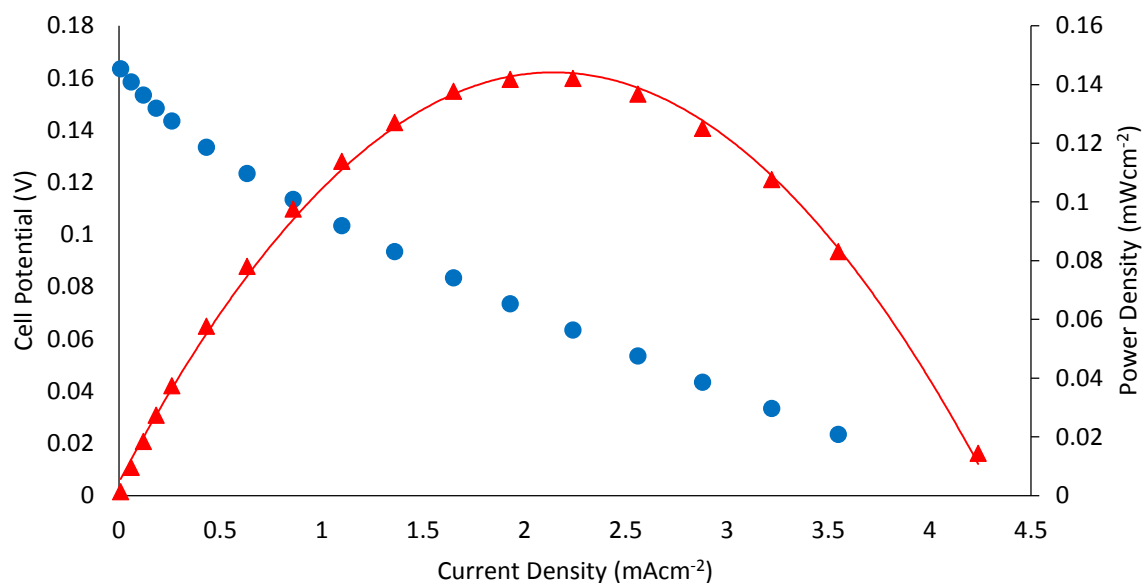
Figure 23: I-V (blue) and I-P (red) curves of a fuel cell constructed with a heat-treated Ni foam anode and a polished Ag plate cathode in a 1M ethylenediamine/1M NaOH electrolyte with 300mM H2O2 added.

Figs. 24 and 25 show I-V and I-P curves of fuel cells were the electrolyte was purged with N_2 gas for several minutes before testing and throughout the duration of the test. This was done to try to reduce the dissolved O_2 content of the electrolyte and observe any differences in the fuel cell performance. This was difficult and may be impossible as during the operation of the fuel cell $O_{2(g)}$ is necessarily

produced at the anode. However, no appreciable difference was observed in the OCP, the limiting current density or the maximum power density when compared to the tests without bubbling.
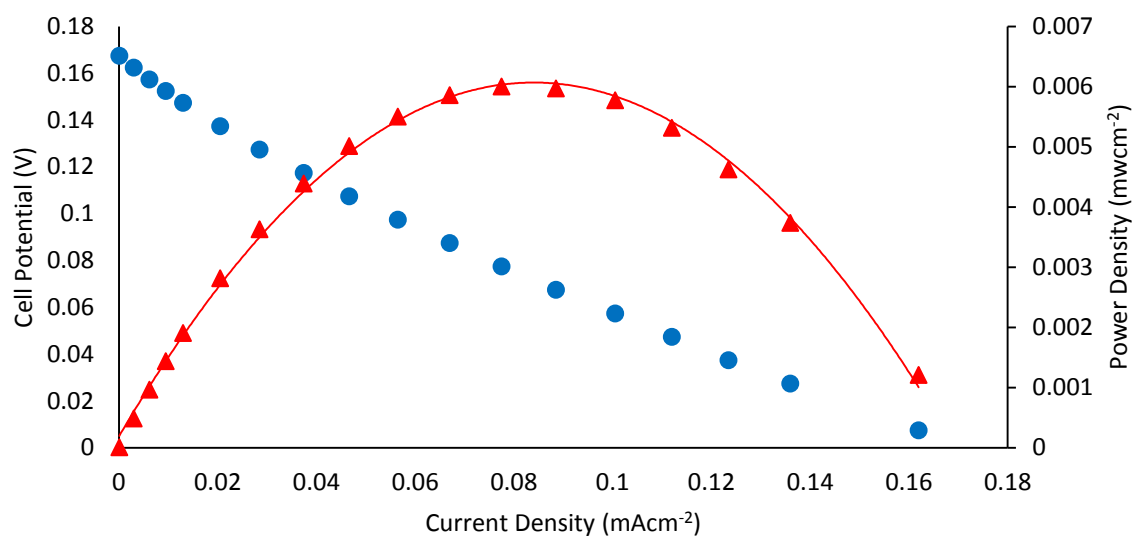

Figure 24: I-V (blue) and I-P (red) curves of a fuel cell constructed with a heat-treated Ni foam anode and a polished Ag plate cathode in 0.05M borate buffer at pH 9.2 with 300mM H2O2 added. Electrolyte bubbled with N_2.
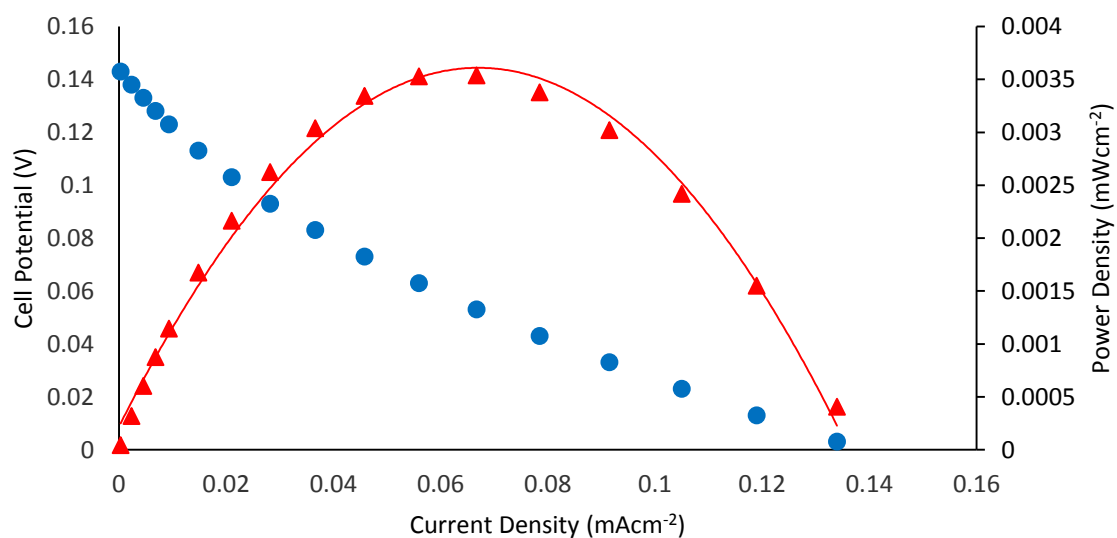

Figure 25: I-V (blue) and I-P (red) curves of a fuel cell constructed with a Ni foam anode and a polished Ag plate cathode in 0.05M borate buffer at pH 9.2 with 300mM H2O2 added. Electrolyte bubbled with N_2.

1.   S. H. Tamboli, G. Rahman and O.-S. Joo, *Journal of Alloys and Compounds*, 2012, **520**, 232-237.

Chapter 4

Reversible Direct H_2O_2 Fuel Cells

4.1 Reversible Direct Hydrogen Peroxide Fuel Cell

4.2 Introduction

Fossil fuels are used in enormous quantities today in both grid energy production and transportation as motor fuels. Their use has grown tremendously since the beginning of the 20th century and as a result their effect on the environment has already begun to manifest itself. Rising atmospheric CO_2 levels are predicted to cause major changes to global climates and increase the risk of extreme weather phenomena. Evidence as to the effect of higher atmospheric CO_2 levels can already be seen in the decreasing pH of the world's oceans and the threat that this poses to calcifying organisms such as crustaceans and corals[1, 2]. To replace fossil fuels as a primary energy source a number of "green" technologies are available such as wind, solar and tidal power. However, unlike fossil fuels, these technologies by themselves are not suited to transportation and need to be paired with a moveable energy storage medium which is also "green" in the sense that it does not produce waste during its operation.

Hydrogen gas is a much studied fuel[3-5] which can be produced electrochemically (directly from "green" energy sources) *via* water splitting and produces nothing but water and energy when it is used in a hydrogen fuel cell[6]. However, it proves to be problematic as a fuel because it has a low volumetric energy density compared to petroleum. In order to be economical hydrogen gas either needs to be pressurized, which requires high-pressure equipment or cryogenics[7] both of which add to the weight, cost and safety risks[8, 9] of the storage tanks. Hydrogen gas may also be stored at higher volumetric densities in materials such as metal hydrides[10-12] or metal-organic frameworks[13, 14] but these either store only low amounts of hydrogen, release hydrogen too slowly or can only release hydrogen at high temperatures.

Alternatively, H_2O_2 may also be used as a fuel because it oxidises to form benign products and, unlike $H_{2(g)}$, has the advantage of being a liquid at room temperature. It can also be produced electrochemically, either by the reduction of oxygen or by water oxidation[15-18]. A direct H_2O_2 fuel cell (DPPFC) has been demonstrated by Hasegawa *et al.*[19] and has been reported subsequently with various improvements to cell design and electrode composition[20-22]. These types of fuel cells make use of two different electrolytes, one alkaline and one acidic, which is problematic because they either require a membrane to separate the electrolytes or are kept stable by utilising microfluidic channels. Membranes can cause resistance in the fuel cell by inhibiting ion transport and have problems associated with leakage while microfluidic channels have low flow rates and are not suited to upscaling. Recently, single-compartment direct hydrogen peroxide fuel cells have been reported which produce power based on the potential difference between the selective oxidation and reduction of hydrogen peroxide at different electrodes[23-26]. Single-compartment fuel cells are advantageous because they do not require a membrane, the cell design is relatively simple and it allows hydrogen peroxide to be produced electrochemically in the same electrolyte. As such, this design has the potential to be used as a reversible fuel cell.
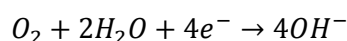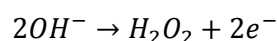
The concept of a reversible fuel cell as defined in this chapter is in essence a self-contained system where the fuel is produced electrochemically in some electrolyte and stored in a tank. This electrolyte/fuel mixture is later flowed through to the fuel cell where the fuel is oxidised and produces power. The electrolyte is then flowed back to the fuel production system. One of the most important aspects of this is the behaviour of the electrolyte during the cycling of fuel production to fuel usage. Ideally, for a reversible system, the electrolyte should be able to be regenerated during the fuel cell operation to the point where it can be used once again in the fuel production step with little to no external input. That is, the only reactants of the fuel producing process should either be

readily available from the surrounding environment (eg. atmospheric O_2) or be the products of the fuel utilisation process and *vice versa*.

For example, the direct H_2O_2 fuel cell described by Hasegawa *et al.*[19] uses Na^+ and SO_4^{2-} ions as the charge carriers between the two compartments of the fuel cell. As a result, during the operation of the fuel cell a salt, $NaSO_4$ is produced and the concentration of Na^+ in the anolyte and SO_4^{2-} in the catholyte is reduced. This means that in order to reproduce the same performance as was seen in the first cycle both electrolytes would need to be regenerated with the addition of $NaOH$ and H_2SO_4 and the remaining $NaSO_4$ would need to be removed. Of course, this system was not designed to be reversible but simply test the concept of a direct H_2O_2 fuel cell. However, it illustrates one of the problems with using two-compartment fuel cells when reversibility is required.
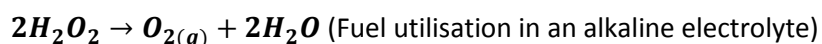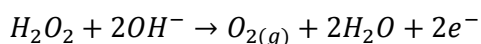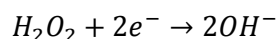
Previously, hydrogen production *via* water oxidation in alkaline electrolytes containing organic salts has been reported by Izgorodin *et al.*[27] where an aqueous solution of butylamine and sulphuric acid at pH10 was used in conjunction with a catalytic manganese oxide film (electrodeposited from a dilute ionic liquid) as a working electrode. This electrocatalytic method for H_2O_2 production is very promising in terms of producing a totally reversible fuel cell system as, when combined with a direct H_2O_2 fuel cell operating in the same electrolyte, the overall reactions taking place as part of the fuel cell cycle would only include:

Fuel Production

$$2OH^- \rightarrow H_2O_2 + 2e^-$$

$$O_2 + 2H_2O + 4e^- \rightarrow 4OH^-$$

$$\boldsymbol{O_2 + 2H_2O \rightarrow 2H_2O_2}$$ (Fuel production in alkaline electrolyte)

And:

Fuel Utilisation:

$$H_2O_2 + 2e^- \rightarrow 2OH^-$$

$$H_2O_2 + 2OH^- \rightarrow O_{2(g)} + 2H_2O + 2e^-$$

$\mathbf{2H_2O_2 \rightarrow O_{2(g)} + 2H_2O}$ (Fuel utilisation in an alkaline electrolyte)

As can be seen in the reactions described above, only oxygen and water are required to produce the fuel and only O_2 and water are produced when the fuel is burned, indicating that the system is fully reversible. If the system is operating in atmospheric conditions air may flowed across the cathode during the fuel production part of the cycle. If the cell is operated in non-atmospheric conditions such as in marine or aerospace applications the evolved gas must merely be collected when the fuel is being used and returned to the cell during fuel production.

The advantage that this type of fuel cell has over the more widely known H_2 fuel cell is that when H_2O_2 is electrochemically produced it remains in the electrolyte where it can be stored over time. H_2 on the other hand must be collected as a gas and, given the low volumetric density of $H_{2(g)}$ must either be compressed, cryogenically cooled or stored in other materials such as metal organic frameworks or metal hydrides, all of which require a significant amount of energy. Alternatively, a H_2O_2 fuel cell combined with the water oxidation method described above has the potential to be integrated into a closed system where the only input required is energy.

This chapter shows some progress into constructing a reversible H_2O_2 fuel cell system where H_2O_2 is generated electrochemically over a period of time and then is transferred directly to a fuel cell where it is used to produce power.

4.3 Experimental

Electrolytes

The butylammonium sulfate solutions used in this chapter were made by the titration of a 1M H_2SO_4 solution with butylamine until the desired pH was achieved.

Catalytic films

MnOx films were produced by electrochemical deposition from a solution of 1M ethylammonium nitrate and 10mM manganese acetate onto a 10cm x 10cm sheet of FTO glass following the method described by Zhou *et al.*[28]. The films were heated at 90°C for 30 minutes.

Electrochemical measurements were performed using a variable multi-channel potentiostat (VMP-2, Princeton Applied Research). Electrochemical generation of H_2O_2 was conducted by chronoamperometry in a three-electrode cell (details are discussed later in the chapter) and final H_2O_2 content was measured using a standard $KMnO_4$ titration method. The titration of the electrolyte after chronoamperometry was conducted according to the reaction:

$$2MnO^{4-} + 5H_2O_2 + 6H^+ \rightarrow 2Mn^{2+} + 5O_2 + 8H_2O$$
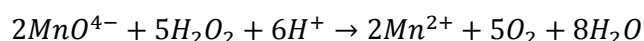
500μL of 2M sulphuric acid was added to 500μL of the electrolyte to acidify the solution and prevent formation of MnO_2. The titration was performed by UV-Vis spectroscopy where absorption was measured at 565nm wavelength. 7.55 x 10^{-3} M potassium permanganate solution was added in volumes of 5μL between each measurement, with 2 minute intervals to allow the adsorption reading to stabilise. Fuel cell testing was performed using chronoamperometry where the potential between the anode and cathode was held constant for 10 seconds at the open circuit potential initially. A bias

was then applied to the working electrode (cathode) incrementally in steps with each potential held for 10 seconds each until the potential difference between the two electrodes was zero. The current was measured at each of these potentials.

4.4 Results and Discussion

DHPFC Performance with Alkaline, Organic-salt Electrolytes

I-V curves were measured for different electrolyte solutions containing 300mM of H_2O_2 in order to determine the performance of these fuel cells in comparison to inorganic electrolytes. Ag metal was use as the cathode and Ni foam as the anode in a two electrode set-up (the reference terminal was connected to the cathode electrode to measure the cell potential). Testing was performed using chronoamperometry where the cell was held at the OCP for 10 seconds. Subsequently, the voltage was increased in steps and held for 10 seconds at a time. The cell potential was measured until it reached 0V indicating that the maximum current of the fuel cell had been reached. Fig. 1 shows a fuel cell constructed with a 1M butylammonium sulfate
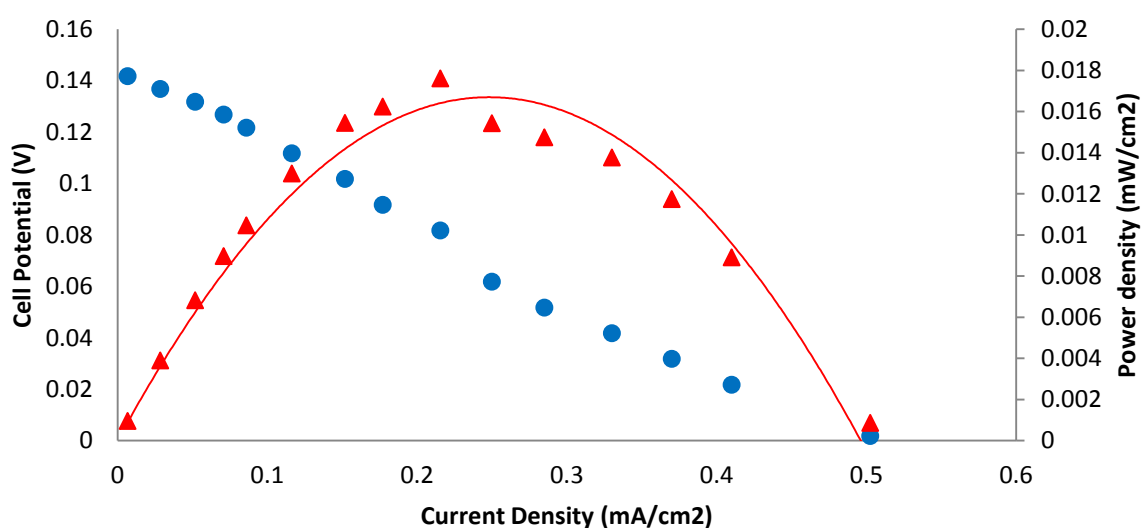
When the same experiment was attempted using a 5M solution of butylammonium sulfate the amount of bubbles that were generated at the Ag cathode caused the results to be inconclusive. Vigorous bubbling occurred even before the electrodes were connected indicating the disproportionation of H_2O_2 due to the highly alkaline environment as discussed in **Chapter 3**.

Integrating H_2O_2 Production and DHPFC

An electrolytic cell that showed high efficiency H_2O_2 production from water oxidation was demonstrated previously[29]. The same system was used here to demonstrate the validity of combining electrocatalytic H_2O_2 production with a direct H_2O_2 fuel cell. For the purposes of this experiment a specialised electrochemical cell was constructed that was designed to increase the surface area of the catalyst compared to the volume of electrolyte. The purpose of this was to try to increase the concentration of H_2O_2 generated and subsequently increase the total power produced by the DHPFC. The working electrode of the cell was a MnOx thin film and the electrolyte was a 1M solution of butylammonium sulfate adjusted to pH 9.95 with the addition of butylamine.
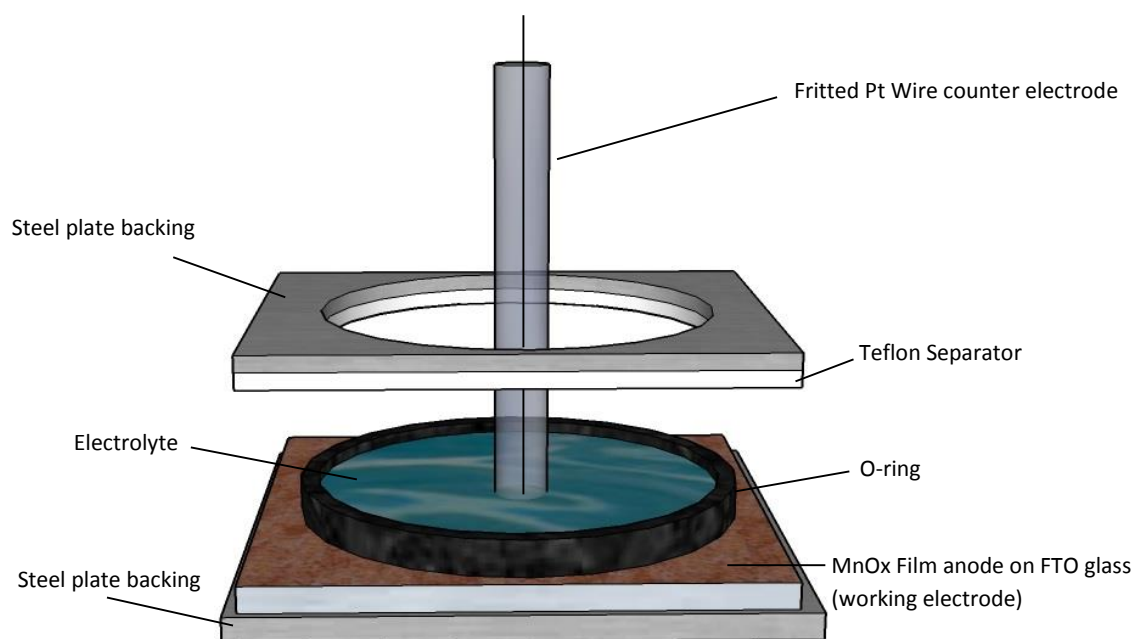
Figure 2: Schematic of the water oxidation cell used to produce H$_2$O$_2$ with a high catalytic surface area to electrolyte volume ratio

The catalytic MnOx film was sandwiched between a steel plate and an o-ring. A Teflon separator was placed on top of the o-ring and another steel plate was placed on top of that. Four screws were threaded through the corners of each of the two steel plates and the Teflon separator and tightened to press the entire cell together and form a seal between the o-ring, the Teflon separator and the FTO working electrode. The electrolyte was pipetted into the space created by the o-ring between the working electrode and the Teflon separator. This created a 21 cm^2 area where the electrolyte was in contact with the catalytic film. The total volume of electrolyte used in the cell was only 3mL. Compared to the method for water oxidation to H$_2$O$_2$ described previously in Chapter 2 where the catalytic surface area of the working electrode was 0.5cm^2 in 0.5mL of electrolyte the ratio of catalytic area to electrolyte is much higher in the new cell. Ideally, this would mean that for the same number of moles of H$_2$O$_2$ produced per active catalytic site the increase in the concentration of H$_2$O$_2$ in the electrolyte would be greater. A coiled platinum wire housed within a fritted glass tube was used as a counter electrode and was

dipped into the electrolyte perpendicular to the plane of the working electrode as shown in Fig. 4. A standard calomel electrode was used as a reference and was inserted into the electrolyte in the same fashion as the counter electrode. Fig. 5 shows a cyclic voltammogram of the cell with a 1M butylammonium sulfate electrolyte that has been adjusted to pH 9.95. The voltammogram shows an increase in current beginning at 0.5V vs SCE applied potential which is most likely the beginning of water oxidation to H_2O_2 as shown in previous work[29]. This suggests that the changes to the geometry of the cell design had no impact on the on the water oxidation potential achieved for H_2O_2 production.
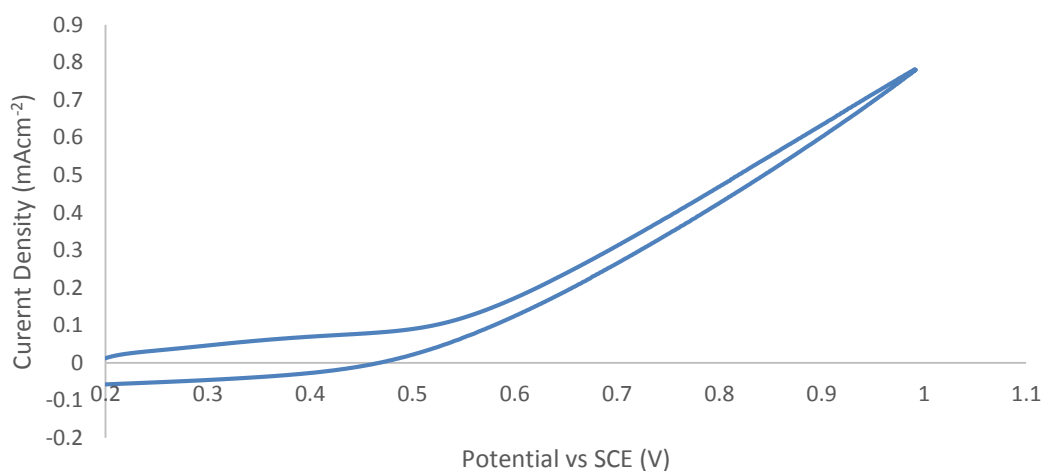

Figure 3: **Cyclic voltammogram of a water oxidation cell including a catalytic MnOx film on FTO as a working, Pt wire counter electrode and a standard calomel reference electrode. The electrolyte was a 1M BAS solution adjusted to pH 9.95. Scan rate of 1mVs^{-1}.**

Long-term hydrogen peroxide production was achieved *via* chronoamperometry with an applied potential of 800mV vs SCE over 5 hours. The current measured over the course of the chronoamperometry is shown below in Fig. 6:
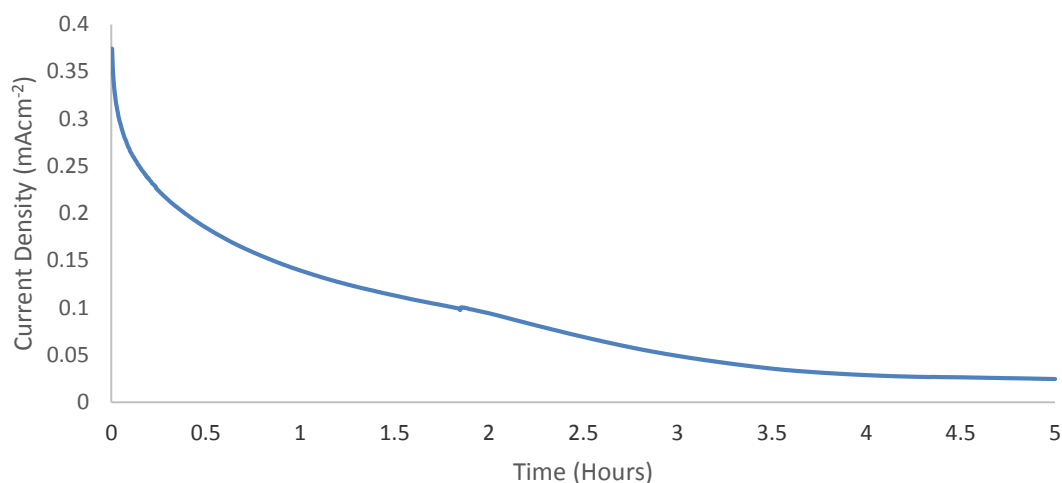
Figure 4: Long-term chronoamperometry of a water oxidation cell with a catalytic MnOx film on FTO as a working electrode, Pt wire counter electrode and a standard calomel reference electrode. The electrolyte was a 1M BAS solution adjusted to pH 9.95. The potential at the working electrode was held at 800mV vs SCE.

The current density produced at the beginning of the experiment when 800mV bias was applied to the working electrode was approximately $0.37mAcm^{-2}$. This current density is expected as it is approximately the same as that in the water oxidation system described in **Chapter 2** using the same electrolyte and the same catalytic material. Given the catalyst and electrolyte have not changed the catalytic activity of the system in the same potential should not change either. However, over the course of 5 hours the current density drops dramatically with the highest rate of current loss occurring in the first 30 minutes of applied potential. Over the next 3 hours the current density drops steadily until it appears to stabilise at $28\mu Acm^{-2}$. This behaviour has been observed in electrodeposited manganese oxide films previously[30-32]. It is also to be expected in this cell configuration that the build up of products will shift the reversible potential and lower the currents. The current could be kept stable by increasing the potential applied between the two electrodes, however, as shown in **Chapter 2** the production of H_2O_2 is limited to a specific range of potentials.

The amount of H$_2$O$_2$ generated after 5 hours of chronoamperometry at 800mV vs SCE was determined by volumetric titration with permanganate. The titration curve measured is shown in Fig. 7.
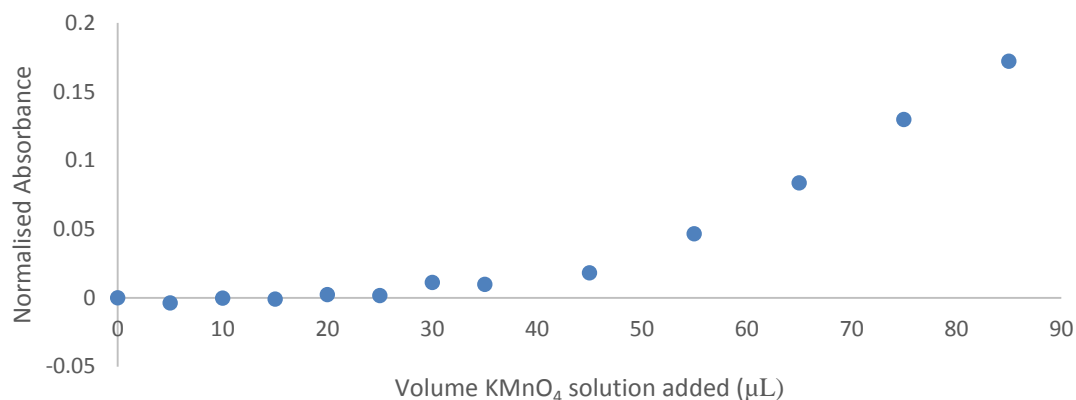
The amount of H$_2$O$_2$ generated with this technique was calculated to be 2.3 ± 0.3µmol (7.9 ± 0.9mM) in the total 3mL of electrolyte. Unfortunately, this is not an improvement when compared to the long term H$_2$O$_2$ production observed in the paper presented in **Chapter 1**[29]. There, using a MnOx catalyst with a geometric surface area of 0.5cm^2 in 0.5mL of electrolyte a total of 3µmol of H$_2$O$_2$ was produced in only two hours at an applied potential of 800mV. This occurred despite the much higher total charge passed through the cell in the high surface area water oxidation cell in the present work. The most probable reason for this is that the geometry of the counter electrode compared to the working electrode is not ideal. As can be seen in Fig. 4 the fritted counter electrode is placed perpendicular to the working electrode surface. This means that although at the centre of the working electrode the counter and working electrode are close together the edge of the working electrode and the counter electrode are approximately 2.5 cm

apart. Due to resistance in the FTO backing of the working electrode this means that the current density will be much lower at these outer edges compared to the centre. As such the total current density achievable by the cell could be much higher if the area of the counter electrode completely matched the area of the working electrode.

Fuel cell testing was performed immediately after the hydrogen peroxide production. The electrolyte was pipetted out of the water oxidation cell into a glass sample tube. A Co_3O_4/C65 catalytic film was use as the cathode and heat-treated Ni foam as the anode in a two electrode set-up (the reference terminal was connected to the cathode electrode to measure the cell potential). Fig. 8 below shows the I-V and I-P curves of the fuel cell using hydrogen peroxide electrogenerated *via* water oxidation.

Figure 6: I-V (blue) and I-P (red) curves of a direct H_2O_2 fuel cell. Hydrogen peroxide was generated *via* water oxidation in a 1M butylammonium sulfate electrolyte. Co_3O_4 cathode and heat treated Ni foam anode were used with a geometric area of 1cm² each.

The open circuit potential (when the current density of the cell is zero) observed in the I-V curve of Fig. 8 is approximately 0.18V which is expected given that similar potentials were observed in Chapter 3 under the same conditions, but adding H_2O_2 to the electrolyte manually rather than electrogenerating it. As the cell potential is reduced the

current density increases which is the expected behaviour for the fuel cell. The limiting current density of the cell (at a cell potential of 0V) is approximately 4µAcm^{-2}. This low limiting current compared to those found when 300mM of H_2O_2 was artificially added to the electrolyte is likely due to the low concentration of H_2O_2 produced by the electrochemical water oxidation. To attempt to improve mass transport of H_2O_2 through the cell the electrolyte was stirred during the fuel cell test. The OCP of the cell while stirring was found to be 0.19V and the limiting current shown in the I-V curve of Fig. 9 is marginally improved to 6.6µAcm^{-2} by stirring, indicating that mass transport is a limiting factor in the current density when the H_2O_2 concentration is this low.
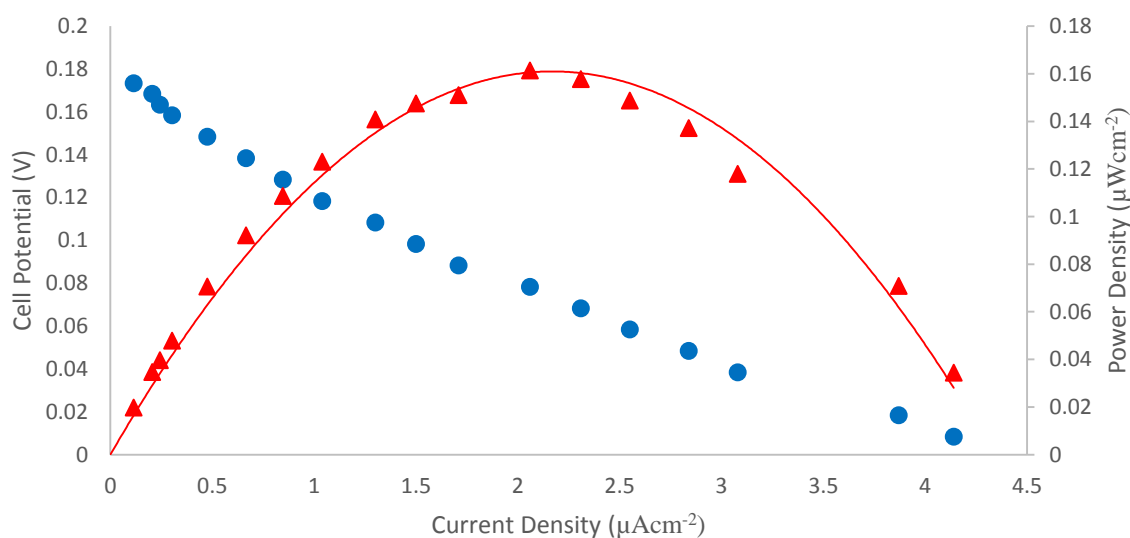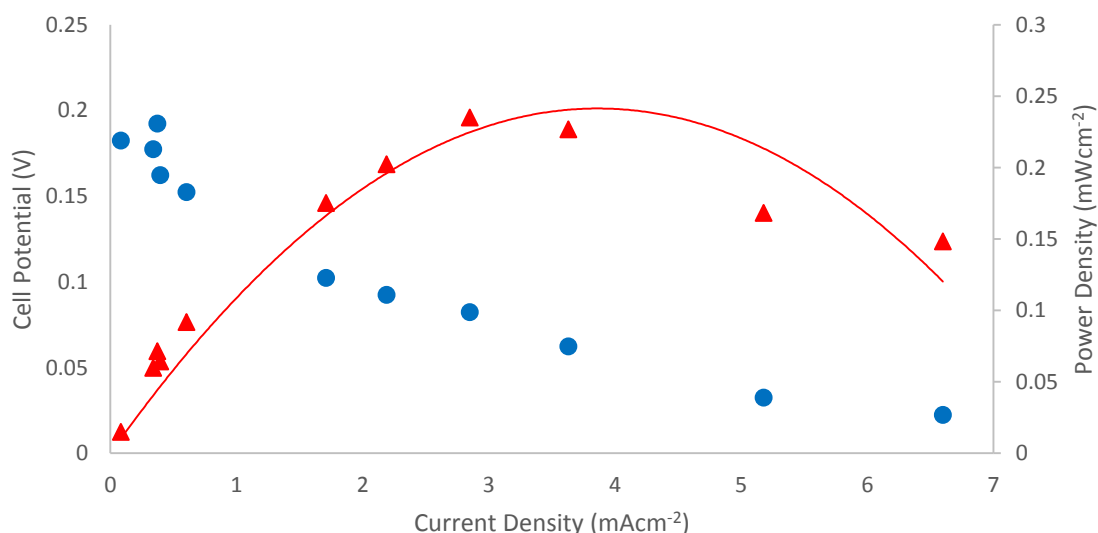

Figure 7: I-V and I-P curves of a direct H_2O_2 fuel cell. H_2O_2 was generated *via* water oxidation in a 1M butylammonium sulfate electrolyte. A heat-treated Ni foam anode and a Co_2O_3/C65 cathode were used with a geometric surface area of 1cm^2 each. Electrolyte was stirred during fuel cell testing.

The viability of this type of system as a reversible fuel cell is dependent on the stability of the electrolyte in both the water oxidation and fuel cell phases. During the oxidation and reduction of H_2O_2 the generation of radicals is likely. Given that amines can be oxidised on certain metals and catalysts and that it is possible that the particular

electrolyte used in these experiments (butylammonium sulfate containing excess butylamine) may be prone to decomposition. However, H^1NMR of the electrolyte after one cycle of water oxidation and fuel cell usage showed that it remained stable with no indication of the oxidation of the amine.

4.5 Conclusions

This chapter demonstrated the combination of a H_2O_2 producing water oxidation cell and a one-compartment direct H_2O_2 fuel cell as part of a reversible fuel generation and utilisation system. A water oxidation cell was designed with the goal of increasing the ratio of catalytic surface area to electrolyte to increase the concentration of H_2O_2. Performing water oxidation using this cell yielded a H_2O_2 concentration of almost 8mM in 3mL of electrolyte. This was then able to be transferred to a fuel cell which reached a maximum power density of $0.25mWcm^{-2}$ when the solution was stirred. Further improvements such as constructing a water oxidation flow cell may help to increase the current and therefore the H_2O_2 production rate as well as inhibit reoxidation of the H_2O_2 at the anode. Additionally, it would be much more electron efficient to also produce H_2O_2 at the cathode simultaneously *via* O_2 reduction while water oxidation was being performed. O_2 reduction to H_2O_2 has been demonstrated previously[17, 33] and such a cell could produce twice as much H_2O_2 for the same amount of current.

4.6 References

1. K. E. Fabricius, G. De'ath, S. Noonan and S. Uthicke, *Proceedings of the Royal Society B: Biological Sciences*, 2014, **281**, 20132479.

2. T. Zielinski, J. Marcin Węsławski and K. Kuliński, *Impact of climate changes on marine environments*, Springer, New York, 2015.

3. J. Tollefson, *Nature*, 2010, **464**, 1262+.

4. in *Production, Transport and Storage*, ed. R. B. Gupta, CRC Press, 2008.

5. A. Szyszka, *International Journal of Hydrogen Energy*, 1998, **23**, 849-860.

6. B. G. Ram and K. K. Pant, in *Hydrogen Fuel*, CRC Press, 2008, pp. 2-32.

7. R. K. Ahluwalia, T. Q. Hua, J. K. Peng, S. Lasher, K. McKenney, J. Sinha and M. Gardiner, *International Journal of Hydrogen Energy*, 2010, **35**, 4171-4184.

8. Z. Li, X. Pan, K. Sun and J. Ma, *International Journal of Hydrogen Energy*, 2013, **38**, 11174-11180.

9. M. Royle and D. Willoughby, *Process Safety and Environmental Protection*, 2011, **89**, 452-462.

10. C. M. Rangel, V. R. Fernandes, Y. Slavkov and L. Bozukov, *International Journal of Hydrogen Energy*, 2009, **34**, 4587-4591.

11. F. Schuth, B. Bogdanovic and M. Felderhoff, *Chemical Communications*, 2004, 2249-2258.

12. B. Sakintuna, F. Lamari-Darkrim and M. Hirscher, *International Journal of Hydrogen Energy*, 2007, **32**, 1121-1140.

13. Y. Yan, S. Yang, A. J. Blake and M. Schröder, *Accounts of Chemical Research*, 2014, **47**, 296-307.

14. I. A. Ibarra, S. Yang, X. Lin, A. J. Blake, P. J. Rizkallah, H. Nowell, D. R. Allan, N. R. Champness, P. Hubberstey and M. Schroder, *Chemical Communications*, 2011, **47**, 8304-8306.

15. W. R. P. Barros, Q. Wei, G. Zhang, S. Sun, M. R. V. Lanza and A. C. Tavares, *Electrochimica Acta*, 2015, **162**, 263-270.

16. M. Gara, E. Laborda, P. Holdway, A. Crossley, C. J. V. Jones and R. G. Compton, *Physical Chemistry Chemical Physics*, 2013, **15**, 19487-19495.

17. T.-P. Fellinger, F. Hasché, P. Strasser and M. Antonietti, *Journal of the American Chemical Society*, 2012, **134**, 4072-4075.

18. T. Murayama and I. Yamanaka, *The Journal of Physical Chemistry C*, 2011, **115**, 5792-5799.

19. S. Hasegawa, K. Shimotani, K. Kishi and H. Watanabe *Electrochemical and Solid-State Letters*, 2005, **8**, A119-A121.

20. F. Yang, K. Cheng, X. Liu, S. Chang, J. Yin, C. Du, L. Du, G. Wang and D. Cao, *Journal of Power Sources*, 2012, **217**, 569-573.

21. A. E. Sanli and A. Aytaç, *International Journal of Hydrogen Energy*, 2011, **36**, 869-875.

22. F. Yang, K. Cheng, X. Xiao, J. Yin, G. Wang and D. Cao, *Journal of Power Sources*, 2014, **245**, 89-94.

23. S.-i. Yamazaki, Z. Siroma, H. Senoh, T. Ioroi, N. Fujiwara and K. Yasuda, *Journal of Power Sources*, 2008, **178**, 20-25.

24. Y. Yamada, M. Yoneda and S. Fukuzumi, *Energy & Environmental Science*, 2015, **8**, 1698-1701.

25. Y. Yamada, M. Yoneda and S. Fukuzumi, *Inorg. Chem.*, 2014, **53**, 1272-1274.

26. Y. Yamada, M. Yoneda and S. Fukuzumi, *Chemistry – A European Journal*, 2013, **19**, 11733-11741.

27. A. Izgorodin, E. Izgorodin, D. R. MacFarlane, *Energy & Enviroonmental Science*, 2012, **5**, 9496-9501.

28. F. Zhou, A. Izgorodin, R. K. Hocking, V. Armel, L. Spiccia and D. R. MacFarlane, *ChemSusChem*, 2013, **6**, 643-651.

29. C. McDonnell-Worth and D. R. MacFarlane, *RSC Advances*, 2014, **4**, 30551-30557.

30. I. Zaharieva, P. Chernev, M. Risch, K. Klingan, M. Kohlhoff, A. Fischer and H. Dau, *Energy & Environmental Science*, 2012, **5**, 7081-7089.

31. T. Takashima, K. Hashimoto and R. Nakamura, *Journal of the American Chemical Society*, 2011, **134**, 1519-1527.

32. F. Zhou, A. Izgorodin, R. K. Hocking, L. Spiccia, D.R. MacFarlane, *Advanced Energy Materials*, 2012, **In print**.

33. J. S. Jirkovský, I. Panas, E. Ahlberg, M. Halasa, S. Romani and D. J. Schiffrin, *Journal of the American Chemical Society*, 2011, **133**, 19432-19441.

Chapter 5

Conclusions and Future Work

5.1 Conclusions

This thesis has discussed the electrochemical oxidation of water to produce H_2O_2 as well as its use in direct H_2O_2 fuel cells. **Chapter 1** gave a perspective on electrochemical H_2O_2 production and how this may be incorporated into a 'green' alternative fuel economy. By taking advantage of the electrochemical properties of H_2O_2 it is possible to design unique fuel cells where H_2O_2 acts as both the fuel and the oxidant. These types of fuel cells are similar in operation to the much more prevalent H_2 gas fuel but given that H_2O_2 is a liquid at room temperature it is potentially much safer as it does not require pressurisation.

Chapter 2 presented a paper published in RSC advances that investigated the electrochemical oxidation of water to selectively produce H_2O_2. Through the combination of a well-known water oxidation catalyst, manganese oxide, and unusual electrolytes (alkaline, aqueous solutions of protic ionic liquids based on ammonium cations) water oxidation takes place at relatively low overpotentials and produces stable H_2O_2. **Chapter 2** demonstrates this process using several different electrolytes at various pHs and found that increasing the alkyl chain length of the ammonium cation above four and changing the ammonium cation from primary to secondary reduced the amount of H_2O_2 that was generated. H_2O_2 production was found to begin at pH9 and reach a maximum at around pH 10.5 and the faradiac efficiency of the process was at a maximum when the potential applied to the catalytic anode was below a certain threshold at which point O_2 was generated in competition with H_2O_2.

The utilisation of this electrogenerated H_2O_2 in direct H_2O_2 fuel cells was explored in **Chapter 3**. Several catalysts, both for oxidation and reduction of H_2O_2, were investigated to try to improve the performance of these fuel cells. Out of the catalysts tested, a combination of a heat-treated Ni foam cathode and a mixed Co_3O_4-carbon black anode was found to perform best in both a conventional inorganic salt solution electrolyte and

in the same butylammonium sulfate solution that could be used to electrogenerate H_2O_2 *via* water oxidation. The effect of the mixed potential of H_2O_2 oxidation and reduction on these catalysts was also discussed in relation to the observed open circuit potential and overall efficiency of these types of fuel cells.

Chapter 4 proposes and demonstrates a fully reversible one-compartment direct H_2O_2 fuel cell which incorporates the concepts investigated in both **Chapter 2** and **Chapter 3**. An electrochemical cell was constructed and chronoamperometric water oxidation was performed to produce H_2O_2 in a 1M butylammonium sulfate electrolyte. This electrolyte was then transferred to a fuel cell where it was used to produce a small but measureable amount of power. Although this was a preliminary device it showed that the concept of using electrogenerated H_2O_2 in a fuel cell is sound without requiring additional treatment of the electrolyte before or after it is cycled.

5.2 Future Work

There are a number of research pathways that will expand upon the work presented in this thesis in a meaningful way. Chapter 2 expounded on the mechanisms behind water oxidation to H_2O_2 by analysing the effect of electrolyte environments on H_2O_2 production rates and required overpotentials. The actual electrochemical mechanism that allows for H_2O_2 production and stabilisation, however, was only hypothesised based on the expected interaction between the catalytic surface and the free amine in the electrolyte. Our knowledge of the mechanism might further be refined through the use of computational experiments that include surface interactions of the catalyst with the surrounding electrolytes. This would give relevant information on the electrocatalytic processes that lead to the formation of H_2O_2 and not just the stabilising effect that the free amine has on the H_2O_2 once it is in solution which was demonstrated by Izgorodin *et al*.

The other aspect of the work presented in this thesis is the practical outcomes that this electrochemical generation of H_2O_2 affords both the fuel industry and various other industrial applications of H_2O_2.

Water Oxidation to H_2O_2

The presence of free amine in the electrolyte of the water oxidation process described in **Chapter 2** is necessary for H_2O_2 production. This limits the pH of the electrolyte to at least 9 using simple amines such as butylamine or diethylamine. This problem may be mitigated by dissolving salts with cations containing multiple primary amines in the electrolyte. These amines contain multiple proton accepting nitrogens that have pKas which will increase after protonation of the first nitrogen. Ideally, this would create a cation with an unprotonated amine group that will be available for bonding with and

stabilisation of the H_2O_2 formed during water oxidation. This may allow for a low-pH electrolyte (less than pH 9) that can be used for water oxidation to H_2O_2.

H_2O_2 as a Fuel

As discuss in this thesis electrochemically generated H_2O_2 is a promising energy storage medium that has a number of practical advantages when compared to other types of "green", non-fossil based fuels. While much progress has been made in this work and in the general research body as a whole there are still a number of improvements to be made to these systems to make them viable for use in the outside world.

Reversibility – Chapter 4 presented the design of a reversible fuel cell system that included both the generation of H_2O_2 and its use as a fuel *in situ*. When designing a fuel cell system to be reversible the preferred outcome is that as few components of the system need to be replaced, regenerated or altered as possible before it can be cycled again. This is desirable when fuel cells need to be operated in remote areas or otherwise where access to them is difficult. It also potentially lowers the cost of the system as fewer external components are required to keep the cell operational. Chapter 4 gave one example of a reversible system, however, as the power density achieved was much lower than needed for an operational fuel cell other it may be beneficial to look at other designs. One option is to make use of the two-compartment cell design that was discussed in the review section of Chapter 1. This type of DHPFC has been shown to have much higher open circuit potentials and subsequently much higher maximum power densities but is limited by the requirement for two different electrolytes (acidic and alkaline) which traditionally has limited the reversibility of these cells. While it was proposed that these cells could be used in conjunction with electrochemical generation of H_2O_2 the only method proposed was oxygen reduction in an acidic medium. This means that for the

fuel cell to function there would need to be an interim step in which half of the electrolyte containing the electrogenerated H_2O_2 would need to be alkalinized.

H_2O_2 distillation – The electrochemical methods described in this thesis do not produce enough H_2O_2 to attain concentrations as large as 70w% which was determined to be of comparable energy density to compressed $H_{2(g)}$ in the introductory **Chapter 1.9**. While the rate of H_2O_2 production may be improved by modifications to the cell such as increasing the surface area of the catalytic working electrode it is possible that H_2O_2 may be disproportionated at the electrode if it becomes too concentrated in the electrolyte. As such, it may be necessary to integrate a H_2O_2 distillation system into the reversible fuel cell and store the concentrated H_2O_2 in a tank that is separated from either the water oxidation cell or the fuel cell.

H_2O_2 in Advanced Oxidation Processes

H_2O_2 is largely used for cleaning and bleaching in industry, however, there are a number of other reactions in which *in situ* electrochemical H_2O_2 production could be used as an oxidant. These include the epoxidation of organic molecules as well as the decomposition of unwanted industrial waste products such as dyes. The advantages of *in situ* production are that reaction rates can be controlled as the process can be switch on and off when desired and the rate of H_2O_2 generation can be increased or reduced as desired. In an industrial setting electrochemical H_2O_2 allows companies to produce their own H_2O_2 relatively easily (compared to the current anthraquinone autoxidation method) for their own particular requirements. Further work could focus on integrating the water oxidation to H_2O_2 electrochemical method with these oxidative processes.